Planetary Probes
Entry and Descent Science

Part 1 - Introduction to EDL Technologies and On-board Instrumentation

Alessio Aboudan (alessio.aboudan@unipd.it), Luca Placco, G. Colombatti, F. Ferri and the AMELIA team

Introduction

Goals and engineering challenges and scientific potential of EDL systems

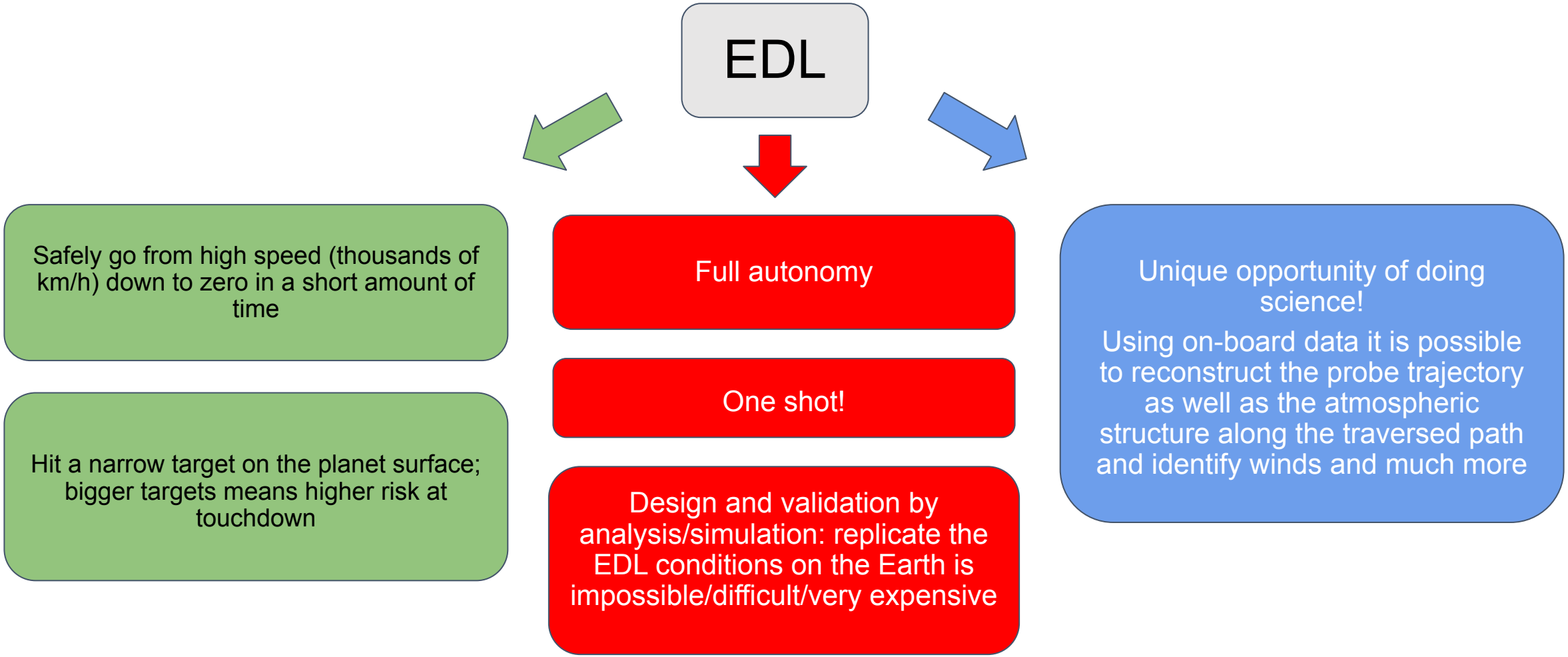

Past and Future Missions

- Atmospheric Structure Instruments
  - Huygens ASI - Titan
  - Galileo Probe ASI - Jupiter
  - Mars Pathfinder ASI - Mars
  - Pioneer - Venus
  - Venera probes

- Instrumentation
  - Temperature
  - Pressure
  - Humidity
  - Accelerometers
  - Optical
    - Radiometers/Spectrometers
  - Entry Instrumentation (shield sensors)
  - Electric Field and Lightning
  - Acoustic

Mars2020 EDL Sequence

State of the art about EDL

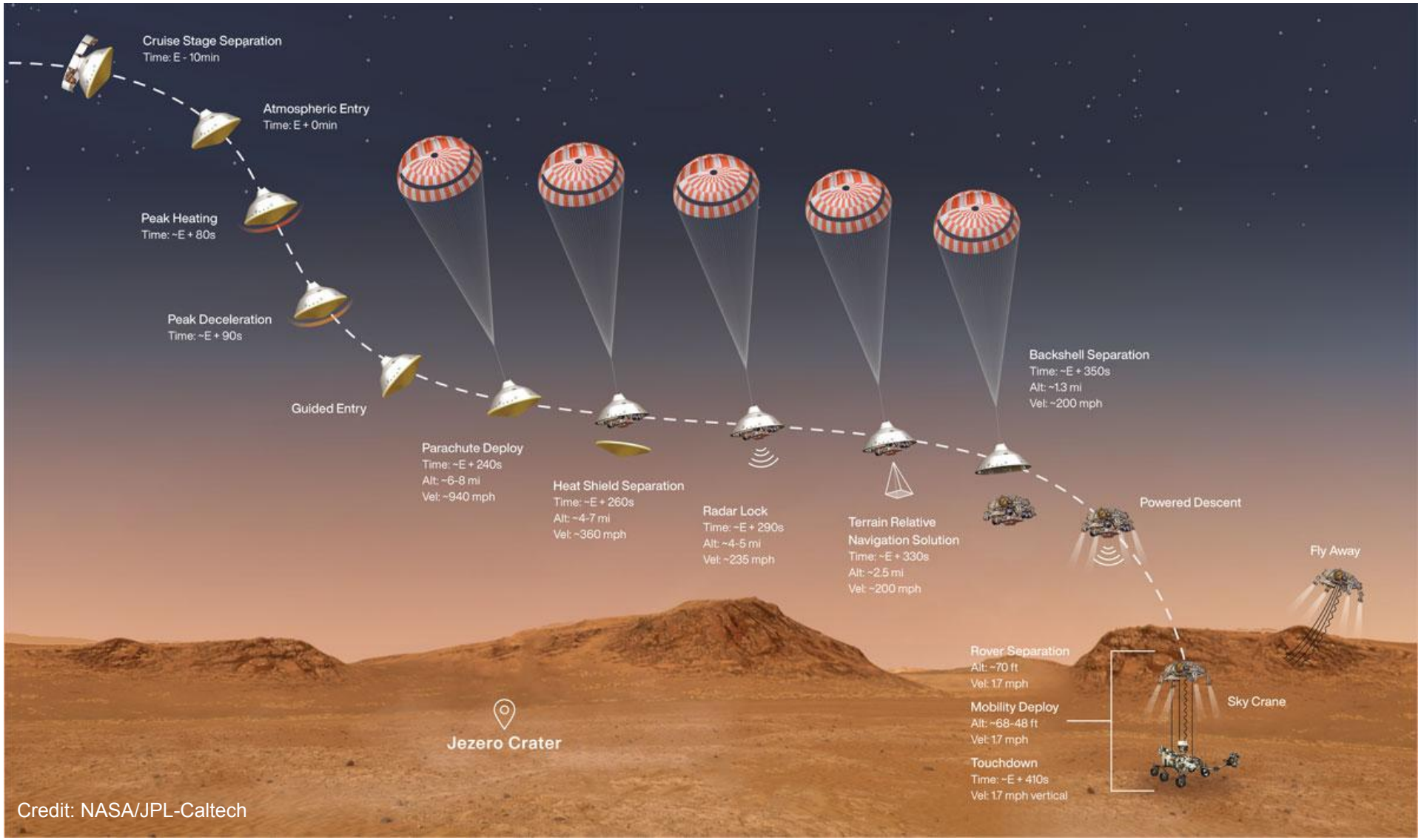

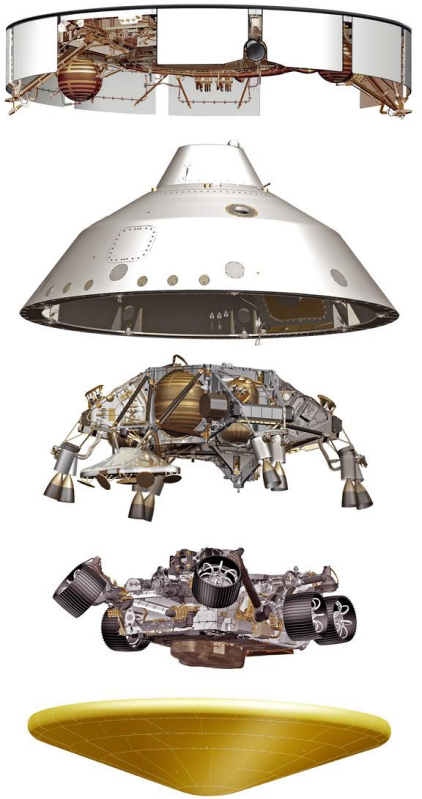

https://mars.nasa.gov/mars2020/timeline/landing/entry-descent-landing/

Cruise stage separation

Spacecraft composite:
Front/rear shields
Surface platform

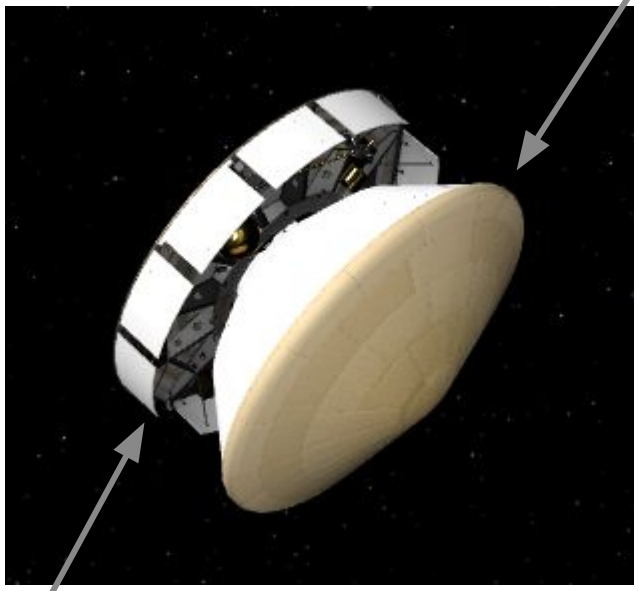

Cruise stage houses:
- Solar panels
- Radio link
- Fuel tanks

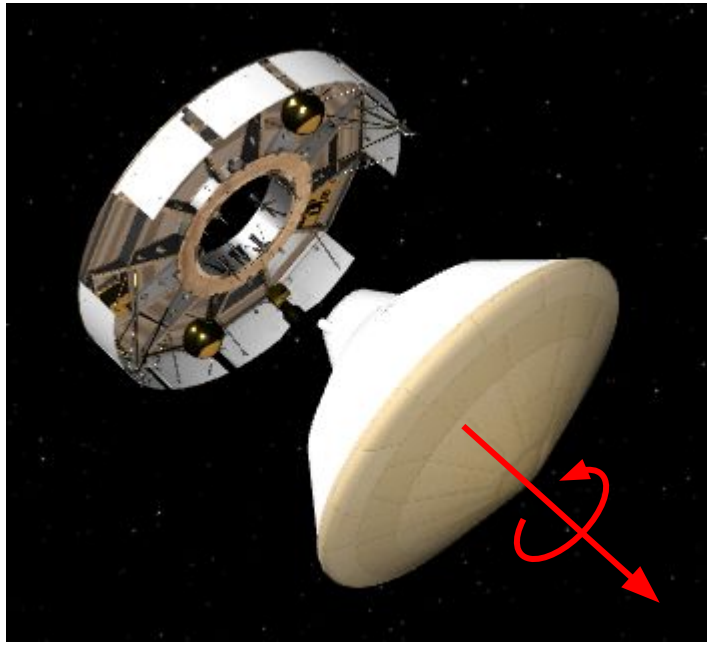

Separation could occur minutes/hours/days before entry interface point (SC encounters the atmosphere)

Separation mechanism is responsible for the right
- Direction
- Attitude
- Spin

Atmospheric entry

Dissipate both kinetic and potential energy of the SC

- Entry is designed to balance
  - Deceleration
  - Heating
  - Accuracy of landing

- Deceleration
  - If the drag is too small
  - Vehicle can bounce-off the atmosphere
  - Accounts also for conditions at parachute deployment
- Heating
  - If the drag is too high
  - Vehicle can burn-up in the atmosphere
- Landing accuracy
  - Keep small the landing footprint to reduce the risk of a failure at the touchdown due to terrain features (craters/rocks/slopes)

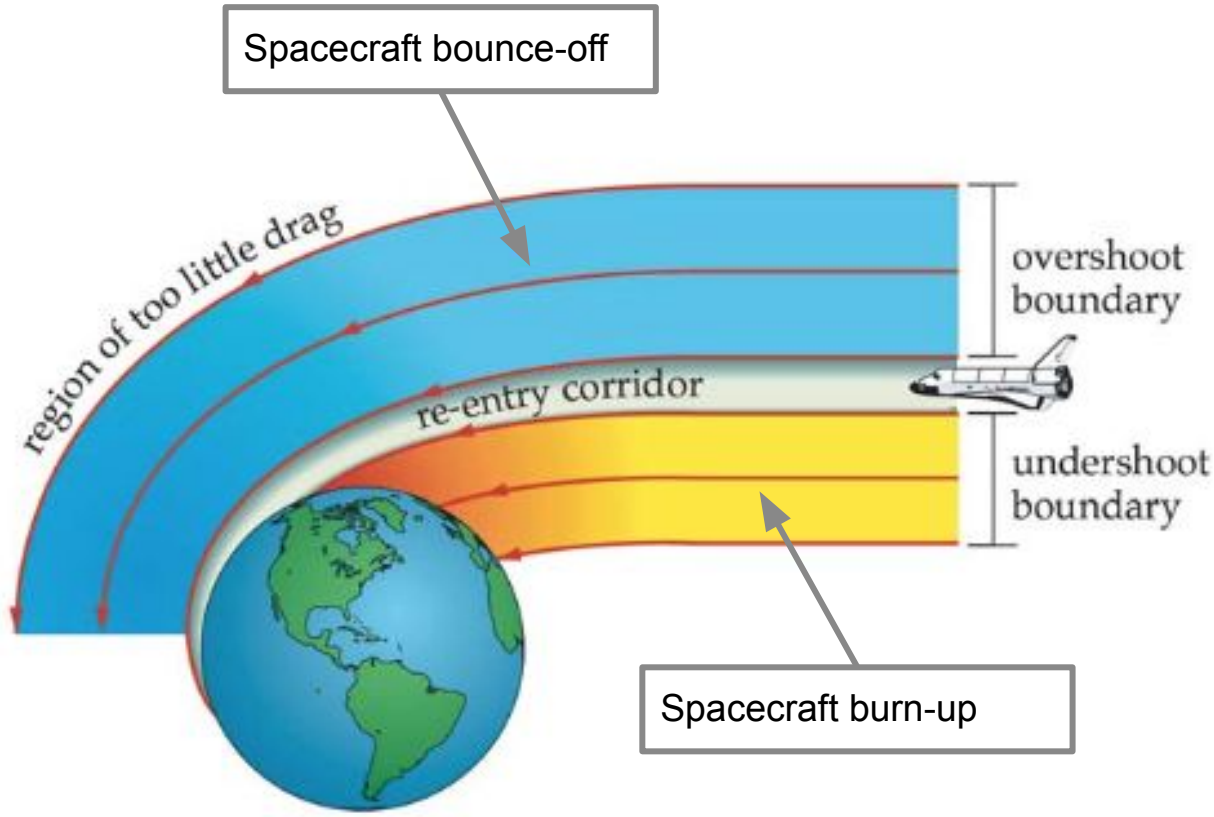

Local frame and basic angles definition

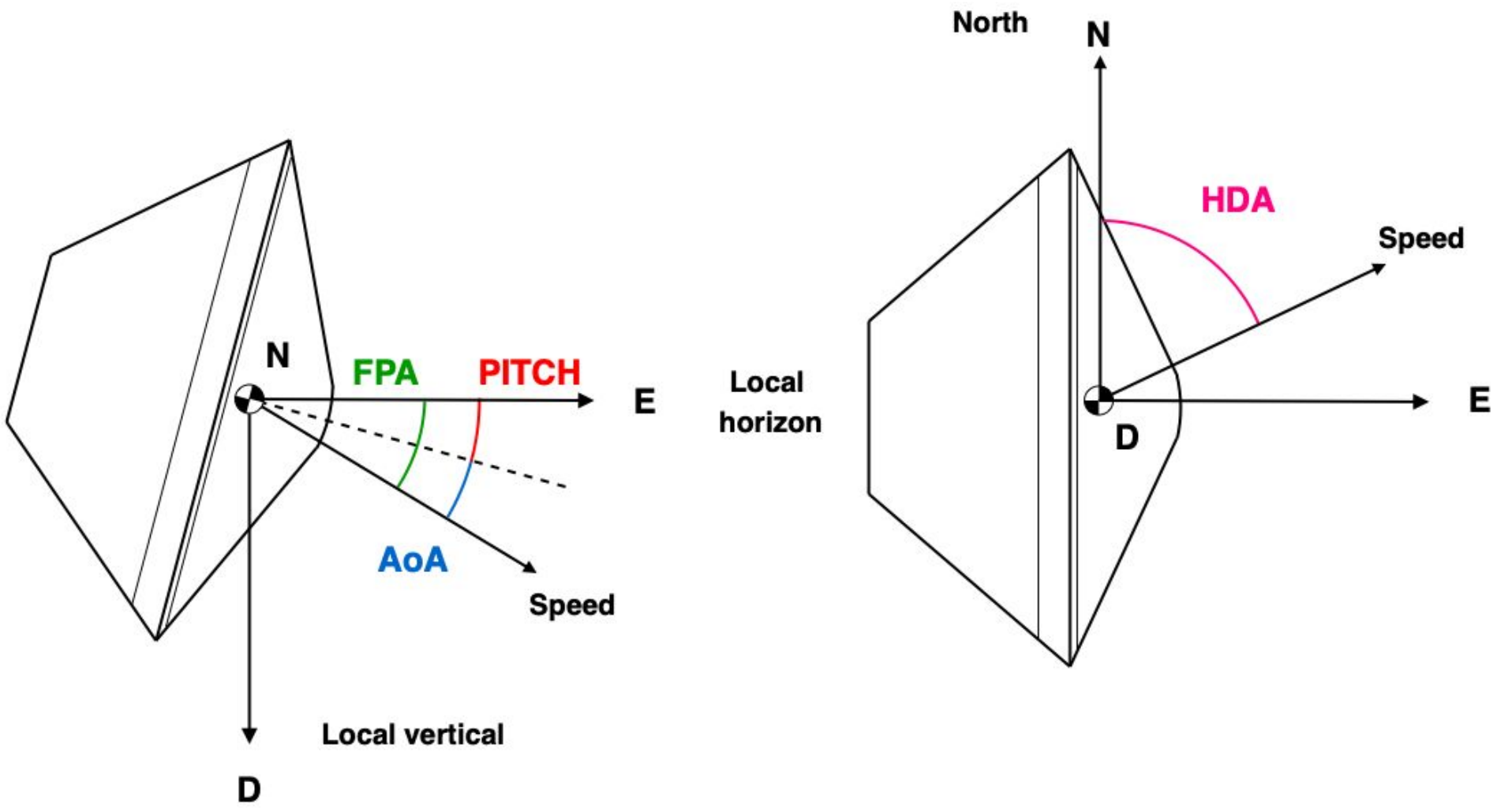

Drag force and the ballistic coefficient

- Drag force definition:

$$f_D = \frac{1}{2}\rho v^2 S C_D$$

atmospheric density (ρ), atmospheric relative velocity (v) reference surface (S) drag coeff. (C_D)

- Drag acceleration is the product of Dynamic Pressure (q) and Ballistic Coefficient (β)

$$a_D = \frac{f_D}{m} = \frac{q}{\beta} \qquad q = \frac{1}{2}\rho v^2 \qquad \beta = \frac{m}{S C_D}$$

hence: low β = high drag, high β = low drag

Entry corridor

Specified as FPA vs β or Speed vs Altitude at the EIP

- Depends on
  - Arrival conditions
  - Landing region and time
  - Atmospheric conditions
- Entry Interface Point (EIP)
  - Altitude at which the atmospheric drag became relevant for the motion of the S/C
  - Fixed altitude used for the design of the GNC
  - During the mission it is defined using the on-board IMU (acc. threshold)
- Acceptable range of FPA vs β is very small
  - Arrival and separation conditions are critical parameters
  - The FPA is an important parameter to be checked during post-flight analysis

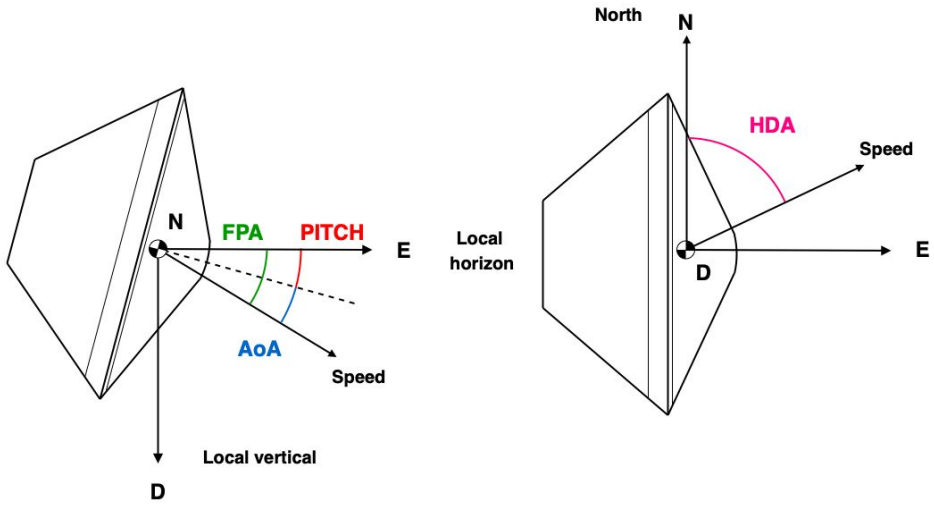

≈ 2 deg

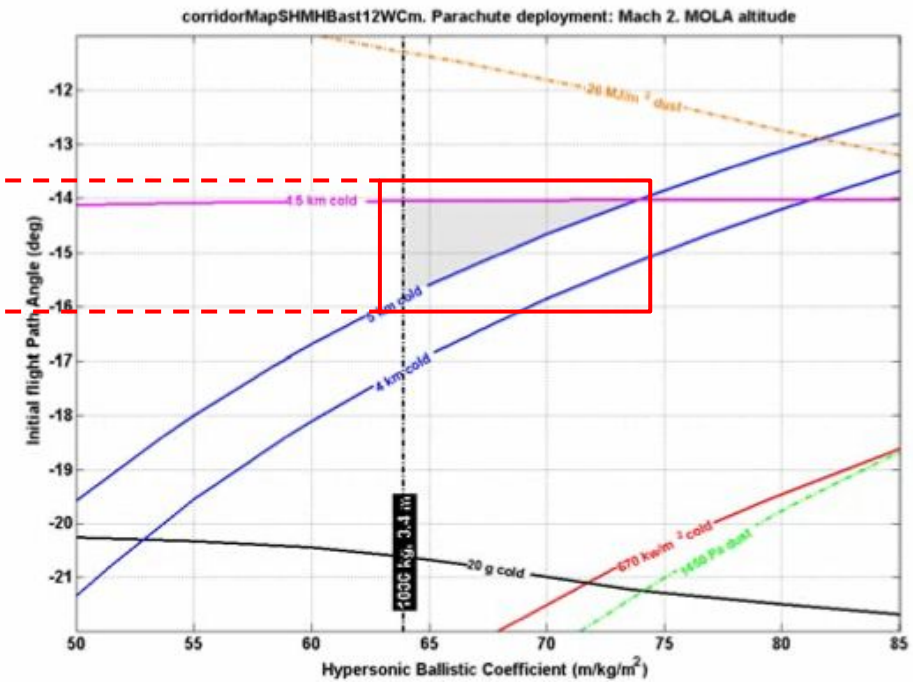

Examples of entry missions

- Share the same design i.e. 70° sphere cone aeroshell (Viking heritage)

Table 2
US robotic exploration of MARS EDL comparative summary.

Mission	Viking I	Viking II	MPF	MER-A	MER-B	Phoenix	MSL
Year	1976	1976	1997	2004	2004	2008	2012
Entry From	Orbit	Orbit	Direct	Direct	Direct	Direct	Direct
Entry Vel (km/s)	4.7	4.7	7.26	5.4	5.5	5.67	6
Entry FPA (deg)	−17	−17	−14.06	−11.49	−11.47	−12.5	−15.2
Ballistic Coefficient(kg/m^2)	64	64	63	94	94	70	142
Entry mass (kg)	992	992	585	832	836	603	3257
Touchdown landed mass (kg)	590	590	360	539	539	364	> 1700
Trim AOA at entry (deg)	−11	−11	0	0	0	−4	−17
Drag Coefficient	0.67	0.67	0.4	0.4	0.48	0.67	0.67
Heat Shield Geometry	70° cone	70° cone	70° cone	70° cone	70° cone	70° cone	70° cone
Heat Shield TPS	SLA-561	SLA-561	SLA-561	SLA-561	SLA-561	SLA-561	PICA
Heat Shield Diameter (m)	3.5	3.5	2.65	2.65	2.65	2.65	4.6
Peak heating rate (W/cm^2)	26	26	100	44	44	58	155
DGB Parachute Diameter (m)	16	16	12.5	14	14	11.5	21.5
Parachute Deployment Mach Number	1.1	1.1	1.57	1.77	1.77	1.6	2
Parachute Deployment Dynamic Pressure (Pa)	350	350	585	725	750	420	750
Landing Site Elevation (MOLA km)	−3.5	−3.5	−2.5	−1.9	−1.4	−3.5	< 1.0
Hypersonic AOA (deg)	−11	0	0	0	0	0	−16
Hypersonic L/D	0.18	0.18	0	0	0	0	0.24
Guided Entry	No	No	No	No	No	No	Yes
Entry Attitude Control	3-Axis RCS	3-Axis RCS	Spin Stabilized	Spin Stabilized	Spin Stabilized	3-Axis RCS	3-Axis RCS
3- σ Landed Ellipse (km)	280×100	280×100	200×100	80×12	80×12	100×21	20×10

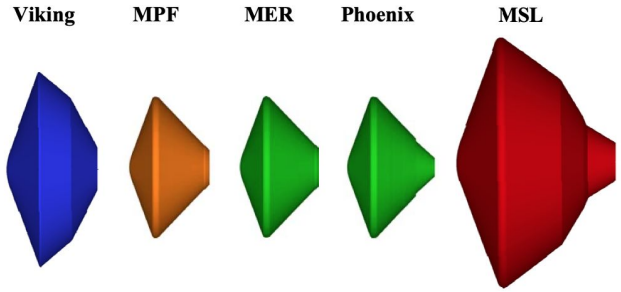

P. Subrahmanyam, D. Rasky, “Entry, Descent, and Landing technological barriers and crewed MARS vehicle performance analysis” Progress in Aerospace Sciences 91 (2017) 1–26, http://dx.doi.org/10.1016/j.paerosci.2016.12.005

- MSL and recently Mars2020 defined a new standard: max. mass and introduced guided entry (bank angle control) to reduce landing position dispersion

Descent phase

Single/double parachute deployment at supersonic or subsonic speed

- Venus/Ice Giants missions could use traditional subsonic parachutes
- For Mars supersonic parachutes are needed; Viking heritage DGB parachute qualified for deployment below Mach 2.1
- Viking legacy includes limitation on system mass, and it is difficult to extrapolate parachute parameters outside qualification ranges

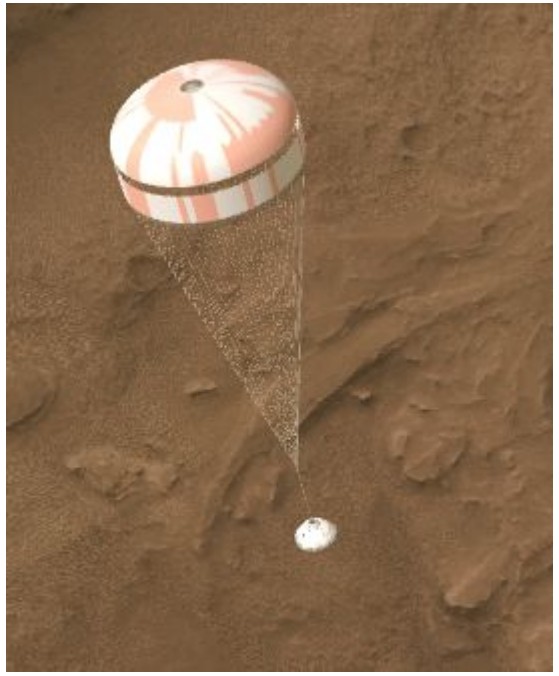

Parameter	Viking	MPF	MER	Phoenix	MSL
Parachute Diameter (m)	16.15	12.4	15.09	11.5	19.7
Mach 24 L/D	0.18	0	0	0	0.24
Landing Site Altitude (km)	-3.5	-1.5	-1.3	-3.5	+1.0

Table 2 – Previous Parachute Deployment Experience

Flight/Test	Mach No.	Dyn. Press. (Pa)	Parachute Diam. (m)
Viking BLDT AV-1*	2.18	699	16.15
Viking BLDT AV-4*	2.13	522	16.15
NASA-TM-X-1575	1.91	555	12.19
NASA-TM-X-1499	1.59	555	19.72
Viking Lander 1	1.04	316	16.15
Viking Lander 2	1.07	330	16.15
MPF	1.71	588	12.40
MER A	1.78	729	15.09
MER B	1.86	763	15.09
MSL	2.05	570	19.70

*NASA-CR-112288

Front shield separation and powered descent

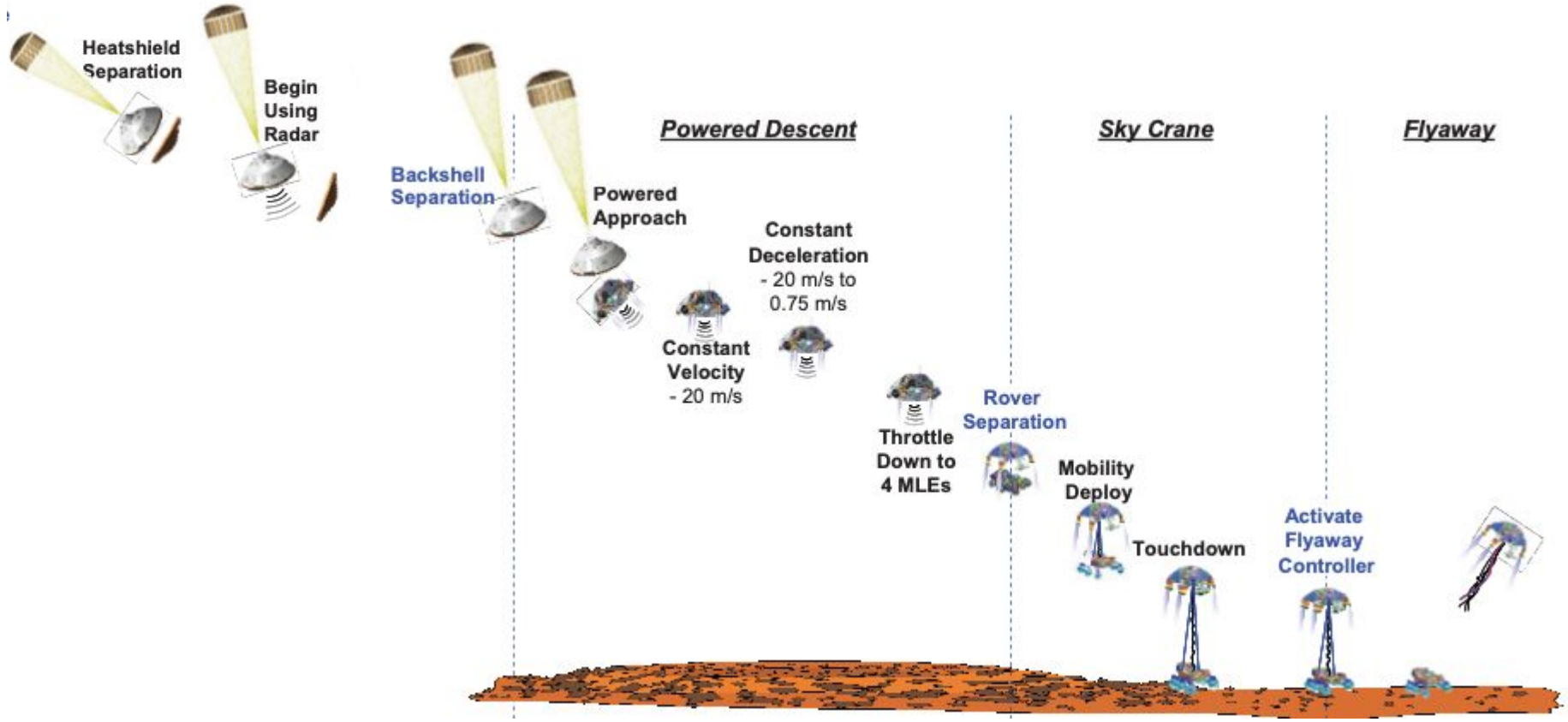

P.D. Burkhart et.al., "Mars Science Laboratory Entry, Descent, and Landing System Overview", IEEE Aerospace Conference Proceedings April 2008

- Retrieve atmospheric parameters during powered descent is difficult/not effective because of low speed and the action of GNC system

On-board Sensors

Upper atmosphere (hypersonic/supersonic phase)

Accelerometers: used to sense deceleration profile and retrieve atmospheric density/pressure/temperature

Front shield radiometer: measure the heat flux during the entry, mainly for engineering purposes

Front shield erosion gauges: measure the ablation of the front shield, for engineering purposes

Lower atmosphere (subsonic phase)

Accelerometers: mainly to identify winds and atmospheric turbulence
(computation of density requires several assumptions while low speed corresponds to high uncertainties)

Temperature: using platinum resistance thermometer (Pioneer/Venus/Huygens)

Pressure: using diaphragm sensors (installed inside the probe to reduce temperature issues with a pipe)

Radiometers and spectrometers: measure the visible and IR heat fluxes () or the entire spectrum of light

Nephelometer: used to characterize clouds/haze

Humidity and chemically-specific sensors: solid state sensors capacitors with moisture-sensitive polymer as the dielectric

Relaxation probes: sensing of electrical conductivity (limited by the effects of the airflow)

Microphones and sonars: to determine the speed of sound or as an anemometer

Planetary Probes
Entry and Descent Science

Part 2 - Basic Aerodynamics of Aeroshells and Parachute Systems, Entry and Descent Modelling and Simulation

Alessio Aboudan (alessio.aboudan@unipd.it), Luca Placco, G. Colombatti, F. Ferri and the AMELIA team

- Reentry vehicles (both capsules and space probes) enter the atmosphere with velocities that spans from 3500-7500 m/s.
  This has strong implications with the phenomena that are generated.

Gas Dynamics

- When the velocity of the object that travels throughout the fluid is progressively comparable with the local speed of sound, discontinuities phenomena arise.
- Thermodynamics quantities around the object tend to change rapidly; in this fluid regime, compressibility effects cannot be neglected.

Fundamentals of Compressible Aerodynamics

Causes of the phenomena

- As an aircraft moves through the air, fluid molecules near the aircraft are disturbed and move around the aircraft.
- At higher speeds, some of the energy of the traveling object is transferred to the fluid flow, locally changing the density and the temperature - *aerothermodynamics*.

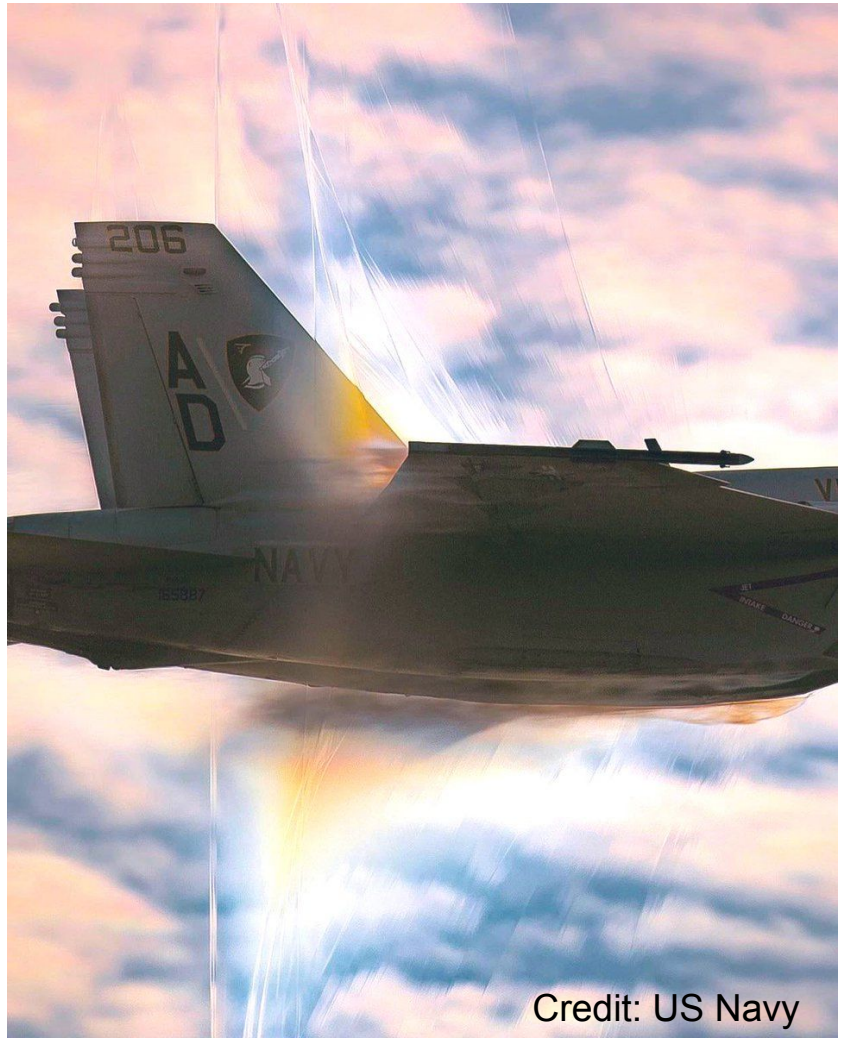

Credit: US Navy

- These quantities change abruptly when particular flow conditions are met.

How do we identify them?

Fundamentals of Compressible Aerodynamics

Parameters of similarity

- When studying a fluid flow, it is convenient to summarize the flow properties by the use of non-dimensional parameters obtained from dimensional analysis; these intrinsically identify the fluid behaviour.

- The parameter Involved are three: **Mach**, **Reynolds** and **Knudsen** numbers.

Name	Definition	Physical significance
Mach number	$M_\infty = \frac{V_\infty}{a_\infty}$	$\frac{V_\infty^2}{a_\infty^2} \equiv \frac{kinetic \cdot energy}{\text{int}\, ernal \cdot energy}$
Reynolds number	$Re_\infty = \frac{\rho_\infty \cdot V_\infty \cdot L_{ref}}{\mu_\infty}$	$\frac{pressure\ forces}{viscous forces}$
Knudsen number	$Kn = \frac{\lambda_\infty}{L_{ref}}$	$\frac{mean\ free\ path}{vehicle\ length}$

- They alter the resulting force on the object and so its aerodynamic response (**coefficients**).

Fundamentals of Compressible Aerodynamics

The role of the geometry on the shock wave

- When the Mach number reaches the value of 1, a shock wave is generated in front of the object, acting as a discontinuity in the flow field.
- The shape and the nature of the shocklayer is associated with the geometry of the object.

↓

- For blunt objects the shock wave at the front detaches. Modeling this condition becomes harder.

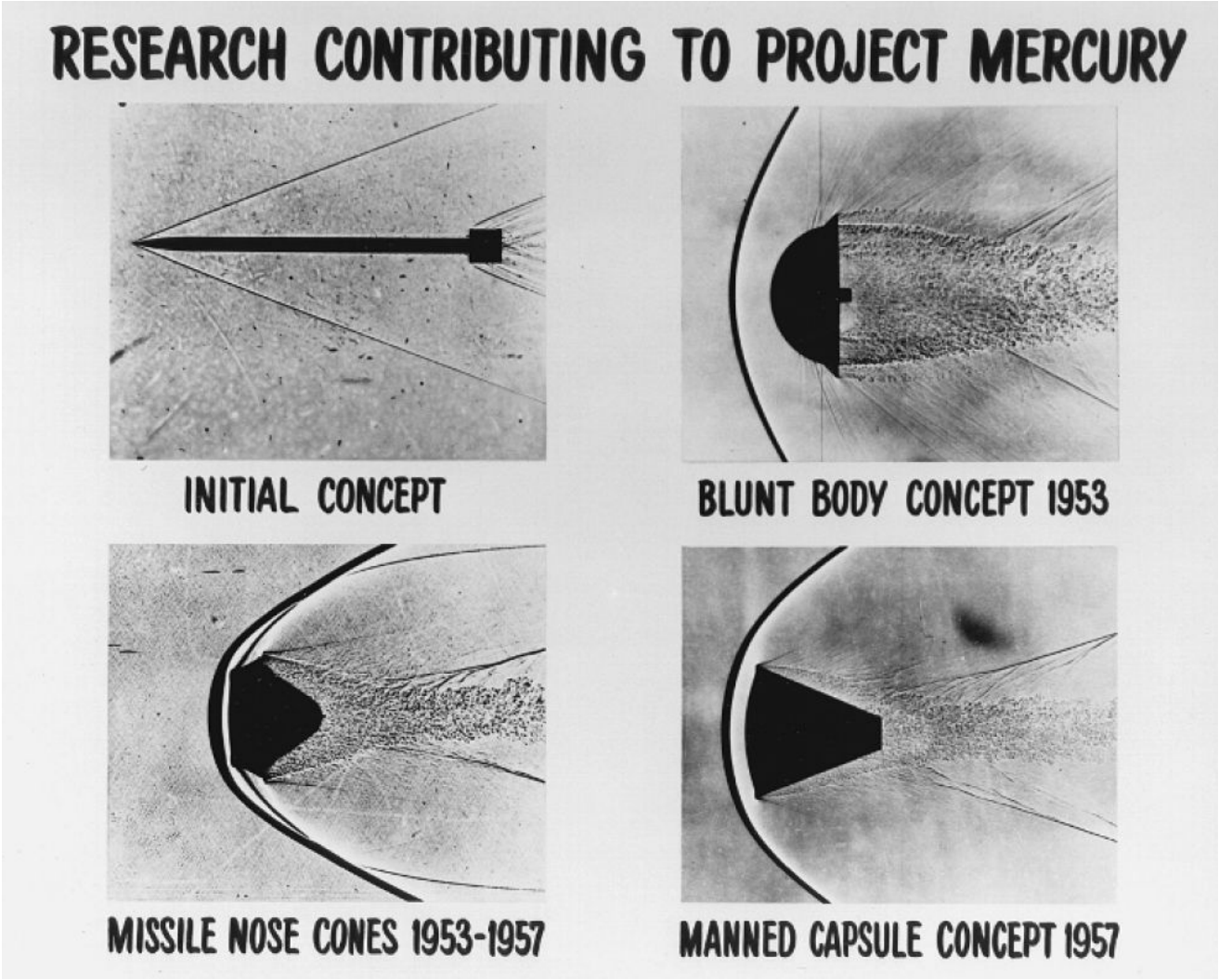

Credit: NASA

Fundamentals of Compressible Aerodynamics

Aerodynamic coefficients and case of study

- In general, aerodynamic coefficients for axisymmetric geometries can be considered as the following:

$$C_{Aw}\left(M_\infty, Re_\infty, Kn_\infty, \bar{\alpha}\right)$$
$$C_{Nw}\left(M_\infty, Re_\infty, Kn_\infty, \bar{\alpha}\right)$$
$$C_{mw}\left(M_\infty, Re_\infty, Kn_\infty, \bar{\alpha}\right)$$

How can we evaluate them properly?

- Reynolds and Knudsen numbers usually are fixed by the flight condition related to the atmosphere.

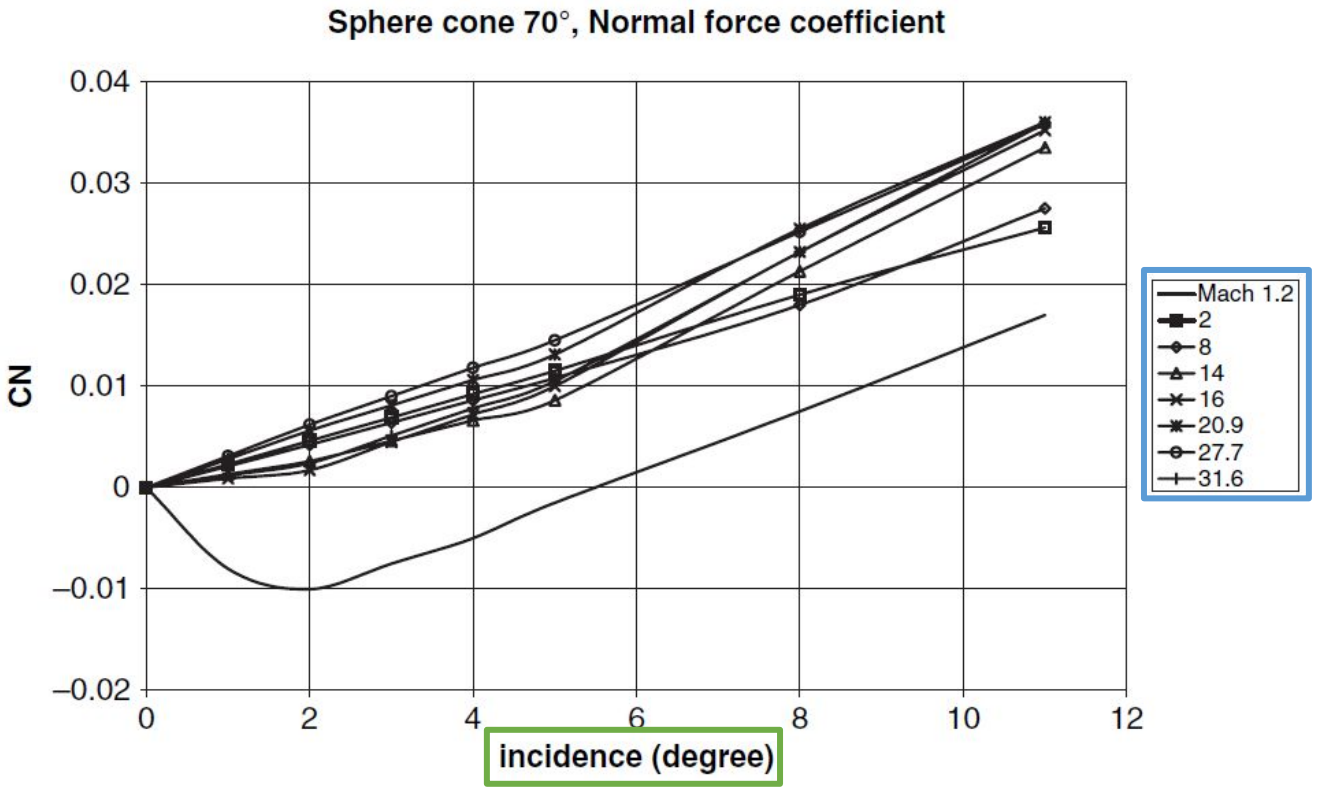

Fundamentals of Compressible Aerodynamics

Role of the Knudsen number

- The Knudsen number characterizes the rarefaction status of the air with respect to dimensions of the vehicle; we can consider three stages during the descent:

1) At very high altitude, Kn >> 1, there are practically no collisions between molecules in the vicinity of the vehicle. We are in **free molecular flow** mode, and each molecule interacts individually with the vehicle wall according to the statistical theory of gases.

2) The intermediate section or **rarefied flow** mode.

3) At low altitudes, when Kn << 1, we are in **continuous flow** mode, governed by classical fluid mechanics theory.

Let's evaluate separately these phase as the altitude decreases.

Fundamentals of Compressible Aerodynamics

Role of the Knudsen number - flow regimes and Reynolds number

Credit: NASA TP2006

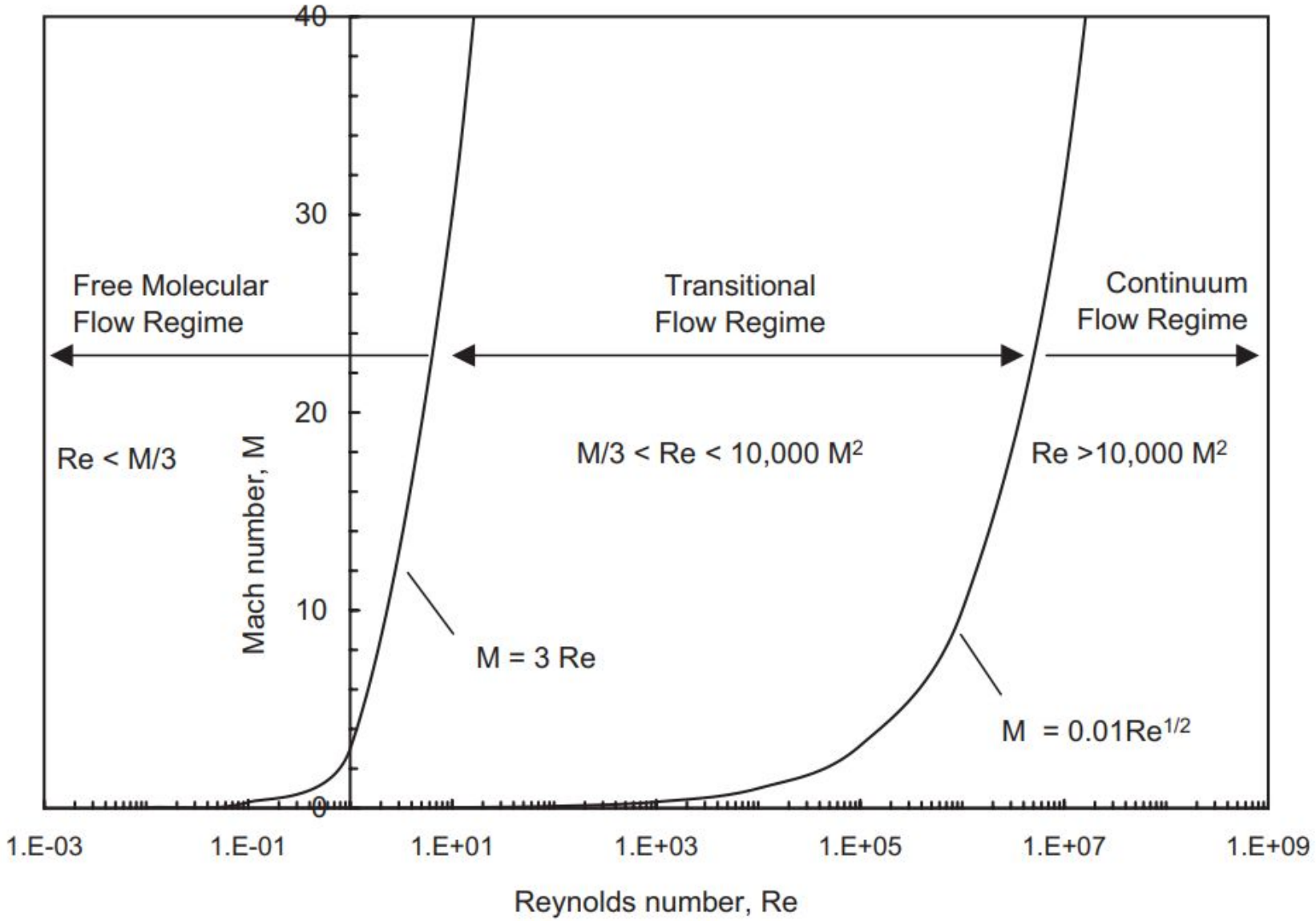

Fundamentals of Compressible Aerodynamics

1. Free molecular flow mode

The effects on the surface of the module are computed by employing the kinetic theory of gases.

- The velocity of every singular incident molecule on a surface is considered different and given by:

$$\vec{v}_R = \vec{V}_R + \vec{\nu}\,(T_\infty)$$

- Particles are reflected on the wall both in an elastic and diffusive way generating pressure and shear stress on the body.

By the integration of these forces on the body we obtain an approximate value of the drag coefficient which only depends on the projected body area in the incidental direction.

$$C_D = 2\frac{S}{S_{ref}}$$

Fundamentals of Compressible Aerodynamics

2. Intermediate rarefied flow mode

This flow represents the transition between free molecular flow and continuous flow; to solve it correctly DSMC is required; bridging functions are then employed.

- Functions are correlated and dependent on Knudsen number, for example:

$$C = C_c + \phi\,(Kn_\infty) \cdot (C_m - C_c)$$

where i.e.

$$\phi\,(Kn_\infty) = \sin^2\left[\pi\left(a_1 + a_2 \log_{10} Kn_\infty\right)\right]$$

or

$$\phi\,(Kn_\infty) = \frac{1}{2}\left[1 + \mathrm{erf}\left(\frac{\sqrt{\pi}}{\Delta Kn} \ln\left\{\frac{Kn_\infty}{Kn_{mi}}\right\}\right)\right]$$

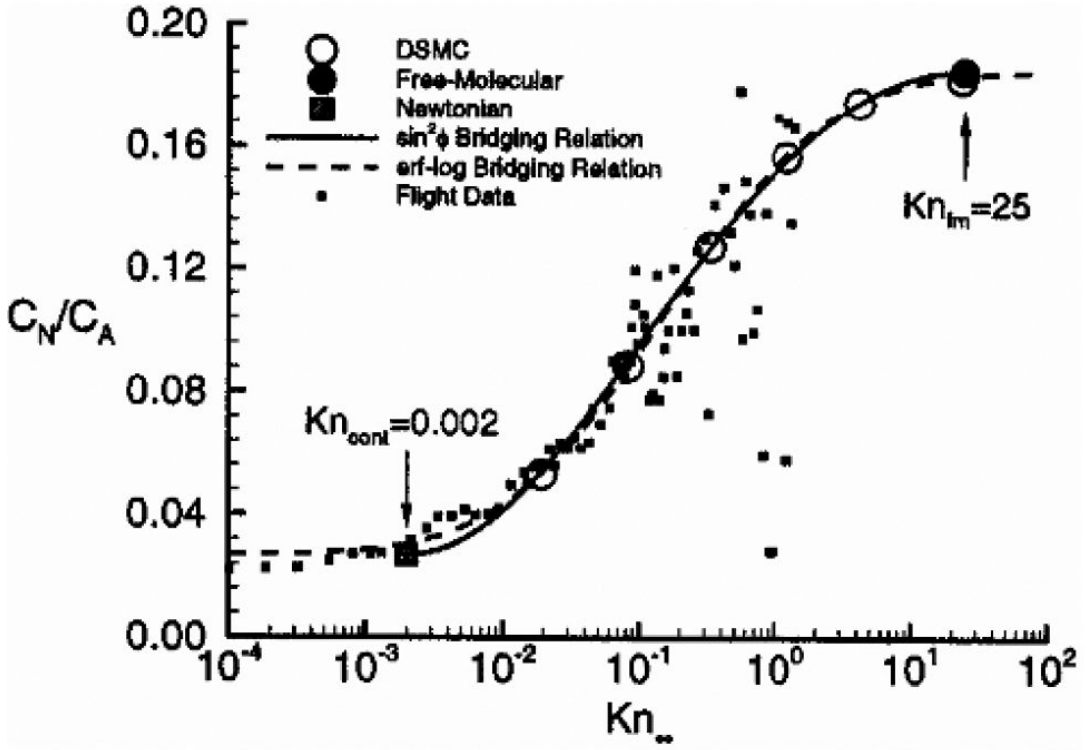

Fundamentals of Compressible Aerodynamics

3. Continuous flow mode - supersonic and hypersonic regimes

need to distinguish between **supersonic** and **hypersonic** regimes;
separation is given by:

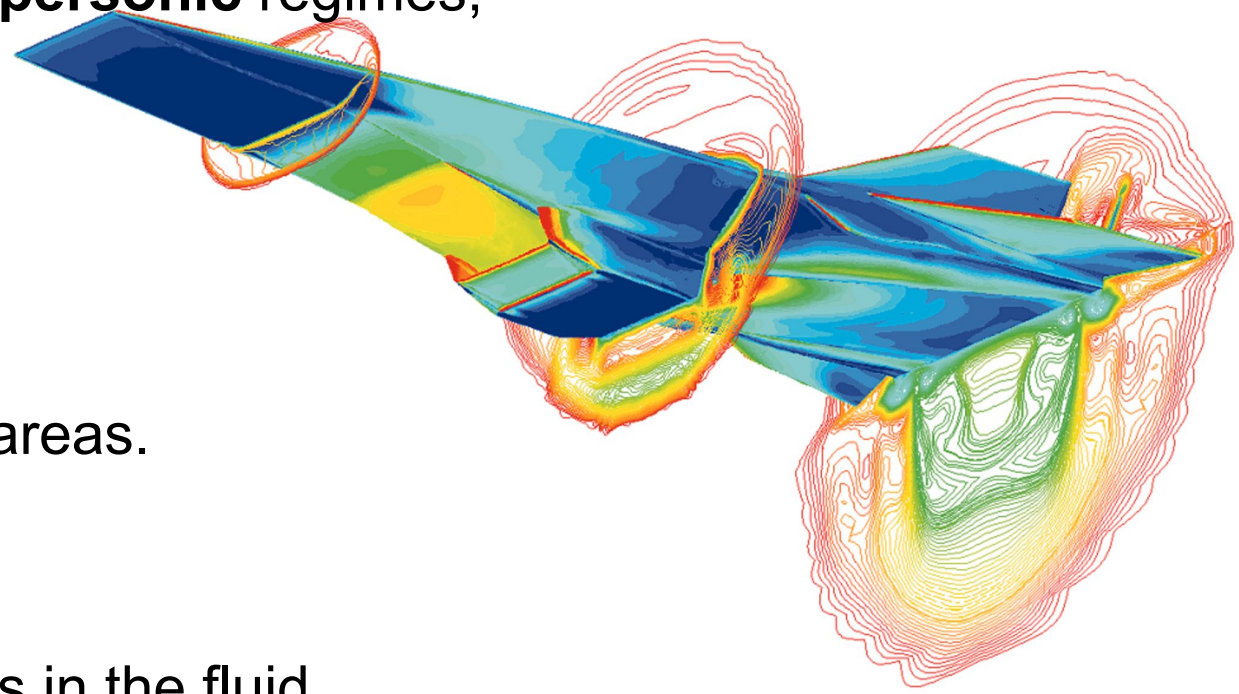

hock wave intensity and volume.

xtension of the vortex and flow recirculation flow areas.

scosity effect on the flow field.

igh temperature causing chemical transformations in the fluid.

rmal separation between the two is fixed at **M = 5**

Dryden Flight Research Center ED97 43968-01
HYPER-X AT MACH 7: This computational fluid dynamic (CFD) image is of the Hyper-X vehicle at the Mach 7 test condition with the engine operating.

- Simple geometry configurations and transonic / supersonic regime can be solved analytically with the use of the **Shock-Expansion Theory**.

$$M_2 = \frac{1}{\sin(\beta-\theta)}\sqrt{\frac{1+\frac{\gamma-1}{2}M_1^2\sin^2\beta}{\gamma M_1^2\sin^2\beta-\frac{\gamma-1}{2}}}.$$

$$\frac{p_2}{p_1} = 1+\frac{2\gamma}{\gamma+1}(M_1^2\sin^2\beta-1)$$

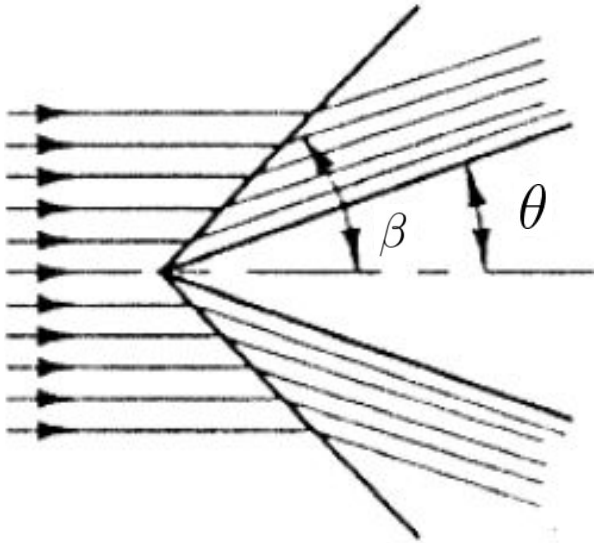

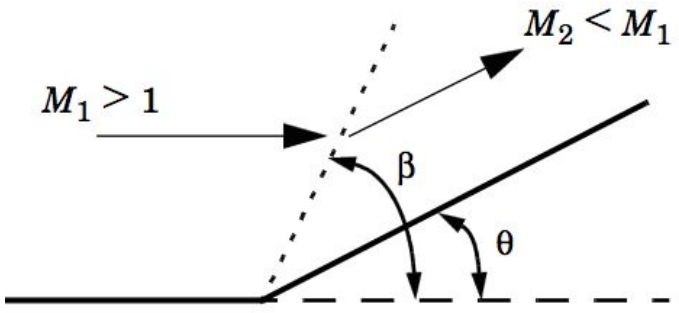

Can we employ it for entry and descent problems?

As Mach rises, discontinuities at the front of the body increase in intensity and decrease in volume. The shock becomes more and more condensed.

Molecular bonds oscillate rapidly, internal vibration
Energy dissipation - Internal energy

Vorticity and flow recirculation

Gas dissociation
Flow ionization

Viscosity of the fluid rises the temperature; flow detaches.

Plasma formation
hypervelocity flow

Fundamentals of Compressible Aerodynamics

3. Analysis of the transition

Credit: NASA TP2006

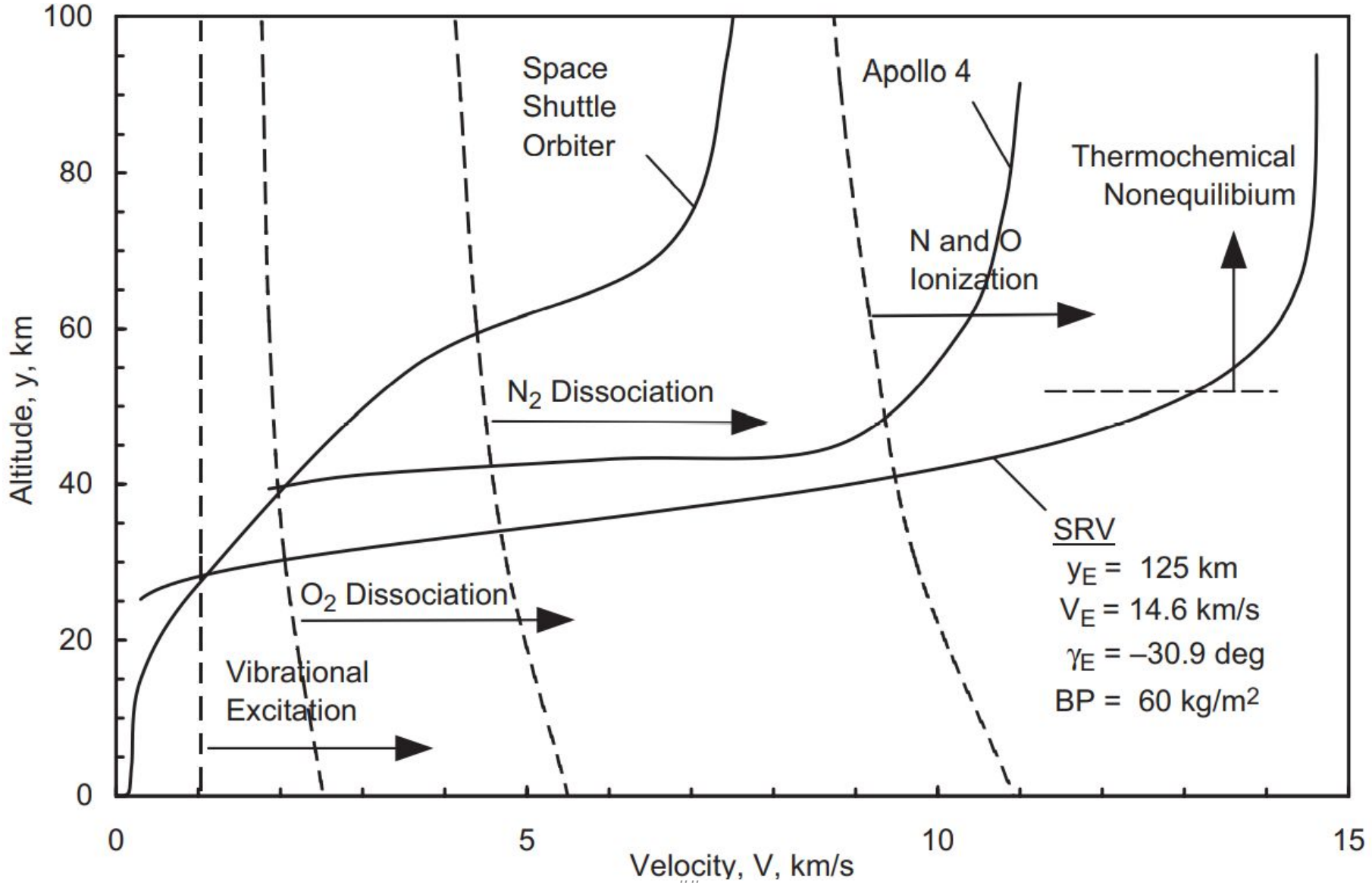

Fundamentals of Compressible Aerodynamics

Shock layer temperatures at different velocities

Credit: NASA TP2006

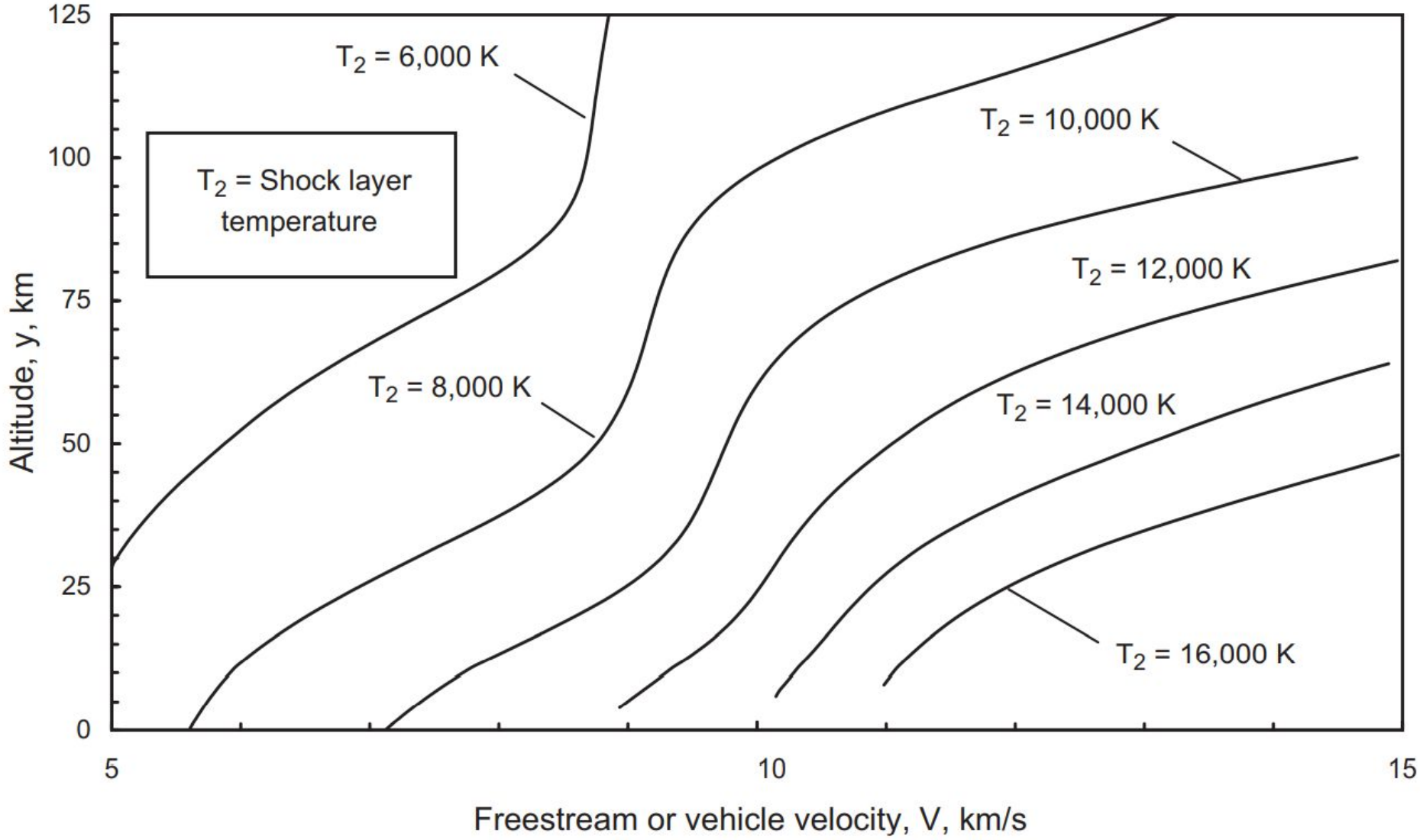

Fundamentals of Compressible Aerodynamics

3. Hypersonic regime

In this regime **Newton Impact Theory** predicts well the pressure distribution along the surface:

$$C_P = 2sin^2\alpha$$

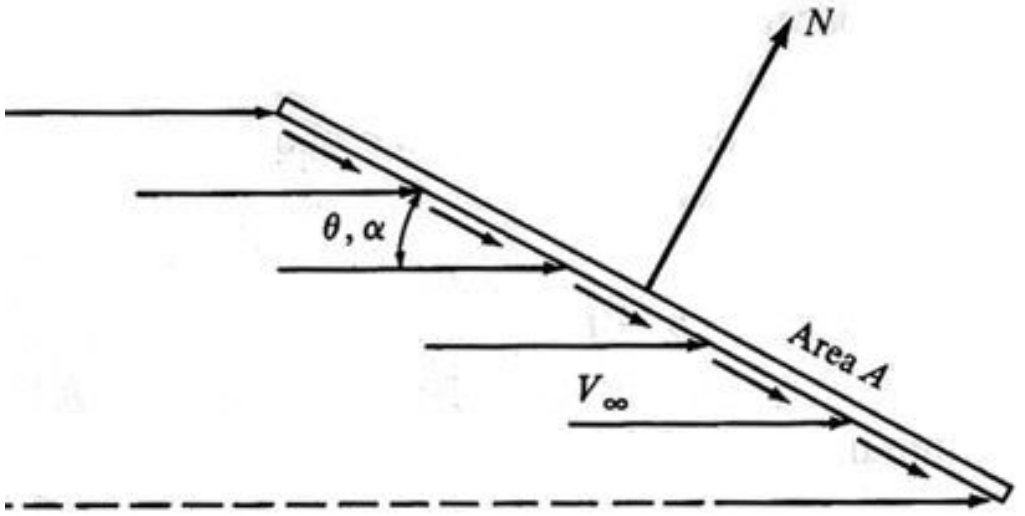

It is considered valid only at a small distance from the wall - instant particles deviation.

- We can obtain the overall effect on a complex geometry by integration of the elementary surface effects in the areas exposed to the fluid. For a convex shape body (cone):

$$C_{Aw} = 2 \cdot \sin^2 \theta_a + \left(1 - 3 \cdot \sin^2 \theta_a\right) \sin^2 \bar{\alpha}$$

$$C_{Nw} = \cos^2 \theta_a \cdot \sin 2\bar{\alpha}$$

Fundamentals of Compressible Aerodynamics

Practical approach for real world applications

- More rounded and complex geometry configurations require the employment of **numerical simulations** or **wind tunnel tests**. Which one do we use?

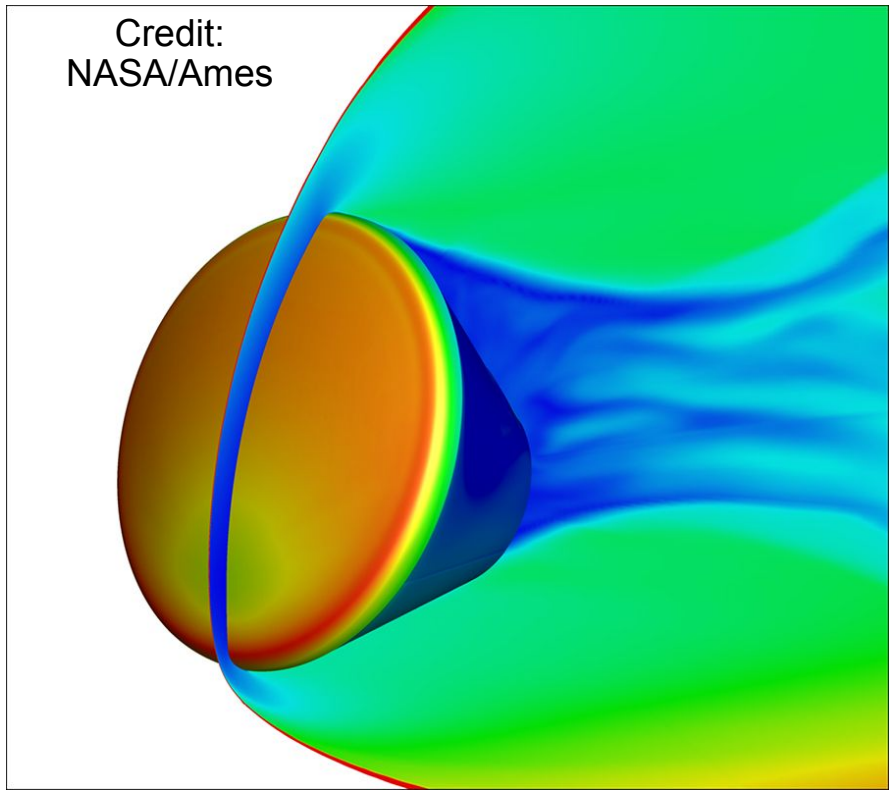

Fundamentals of Compressible Aerodynamics

Numerical simulations or wind tunnels?

Numerical Simulations

PROS:

- Give (theoretically) the best results since they solve the fluid equations.
- Faster to prepare and inexpensive if compared to experimental evaluations.

CONS:

- Limited to the computational power of the machine.
- Difficult to setup and calibrate. Turbulent flows are tough to solve.

Wind Tunnels

PROS:

- Have more authority on the solution; results have higher acceptance.
- Can be employed also for large external flows (buildings, bridges …)

CONS:

- Subjected to setup errors that can lead to faulty results. Ad-hoc corrections are typically needed.
- Expensive to build and to employ.

Neither is better or worse, it depends on the situation.

Aerodynamics of aeroshells and capsules

Properties and characteristic structures - what to expect?

- Shock wave is detached and forms a **bow shape**.
- Shock waves gets closer to the body as the capsule accelerates towards hypersonic regimes.
- In front of the capsule the shock is normal respect to the fluid flow.
- **Flow separates** from the side walls of the capsule and recirculates at the back: **wake generation** and suction effect.
- Wake flow accelerates gradually as it travels through the trailing shock.

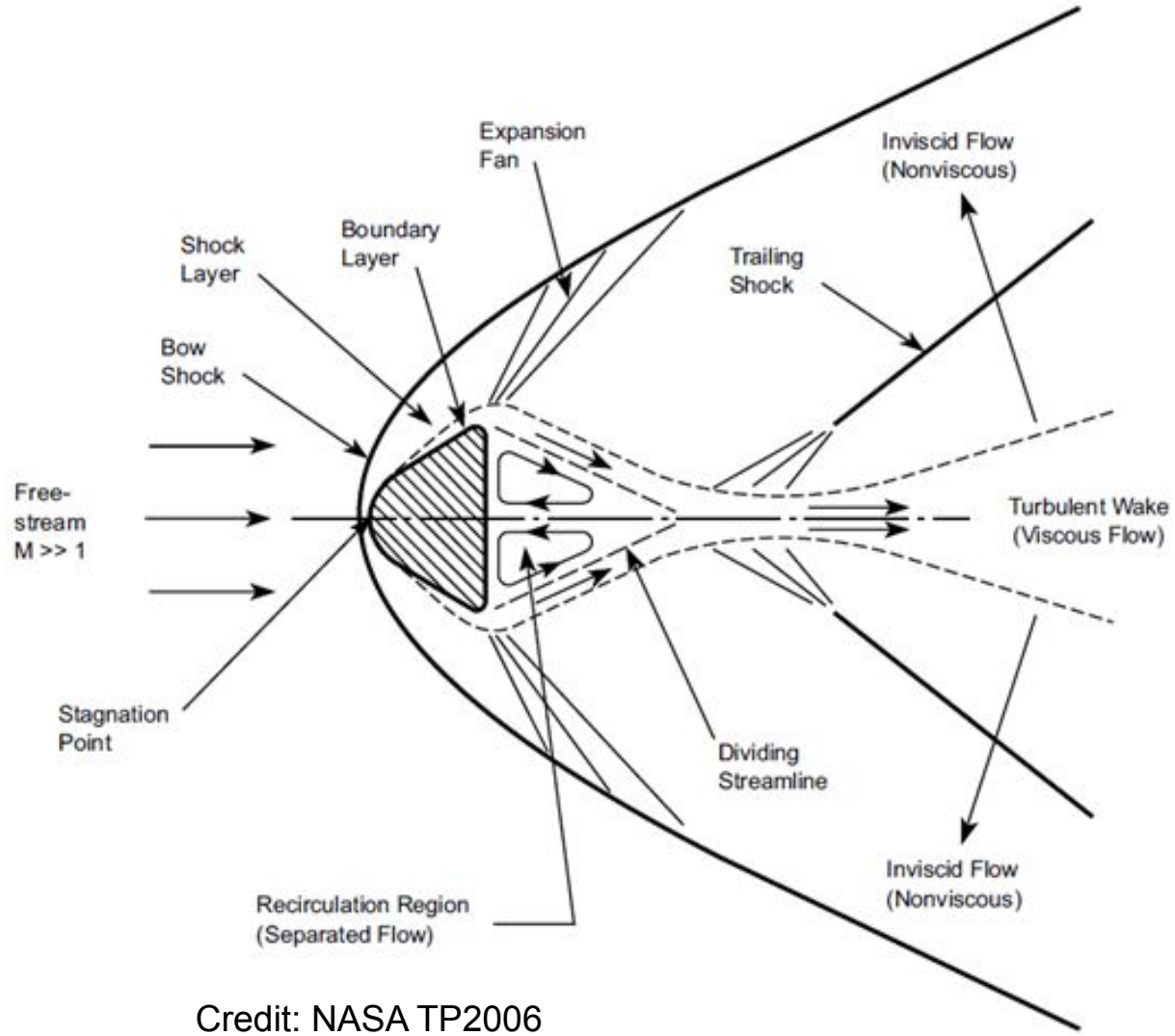

Credit: NASA TP2006

Aerodynamics of aeroshells and capsules

Video of a complete simulation - detail

- In collaboration with M. Bernardini, F. Picano and M. Cogo; performed on the supercomputer Marconi100 at CINECA.

https://www.youtube.com/watch?v=54XC59j-HyE

Aerodynamics of aeroshells and capsules

Numerical simulation - an example

- Computational fluid dynamics allow us to solve the fluid flow iteratively in time and space by discretizing the computational domain.

$$Ma = 2$$

$$Re = 10^6$$

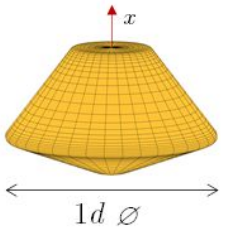

Mesh size:
2048 x 672 x 672
924 844 032 nodes

(40 GB of measurements at every instant!)

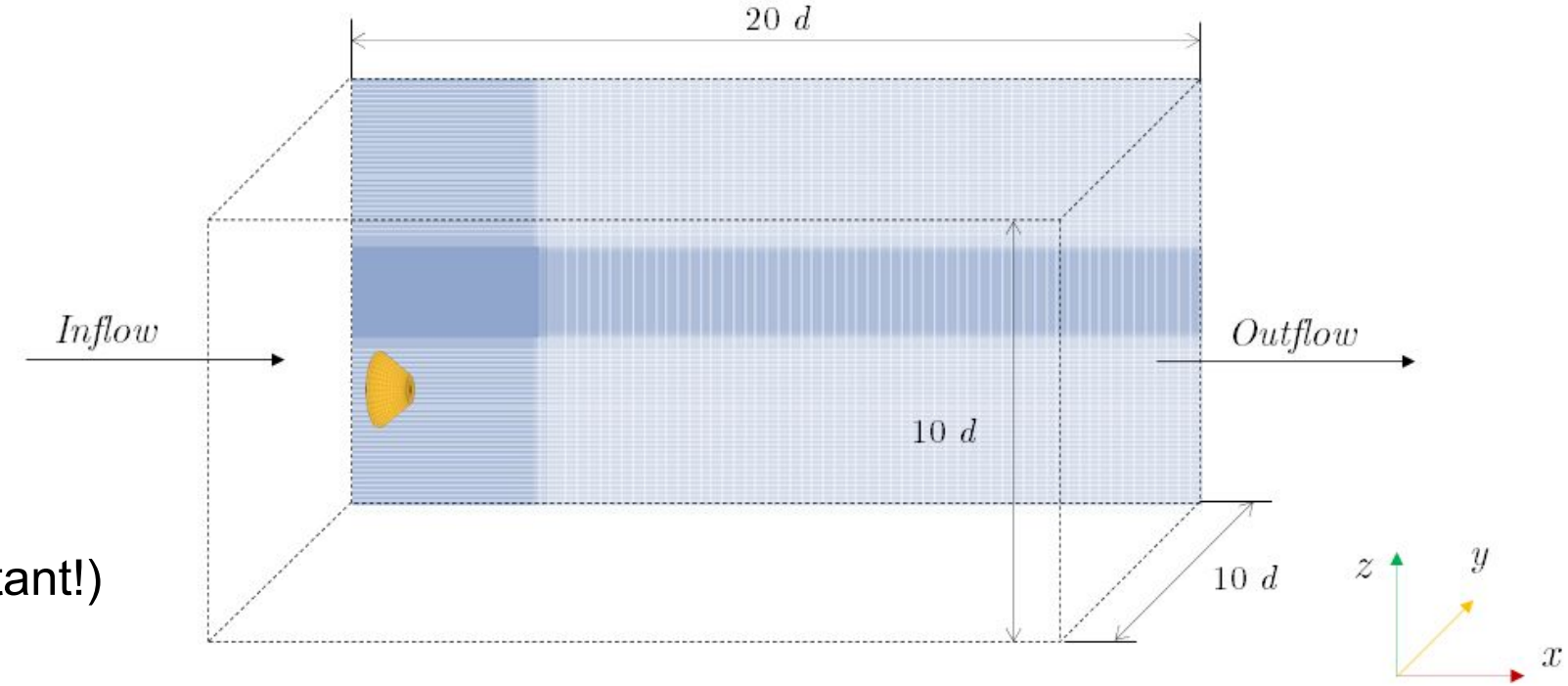

- In collaboration with M. Bernardini, F. Picano and M. Cogo; performed on the supercomputer Marconi100 at CINECA.

Aerodynamics of aeroshells and capsules

Analysis of the major properties and aspects - average fields

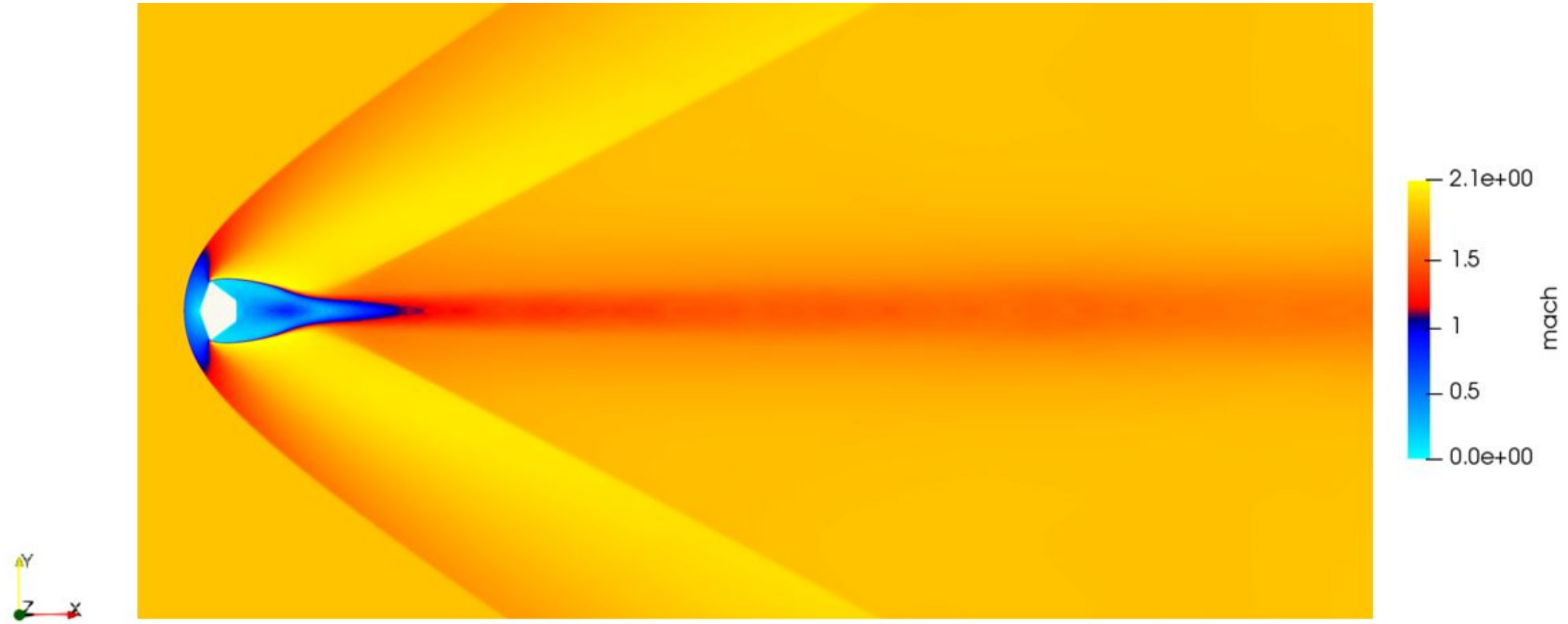

- In collaboration with M. Bernardini, F. Picano and M. Cogo; performed on the supercomputer Marconi100 at CINECA.

Aerodynamics of aeroshells and capsules

Analysis of the major properties and aspects - average fields

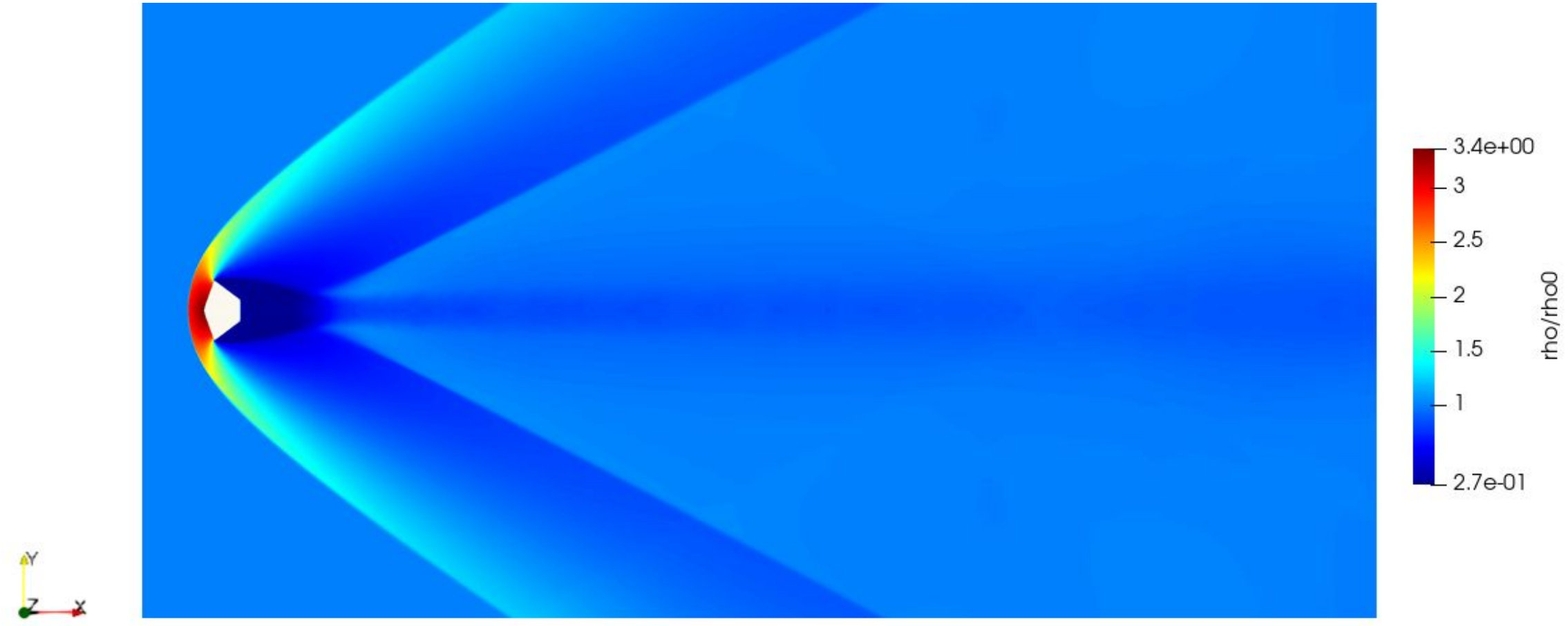

- In collaboration with M. Bernardini, F. Picano and M. Cogo; performed on the supercomputer Marconi100 at CINECA.

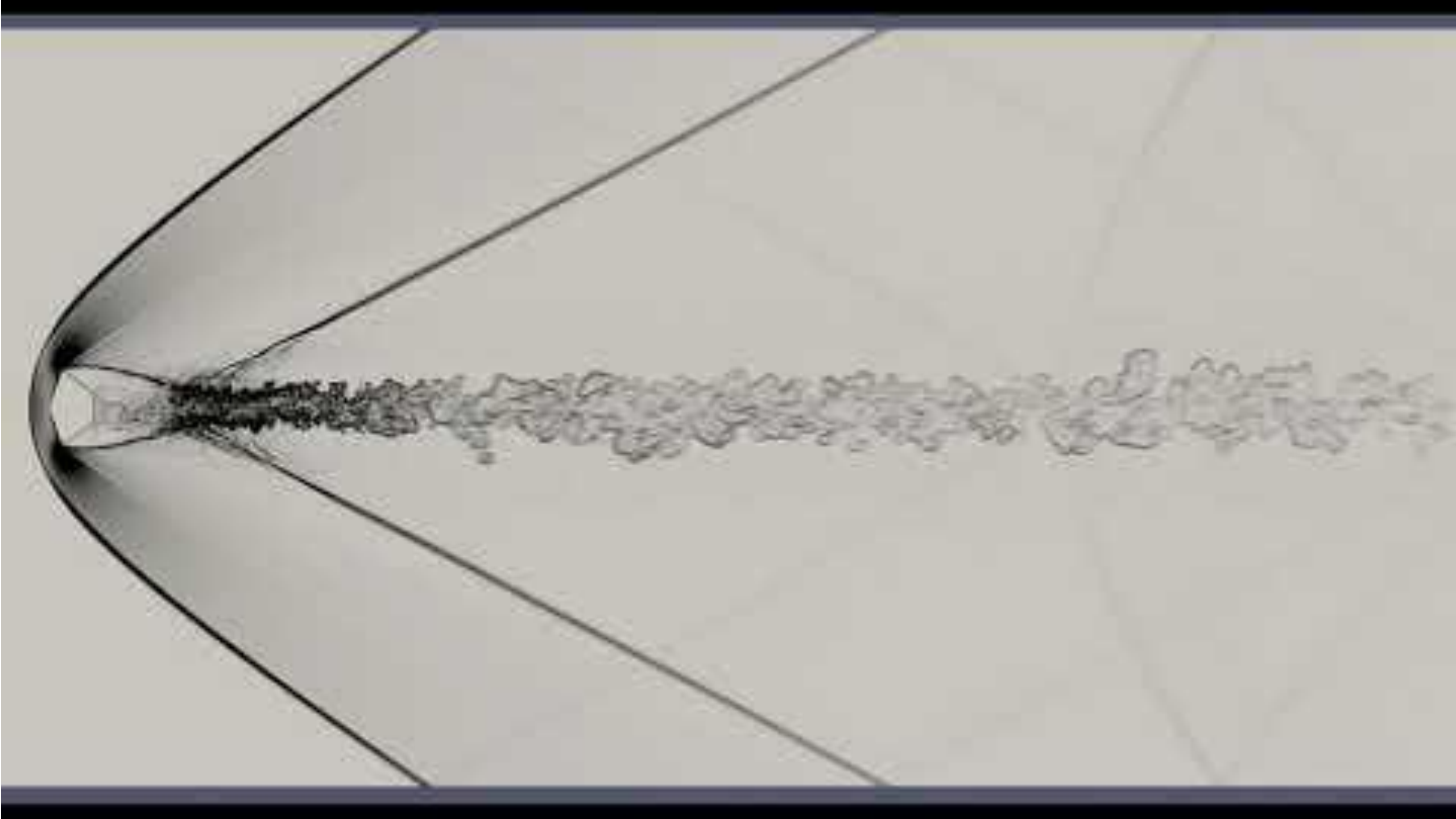

Aerodynamics of aeroshells and capsules

Wake flow behaviour and properties

- Essential to evaluate design choices associated to parachute deployment:

Credit: J. Campbell

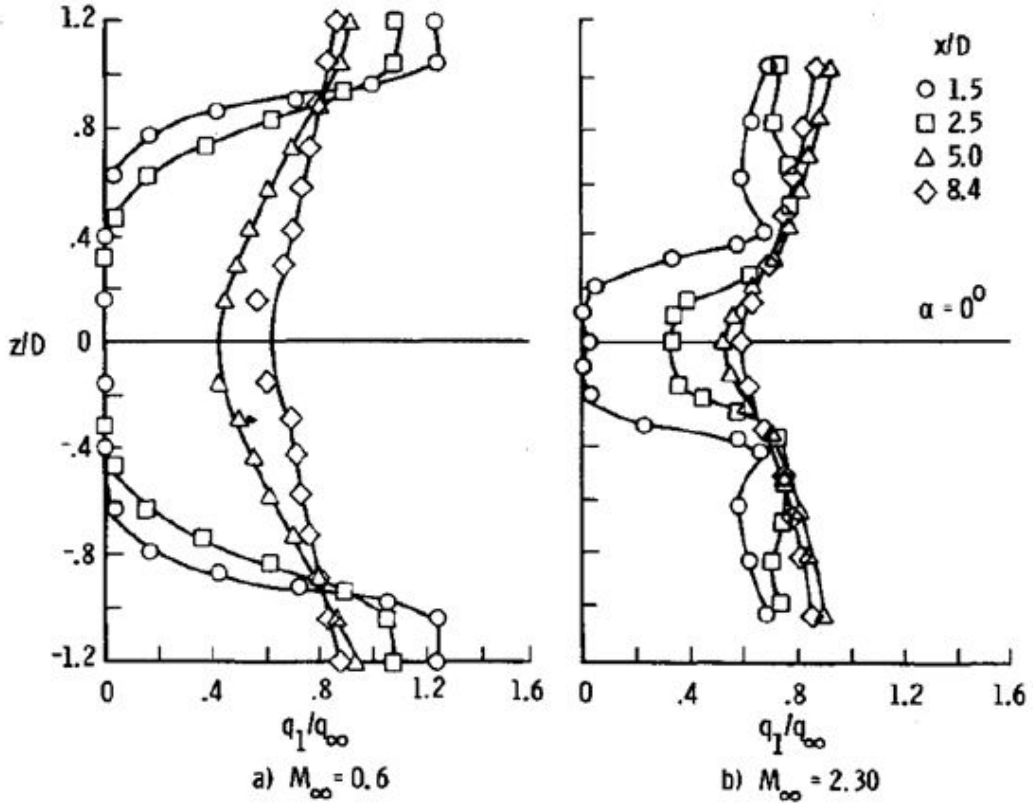

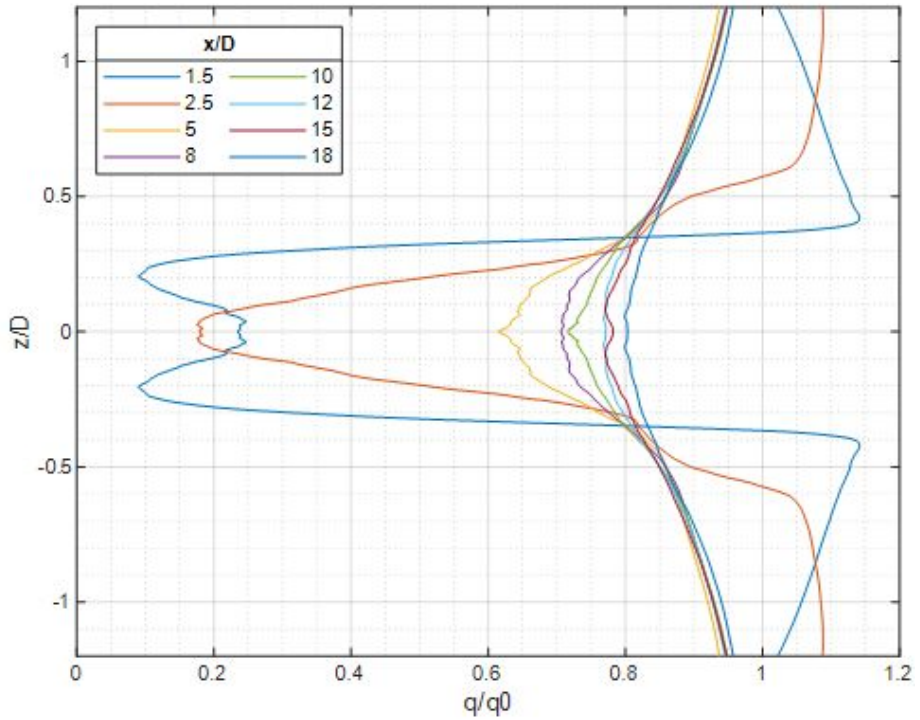

How parachute design and position is influenced by the re-entry configuration?

Parachute system design and modeling

Purpose of aerodynamic deceleration

They are one of the possible solution for slowing down the capsule to a safe landing.

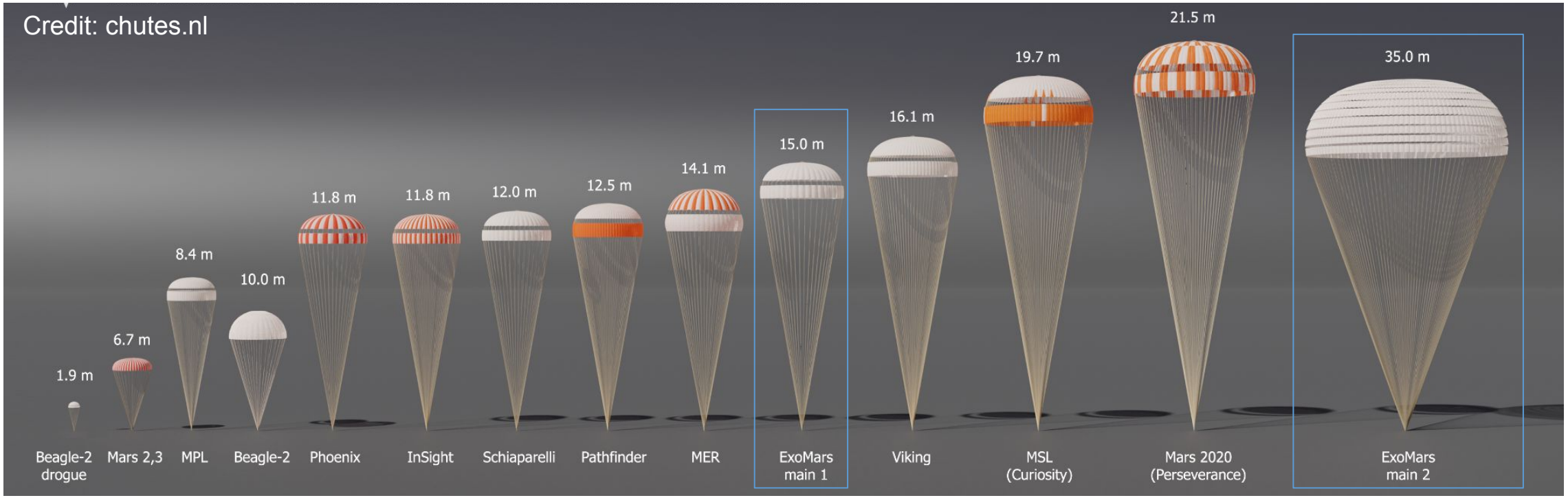

Design procedures are strongly based on empirical and legacy evaluations.

Parachute system design and modeling

Purpose of aerodynamic deceleration

- Given the complex shape, the design process of parachute systems employs empirical evaluations.

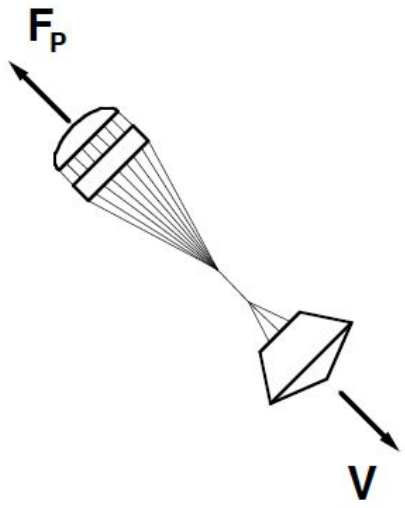

$$F_P = qC_{D0}S_0$$

Let's evaluate separately their role and dependance.

Credit: E. Knacke

Type	Plan	Profile	Shape $\frac{D_c}{D_o}$	Shape $\frac{D_p}{D_o}$	Coef. C_{D_o} Range	Load Factor C_X (Inf. Mass)	Average Angle of Oscillation	General Application
Flat Ribbon	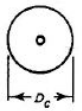		1.00	.67	.45 to .50	~1.05	0° to ±3°	Drogue, Descent, Deceleration
Conical Ribbon	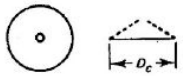		.95 to .97	.70	.50 to .55	~1.05	0° to ±3°	Descent, Deceleration
Conical Ribbon (Varied Porosity)	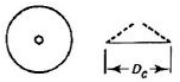		.97	.70	.55 to .65	1.05 to 1.30	0° to ±3°	Drogue, Descent, Deceleration
Ribbon (Hemisflo)	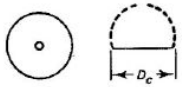		.62	.62	.30* to .46	1.00 to 1.30	±2°	Supersonic Drogue
Ringslot	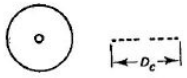		1.00	.67 to .70	.56 to .65	~1.05	0° to ±5°	Extraction, Deceleration
Ringsail			1.16	.69	.75 to .90	~1.10	±5° to ±10°	Descent
Disc-Gap-Band			.73	.65	.52 to .58	~1.30	±10° to ±15°	Descent

Parachute system design and modeling

Nominal drag coefficient for parachute

- It is strongly dependent on the Mach coefficient and the porosity of the parachute cloth.

Credit: J. Cruz

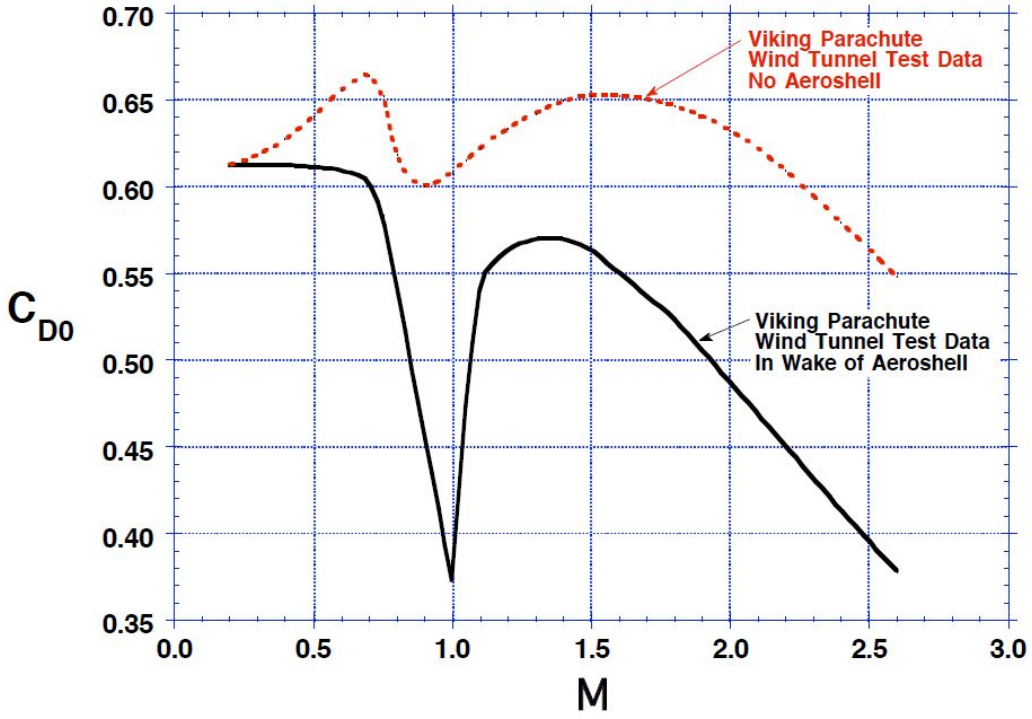

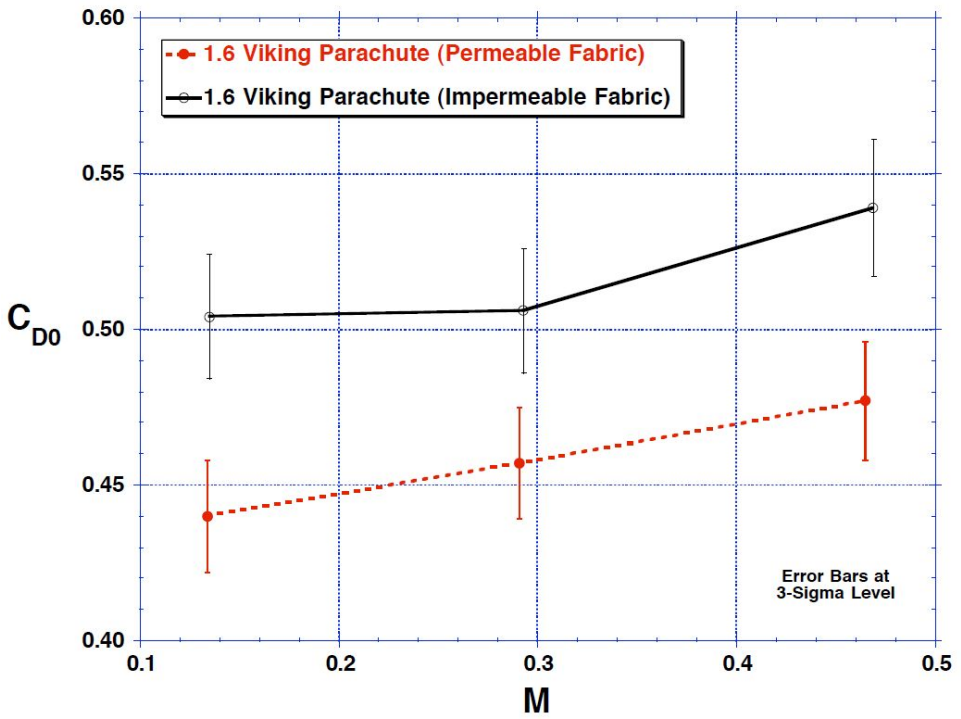

Also geometric porosity (vented area over total area) presents the same behaviour.

Parachute system design and modeling

Nominal drag coefficient for parachute

Other design choices are associated with the different geometry parameters due to wake effects:

- Increasing suspension line increases CD0
- Increasing trailing distance increases CD0
- Reducing the capsule diameter over trailing length increases CD0

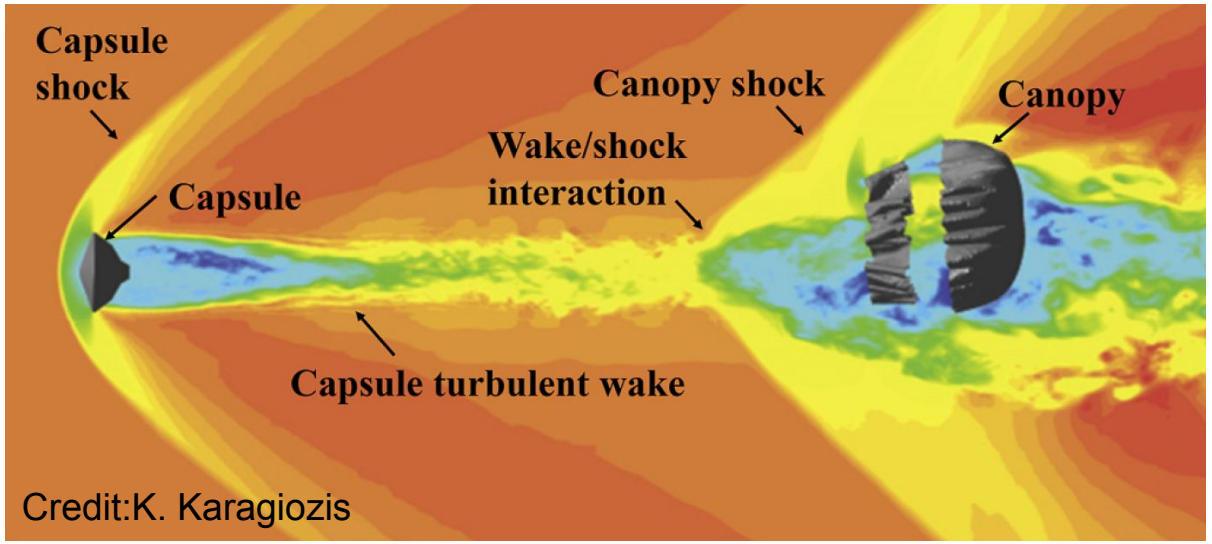

Credit:K. Karagiozis

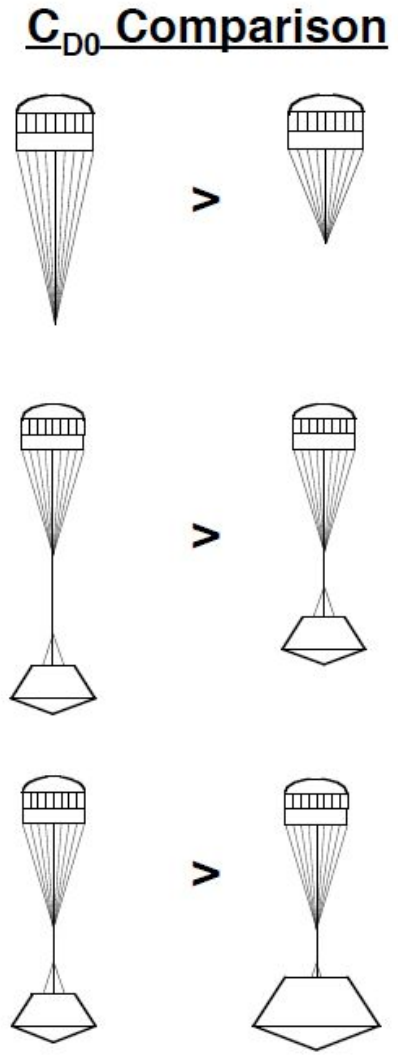

Parachute system design and modeling

Terminal descent model

A simple model can be proposed in order to evaluate the terminal descent condition and determine the sizing of the system:

$$F_P + F_{EV} = q(C_{D0}S_0 + C_{EV}S_{EV})$$

$$q = \rho V^2/2$$

$$F_P + F_{EV} = mg$$

We can determine the parachute dimension knowing CD0 and imposing an acceptable terminal velocity:

$$S_0 = (mg/q - C_{EV}S_{EV})/C_{D0}$$

Drag force is given however by the resultant of the forces on the parachute.

Parachute system design and modeling

Static coefficient model

The resultant force generated by the parachute also depends on its orientation.

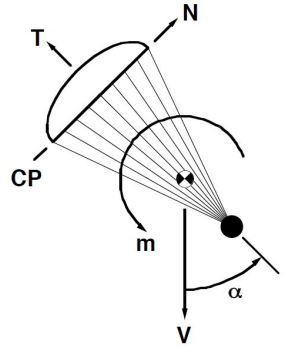

- Tangential direction T is dominant over the normal N

$$C_{D0} = \sqrt{(C_T^2 + C_N^2)}$$

Credit: J. Cruz

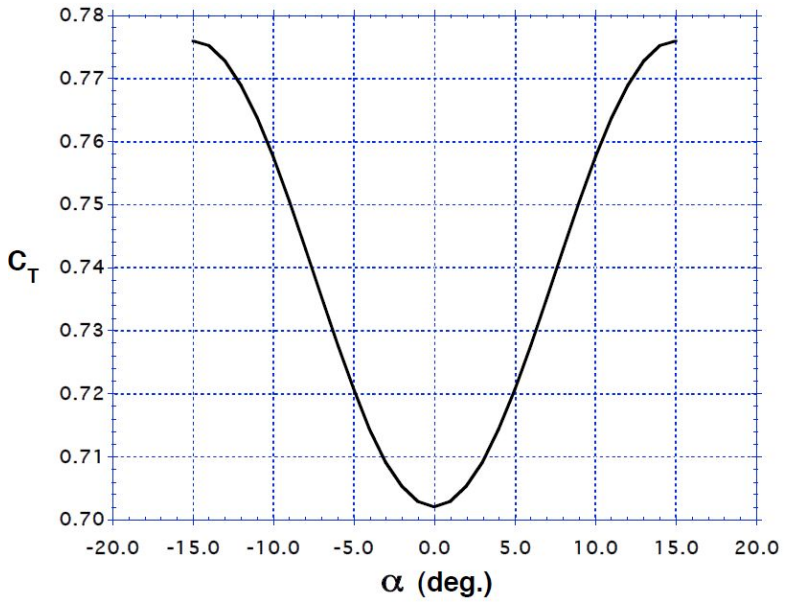

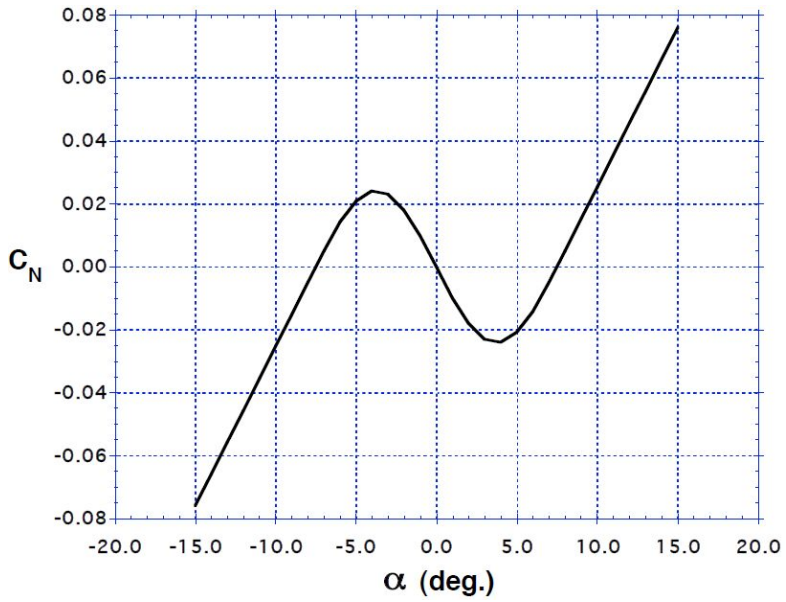

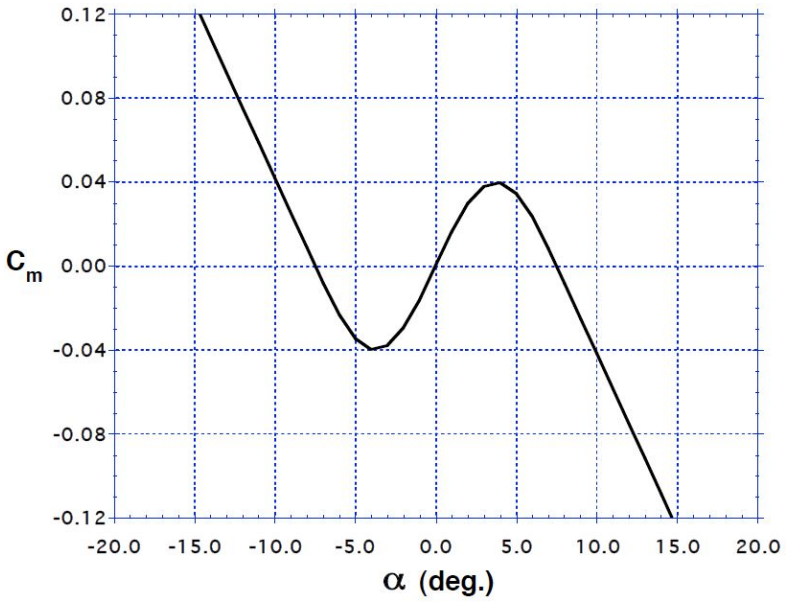

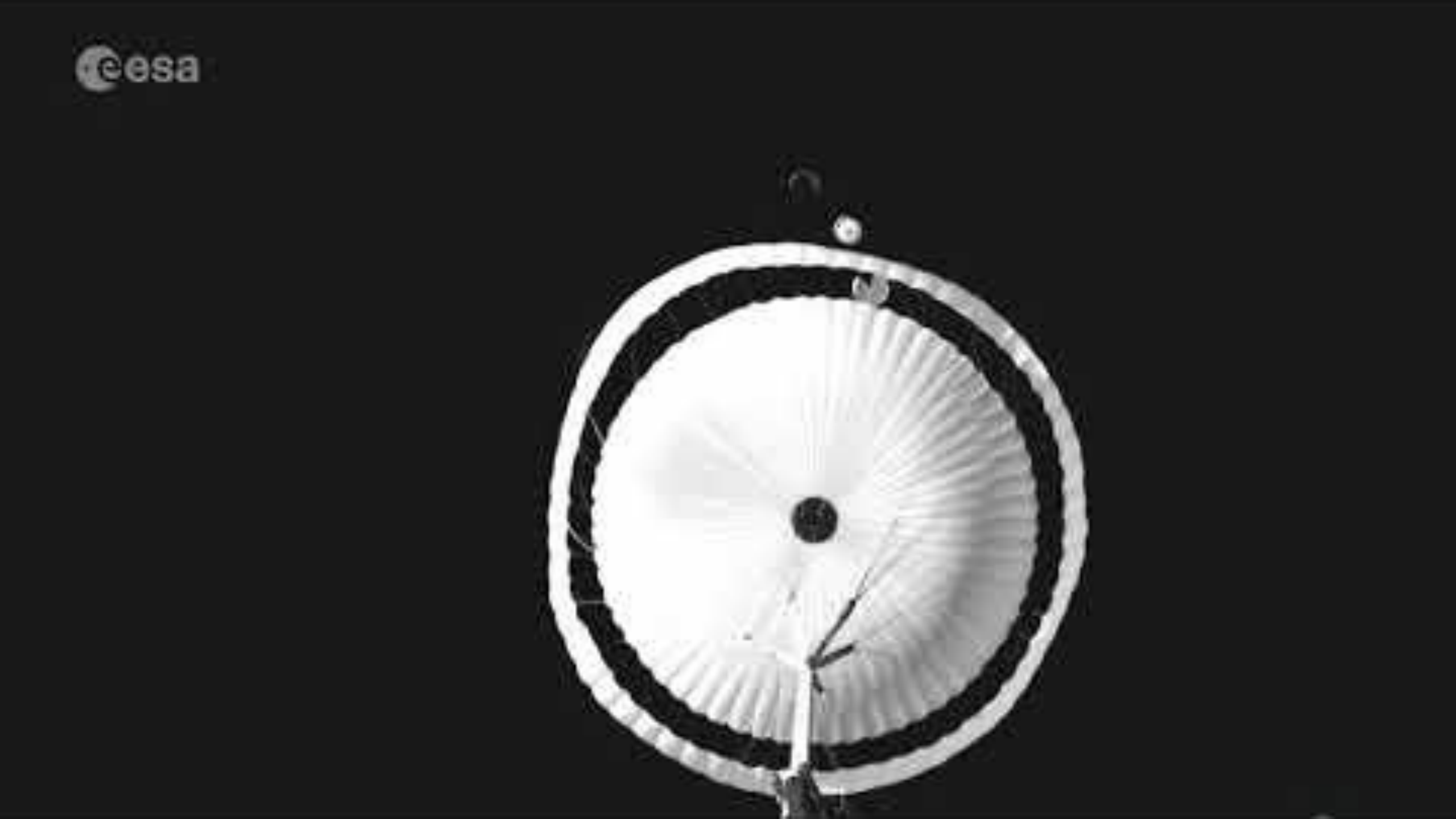
esa

Parachute system design and modeling

Deployment and inflation modeling

- Evaluate the **time** from line-stretch to fully open.
- Evaluate how the **drag** gradually increases during this phase.
- Evaluate the **peak load** of the parachute.

The type of inflation can be:

- Finite-mass type
- Infinite-mass type

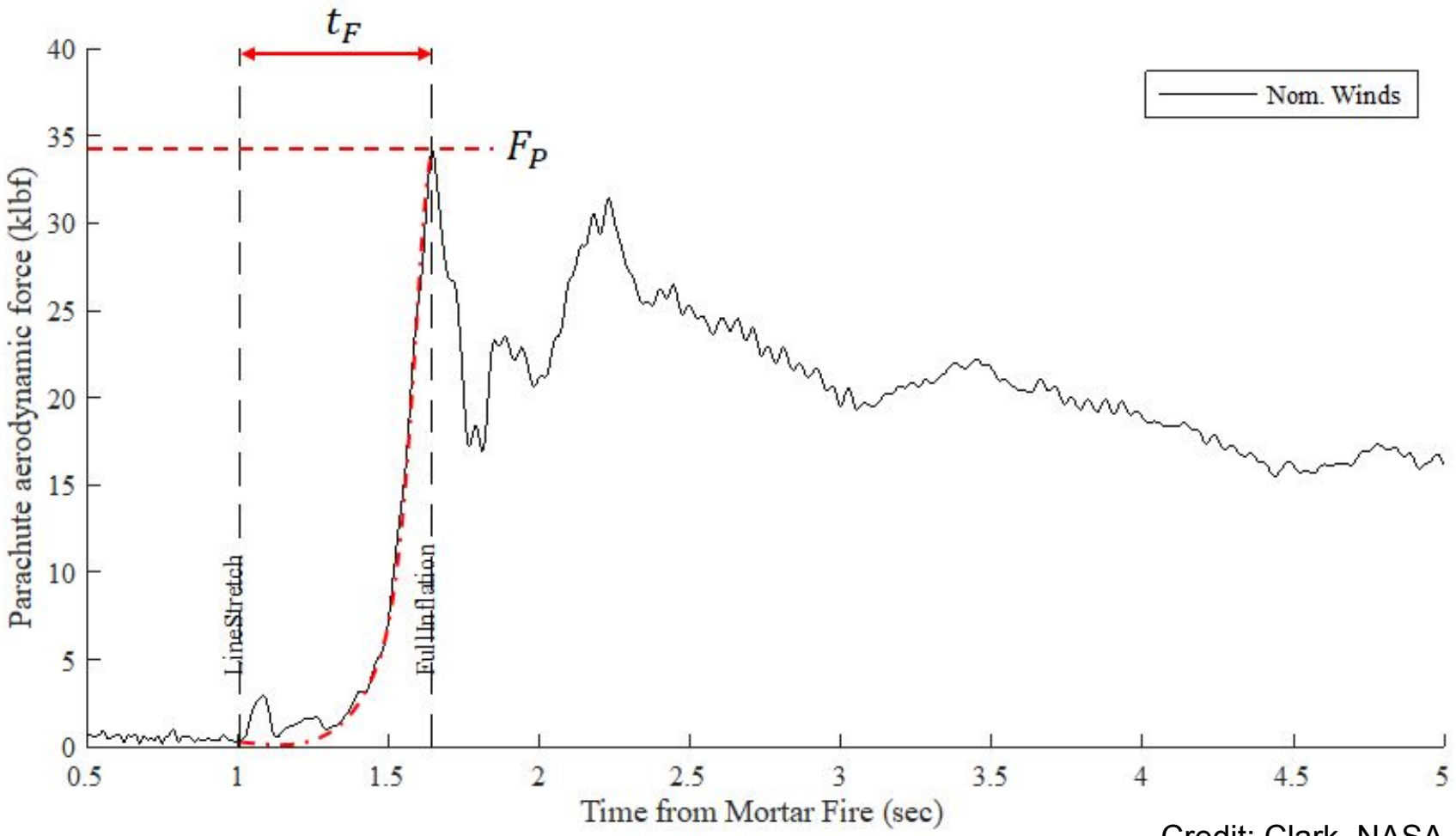

Credit: Clark, NASA

Parachute system design and modeling

Estimate the time of inflation

- Different models exist and are employed for different opening configurations.
- The most basic one is:

$$t_F = n_F D_0 / V_S$$

or

$$t_F = \alpha D_0 / V_S (\rho_c / \rho_\infty)$$

- An accurate estimate of the inflation time is required in order to assess the peak load and the drag profile.

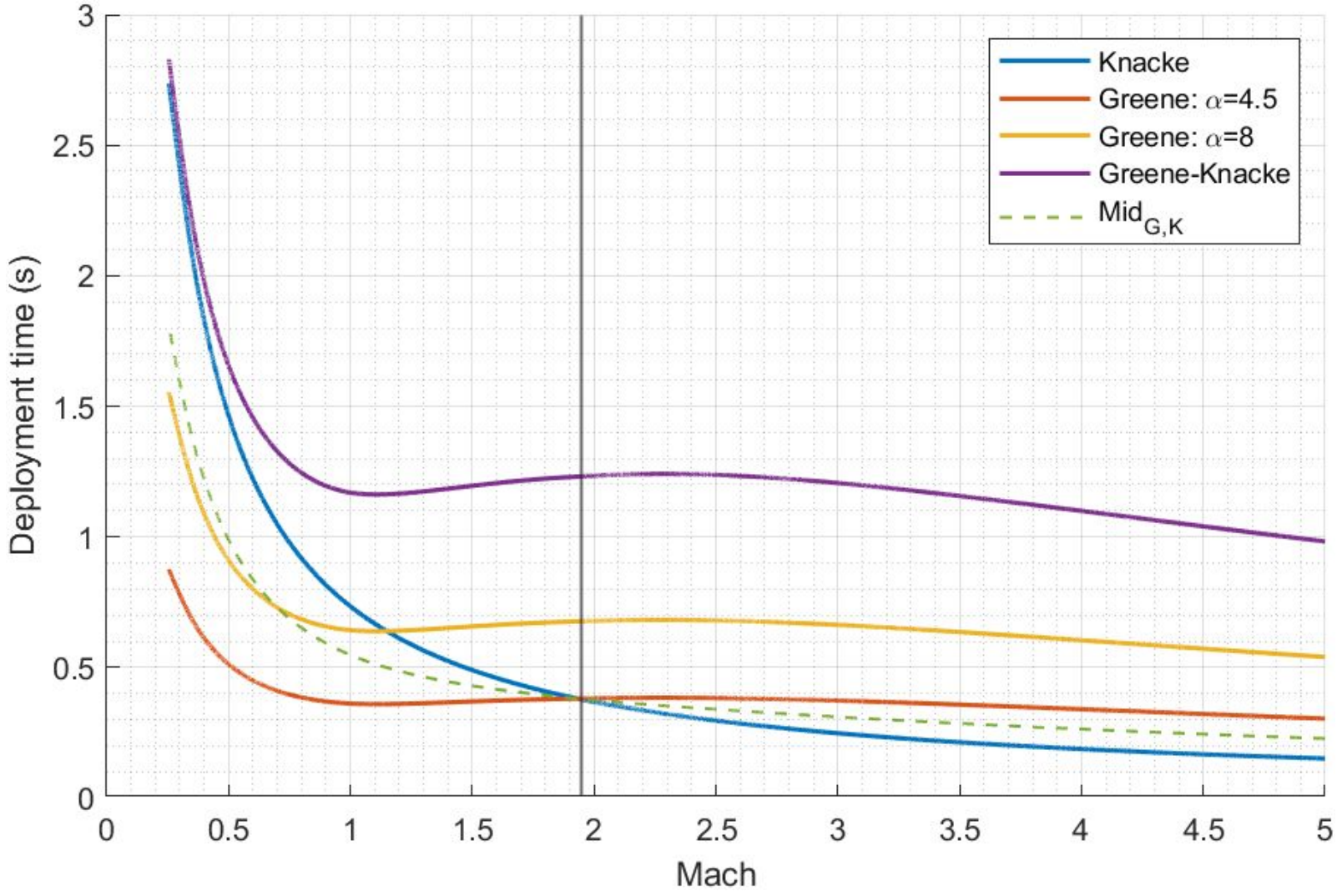

Parachute system design and modeling

Inflation drag profile and peak loading

- Computation of the inflation drag profile typically requires the peak loading:

$$F_{max} = qC_{D0}S_0C_XX_1$$

Drag profile in this way is tuned using the value obtained from the peak load.

For example:

$$C_{D,inf}(t) = C_{D0}C_F\left[(1-\eta)\left(\frac{t}{t_F}\right)^3 + \eta\right]^2$$

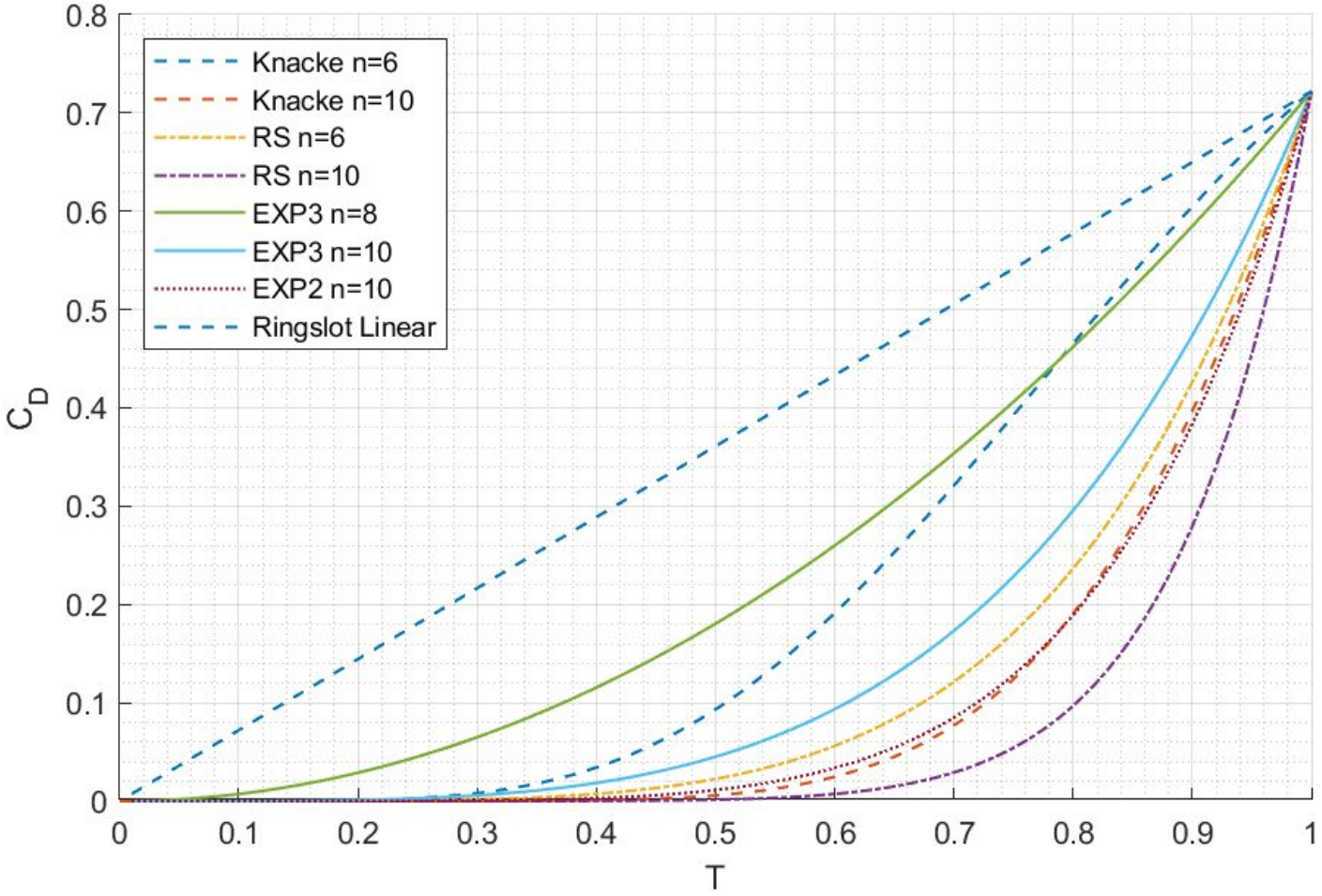

Parachute system design and modeling

Some extras ...

MSL Parachute oscillation model

Models the variations of the drag coefficient after reaching full-inflation condition.
Generates random oscillations of the parachute area in order.

Different scenarios have been analyzed in order to study the overall behaviour of the model.

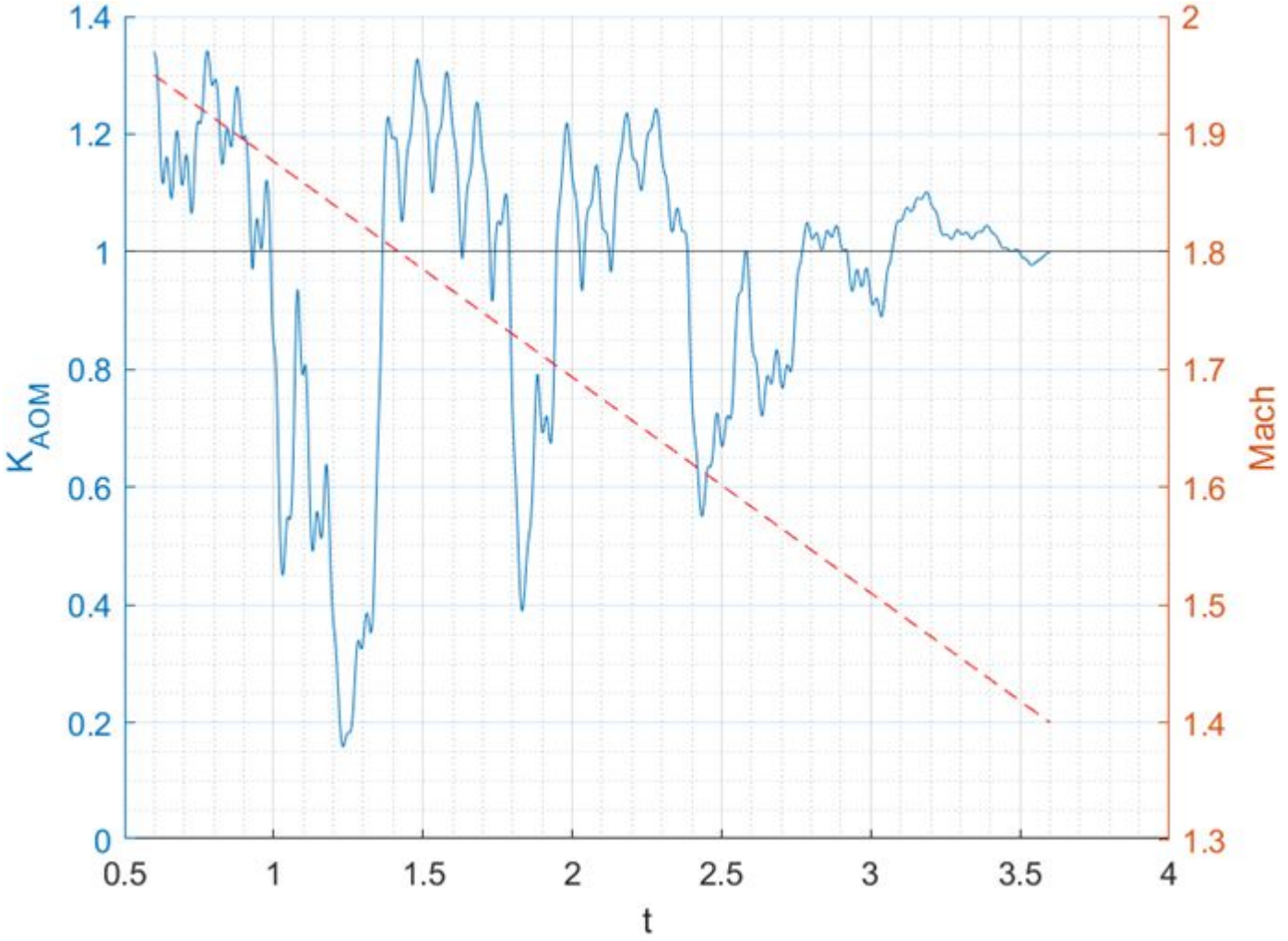

Parachute system design and modeling

Some extras ...

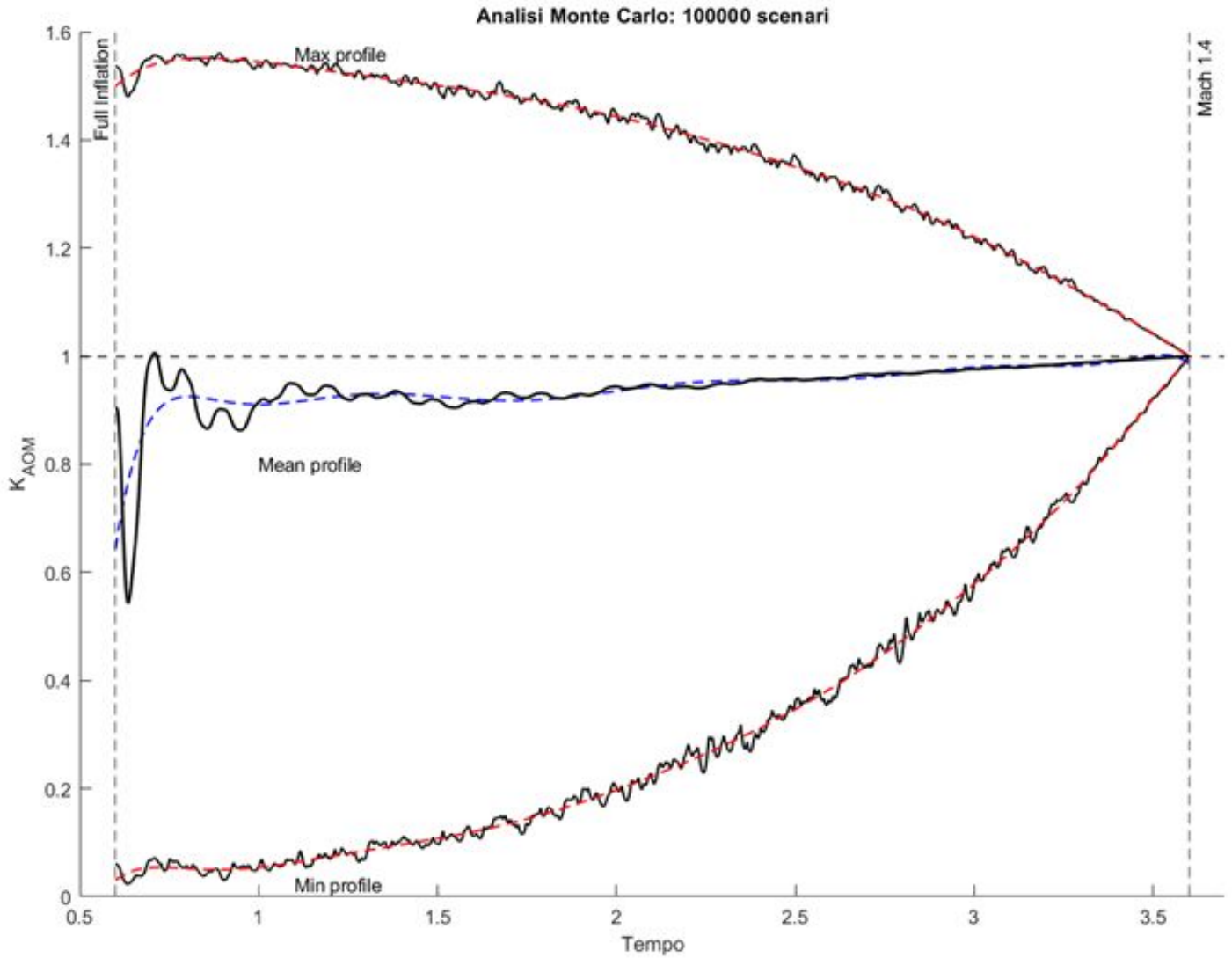

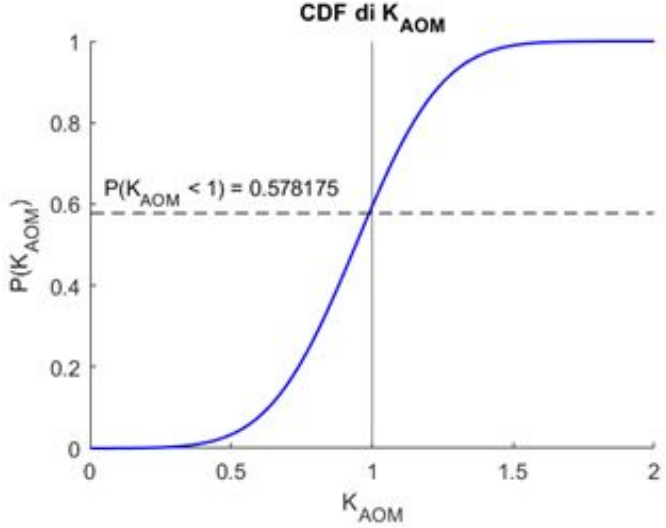

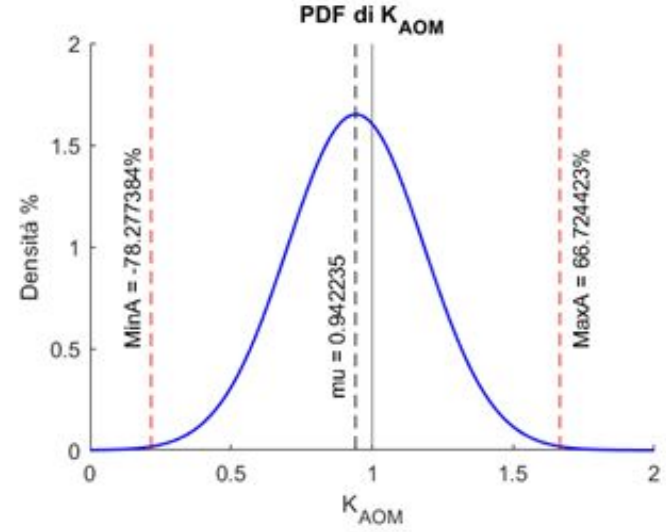

Parachute system design and modeling

Some extras ...

Modeling for MSL descent-landing sequence - from deployment to separation:

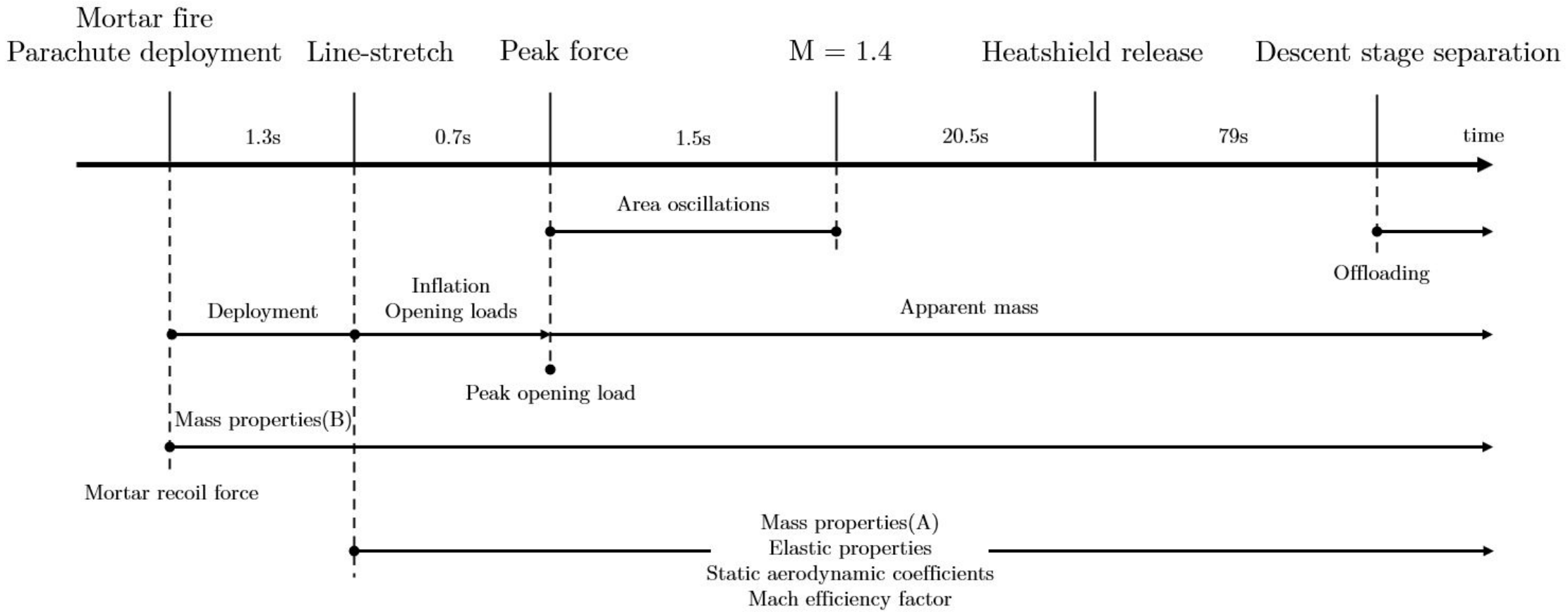

End of part 2

Thank you for your attention

Any questions?

Planetary Probes
Entry and Descent Science

Part 3 - ED(L) Simulation

Alessio Aboudan (alessio.aboudan@unipd.it), Luca Placco, G. Colombatti, F. Ferri and the AMELIA team

Introduction

- Modelling and simulation of EDL is a key aspect
  - To support both design and qualification of the EDL
  - To perform post-flight analysis i.e.
    - verification of engineering requirements
    - scientific analysis of ED (L) data

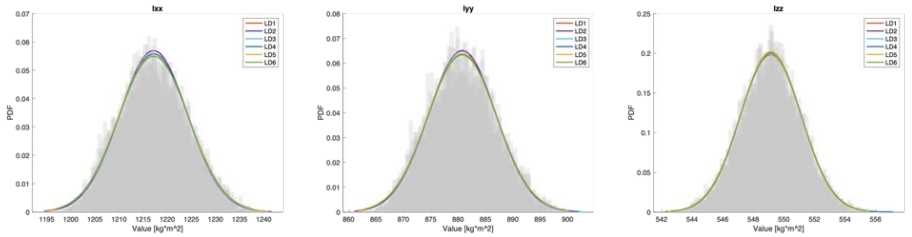

Montecarlo simulation is used to investigate the variability of each output according to inputs uncertainties

Montecarlo simulation

Inputs:

- S/C mass/inertia/shape
- Aerodynamic Database of each component (aeroshell/parachute-s)
- Environment: gravity, atmosphere, terrain (e.g. DTM)
- EDL timeline and main events (GNC)
- On-board sensors location and models
- Initial state vector (position, velocity and attitude)

Outputs:

- Position/velocity/attitude
- Aux parameters:
  - Flow angles (AoA, SSA)
  - Aerodynamic parameters (Knudsen, Mach, C_D, C_A, ecc...)
- On-board sensors predicted measurements

Reference Frames

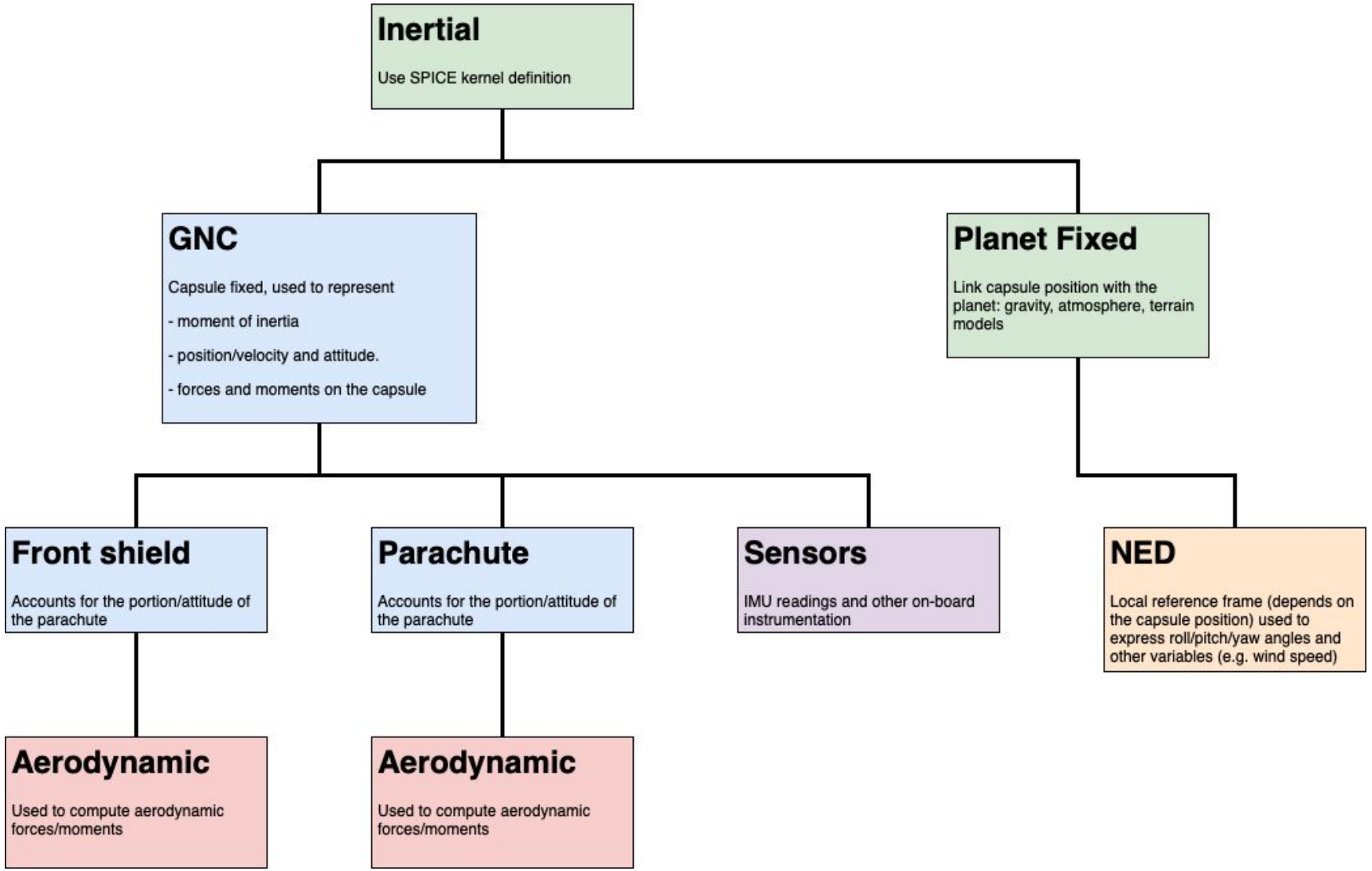

State Space Model

- Probe dynamics and sensor measurements are represented using a state-space model (first order ODE, non-linear)

$$\dot{x} = f(t, x, u) \qquad \text{State equation}$$

$$y = g(t, x, u) \qquad \text{Measurement equation}$$

- State x usually contains capsule angular rate/attitude/velocity/position
- The state vector x can be augmented to include other time-varying parameters and/or state covariance and state transition matrix
- Input u corresponds to force/moments (simulation) and IMU readings for the reconstruction
- The measurements vector y depends only on the state x

Numerical Solution of the Equations of Motion

Equations of motion are integrated over a fixed time interval

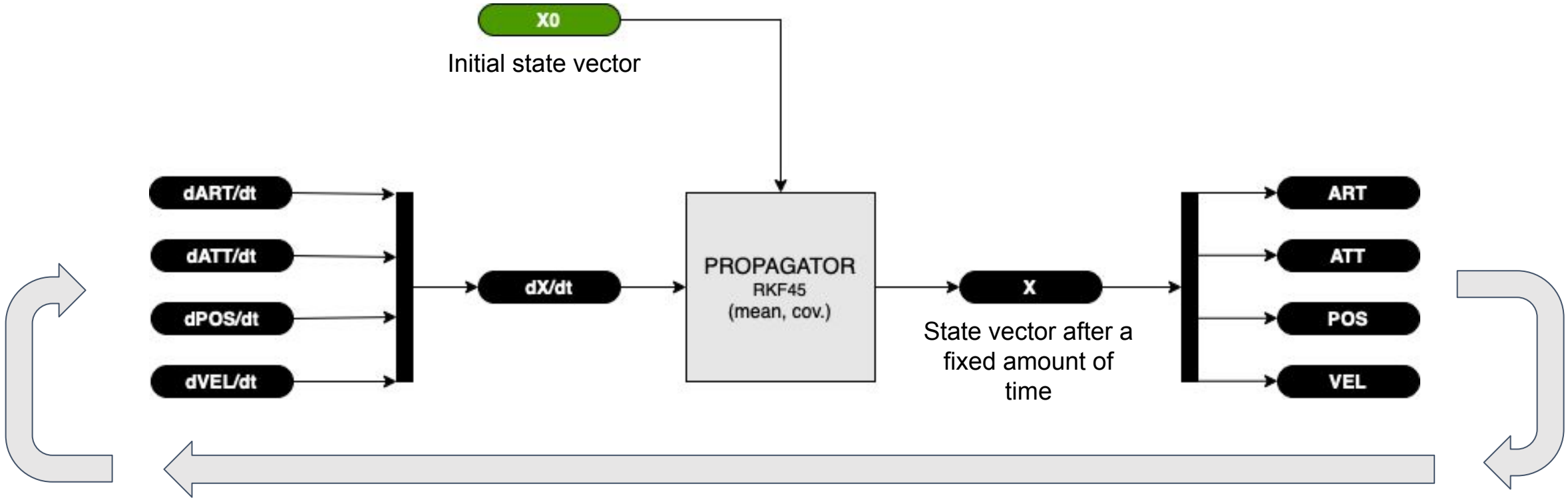

- State equation is an input to the ODE solver
- Complete representation of the capsule dynamical conditions
- ODE solver: Euler 1st order or RKF45 are both effective

Equations of Motion

Entry 6 DoF or Descent 9 DoF equations of motion are integrated over time

- Several implementation options:
- Vel/pos: cartesian/radial, inertial frame/local frame
- Attitude: quaternion/euler angles, ecc…

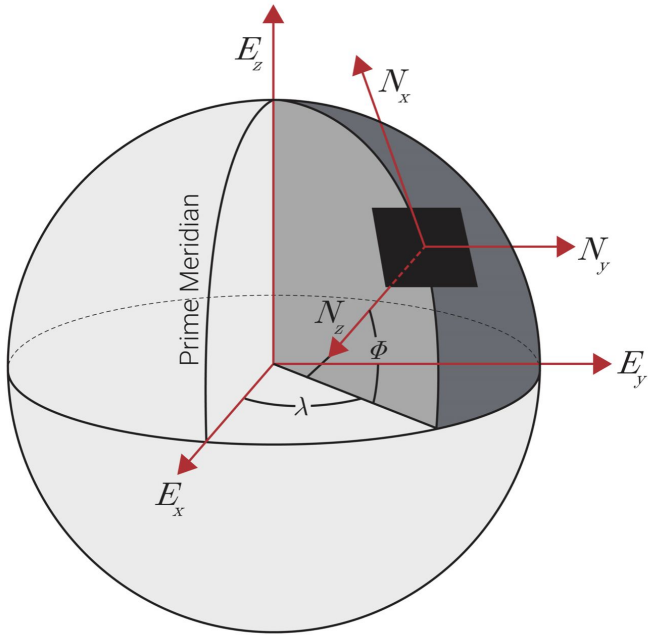

https://www.vectornav.com/resources/inertial-navigation-primer/

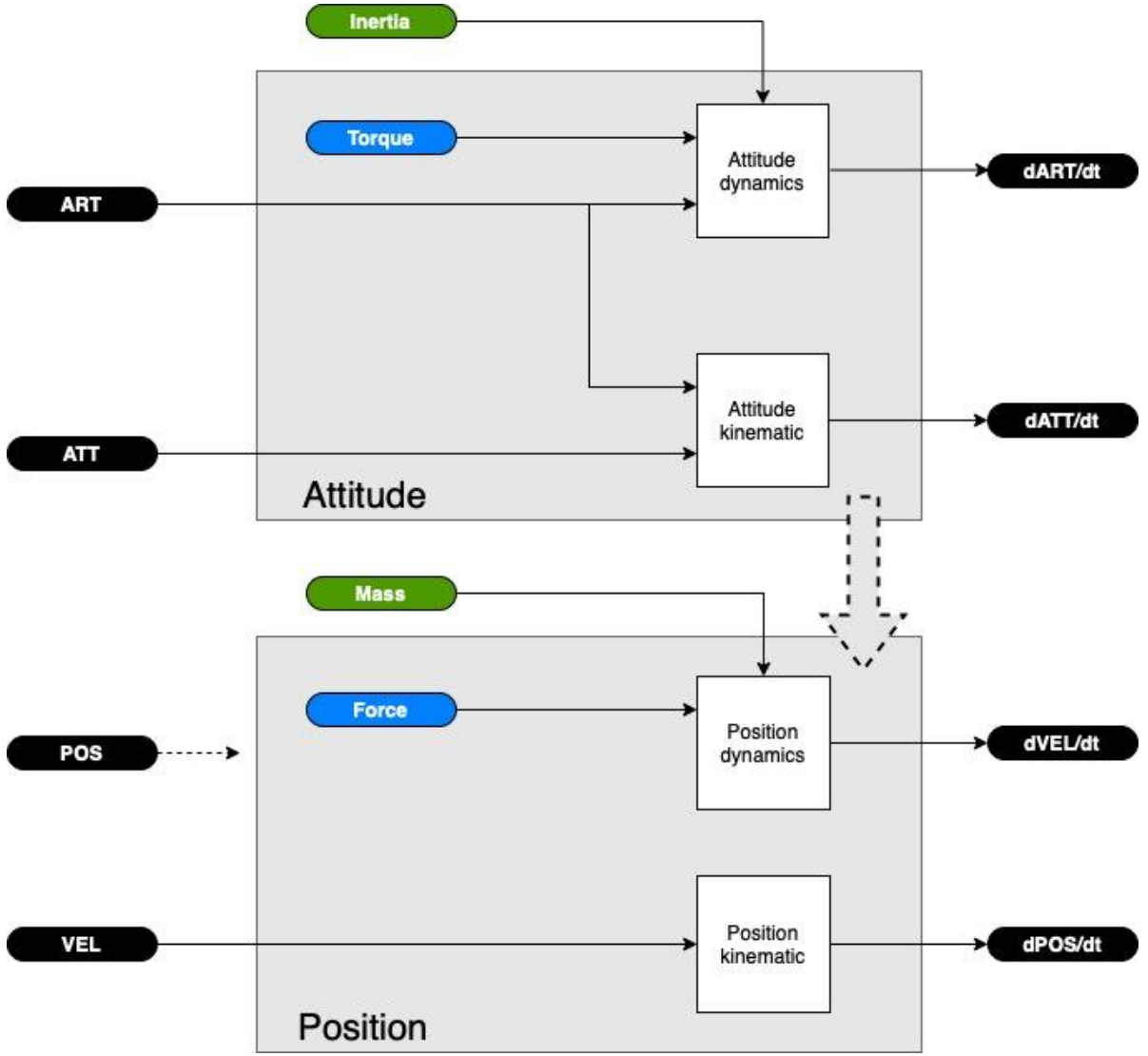

Force and Moments

Computed at each integration step using the current state vector

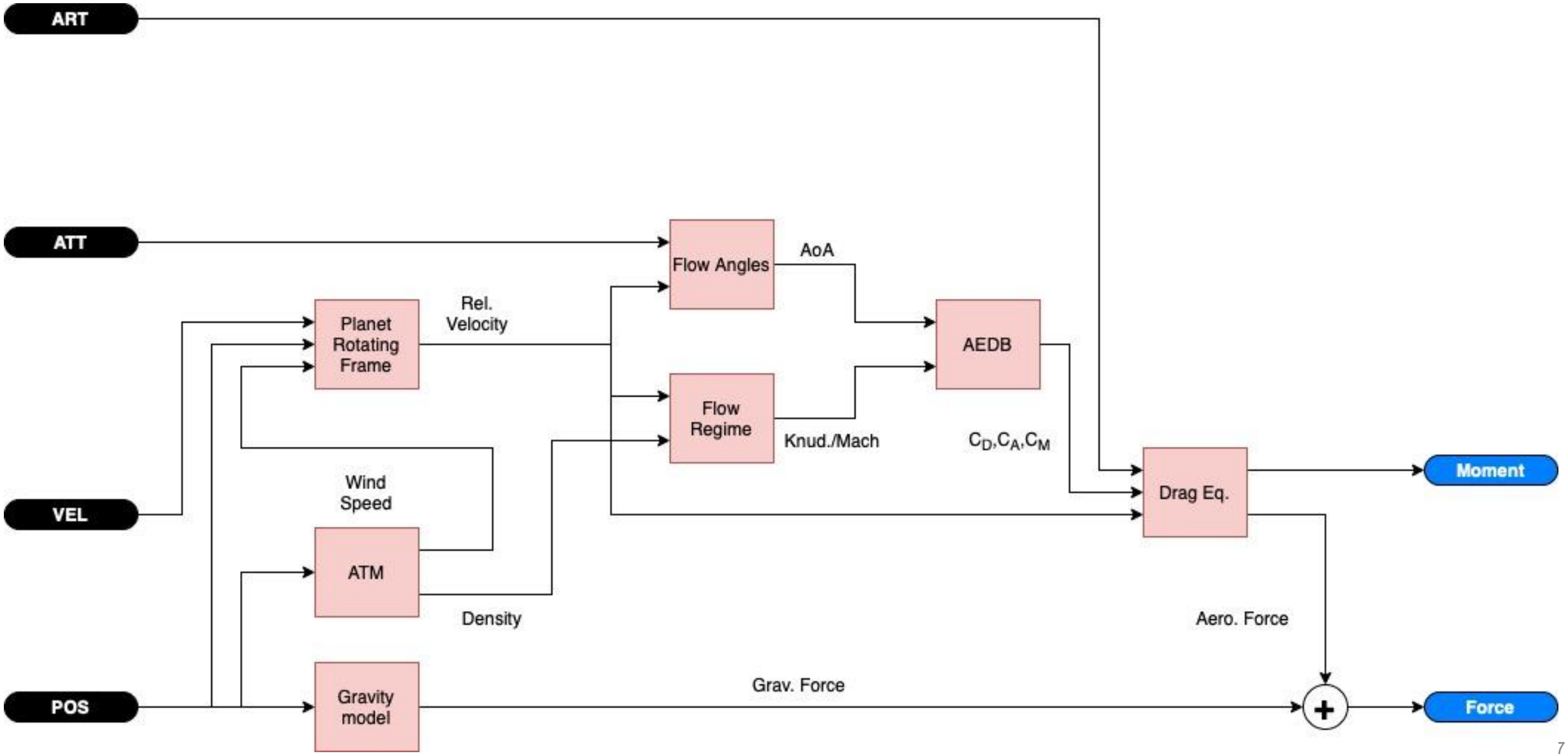

State and Measurement Generative Model

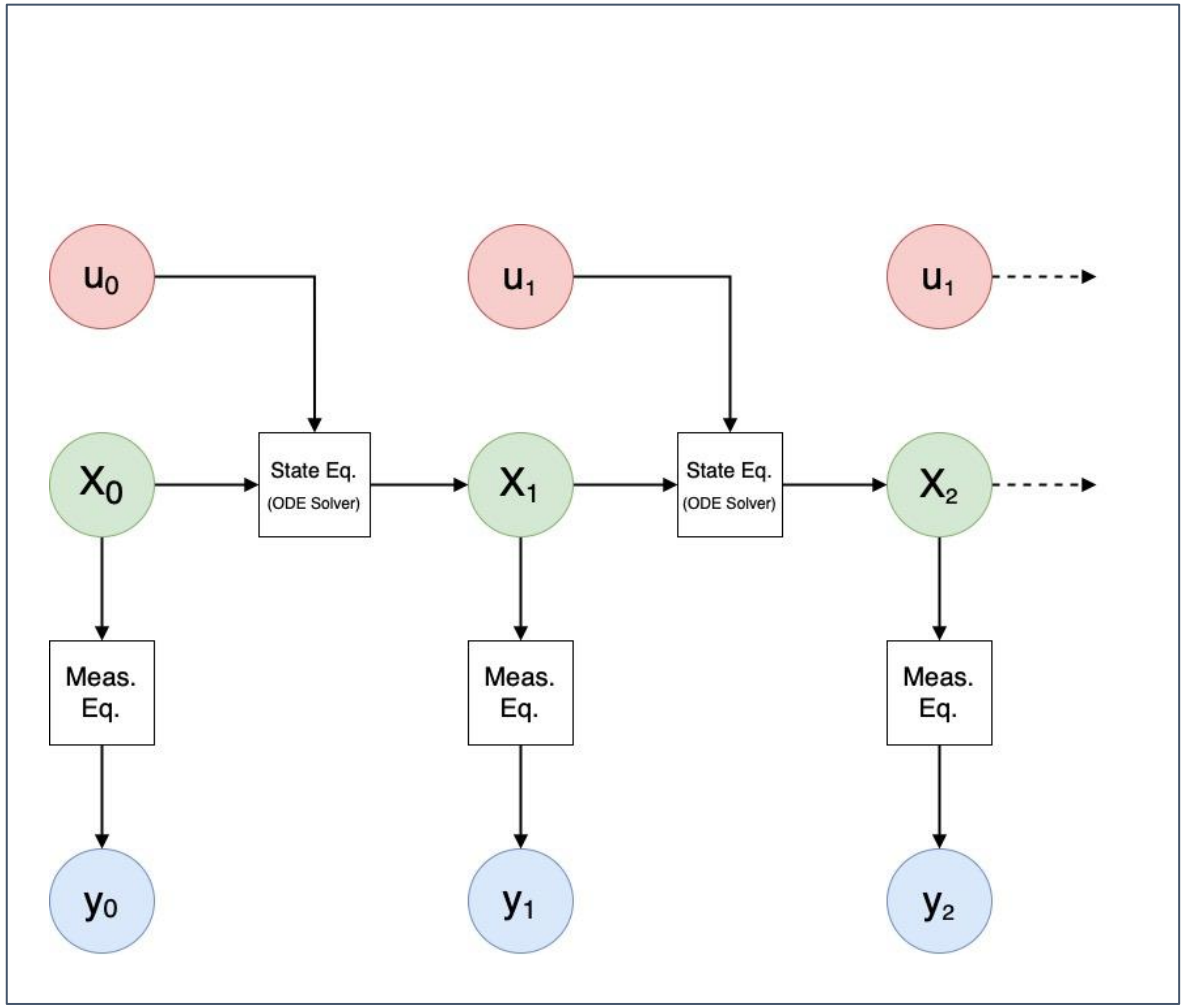

General model

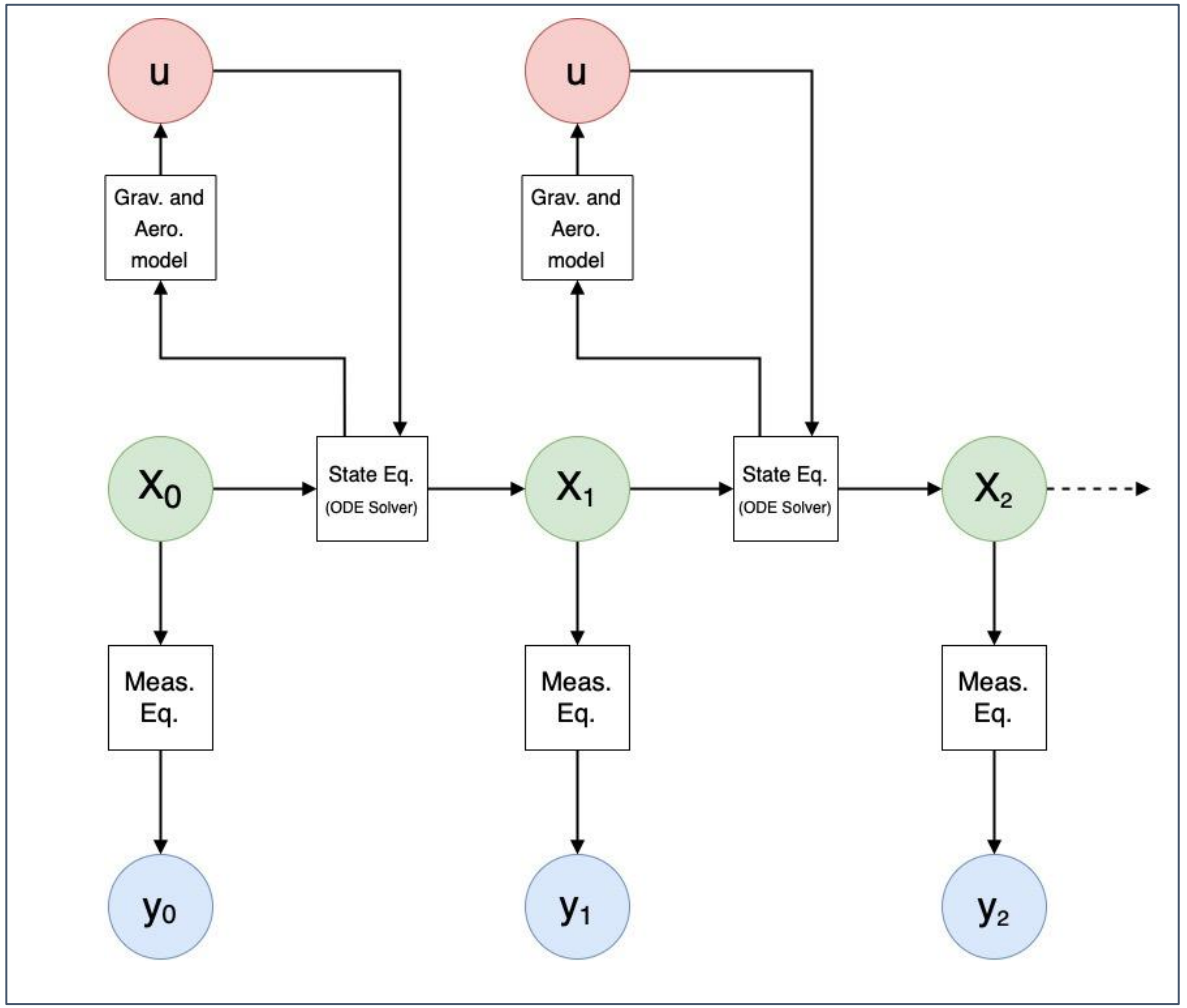

Simulation model

ExoMars-2016 Simulation

State vector fully represents the dynamic of the capsule but relevant infos are hidden

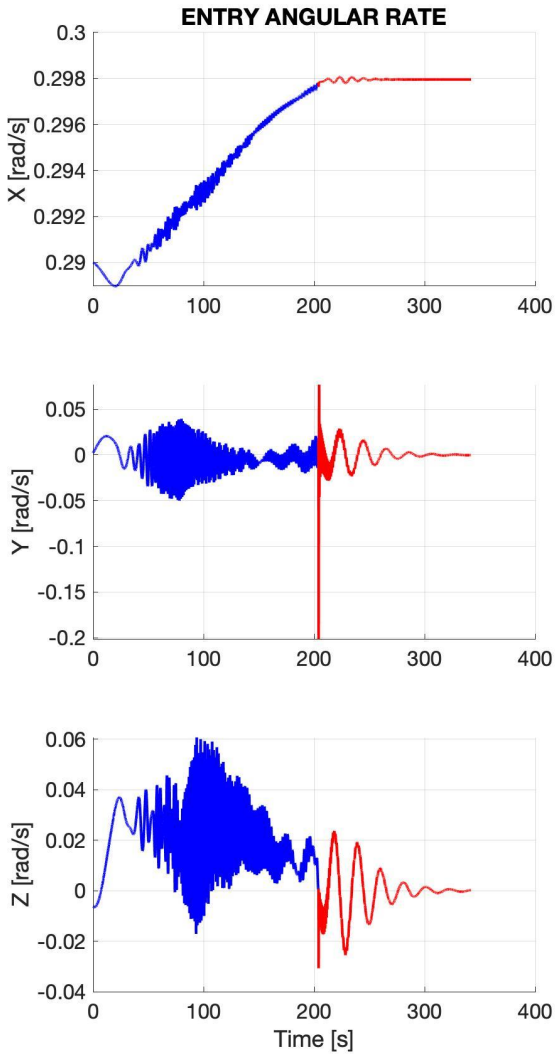

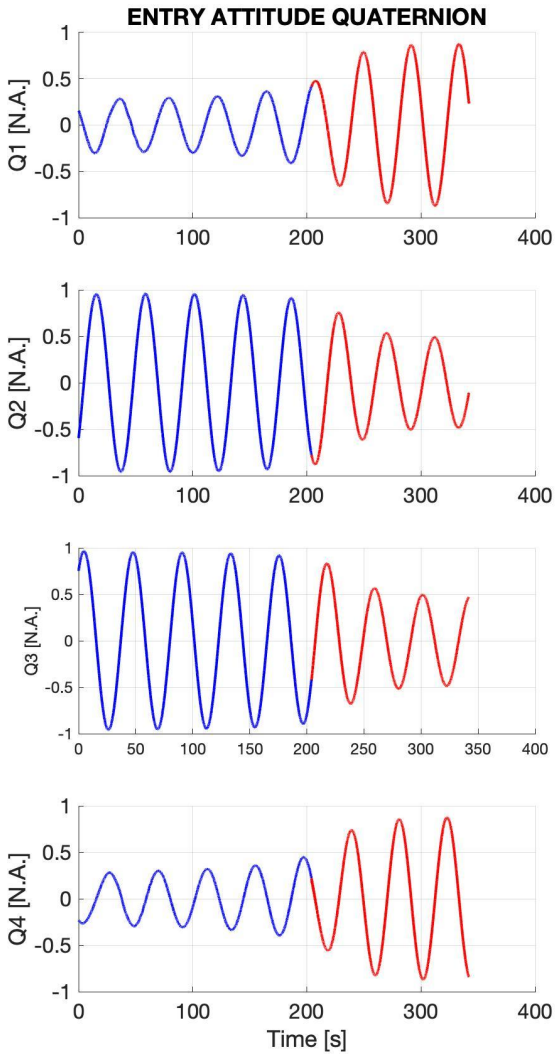

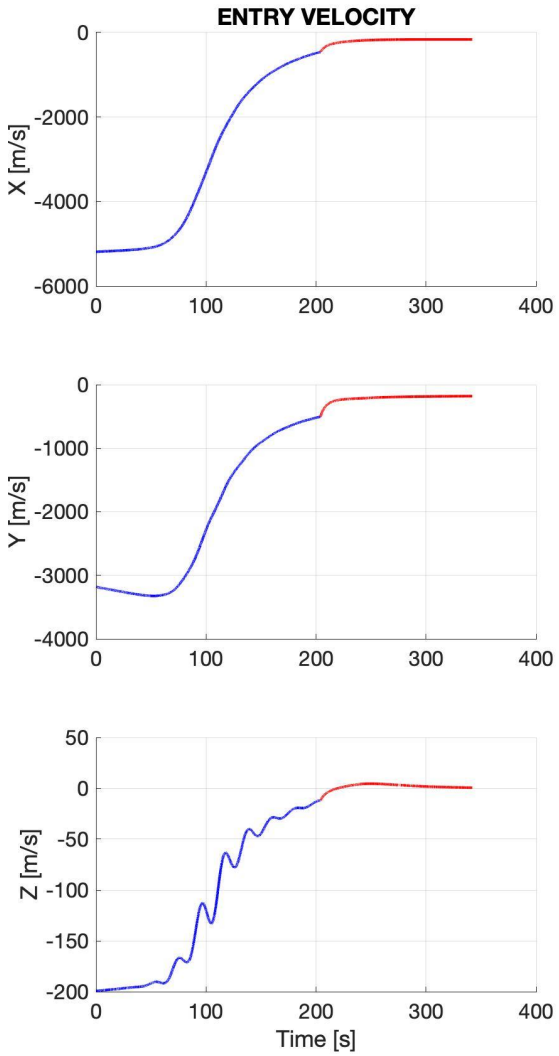

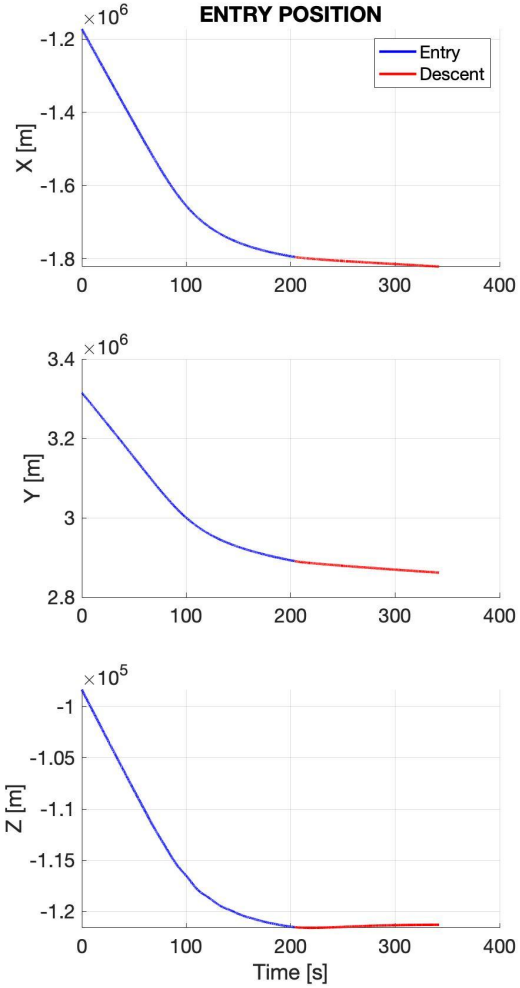

ExoMars-2016 Simulation

Consider for example the inertial vs rel. speed (module), the descent speed and RPY angles

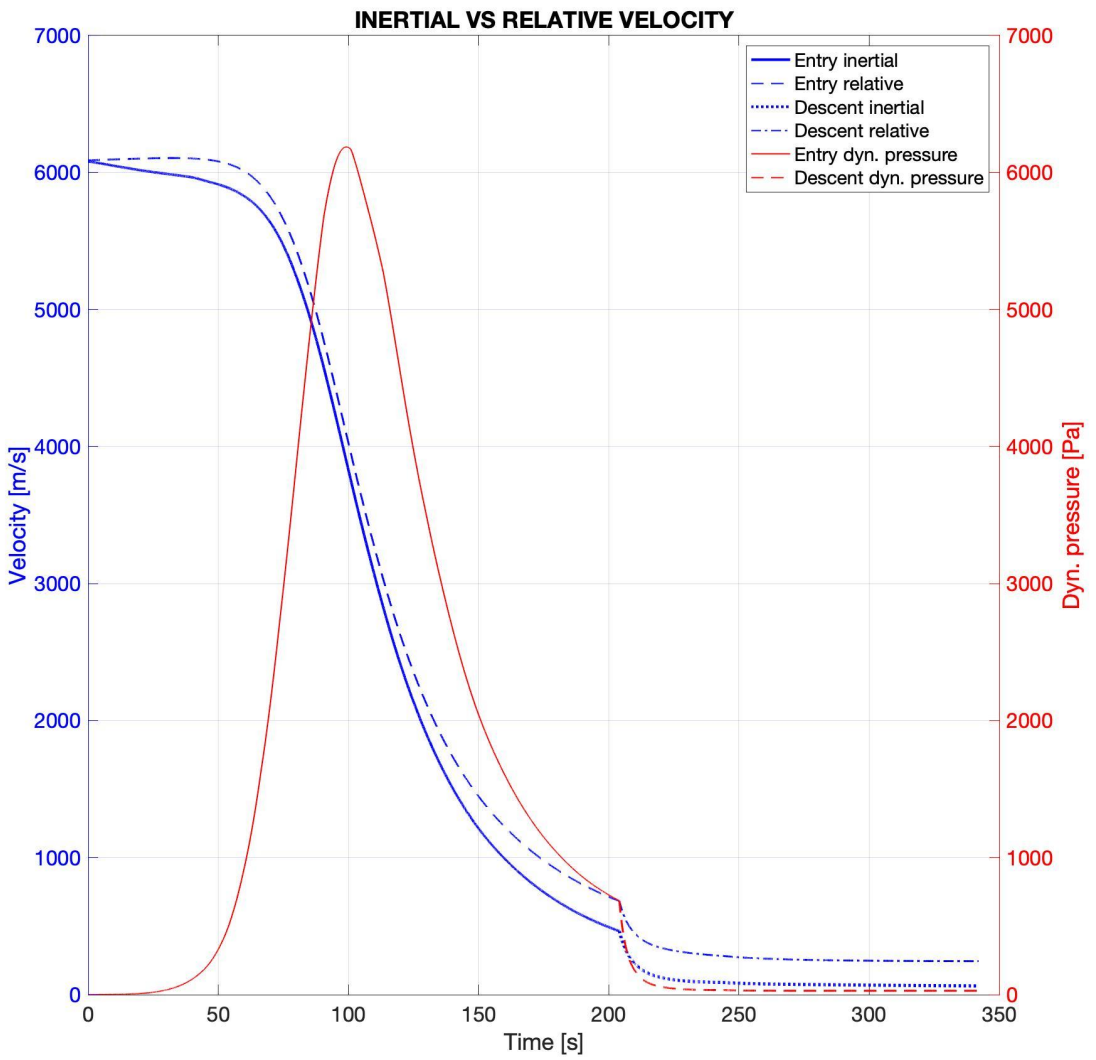

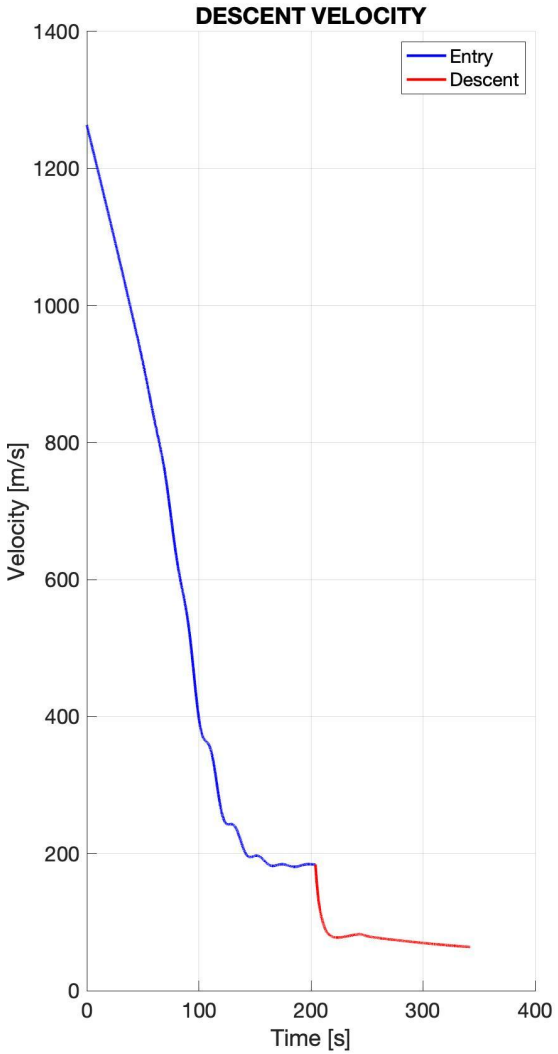

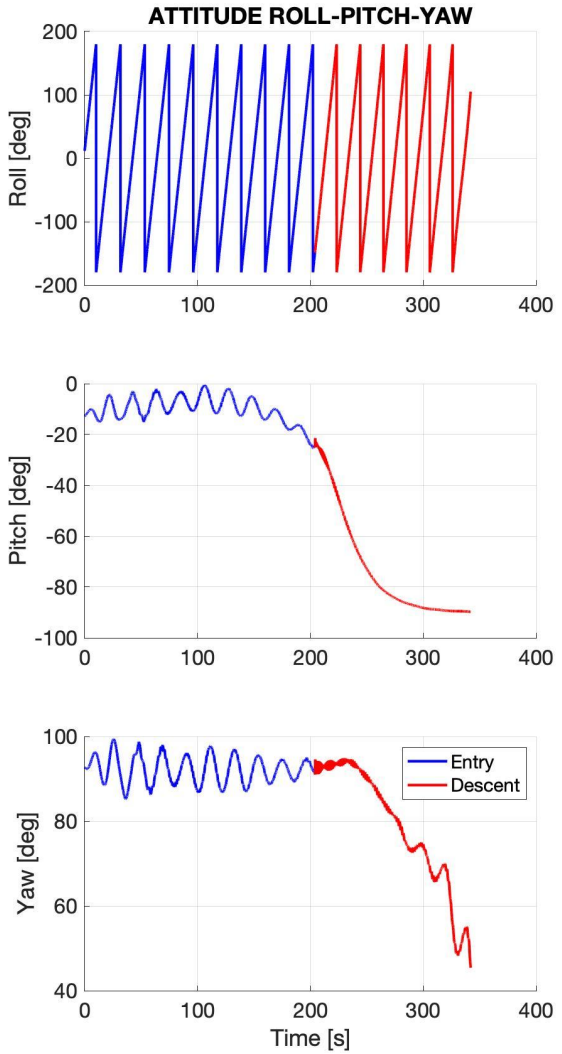

ExoMars-2016 Simulation

Angle of attack, aerodynamic parameters, forces and moments

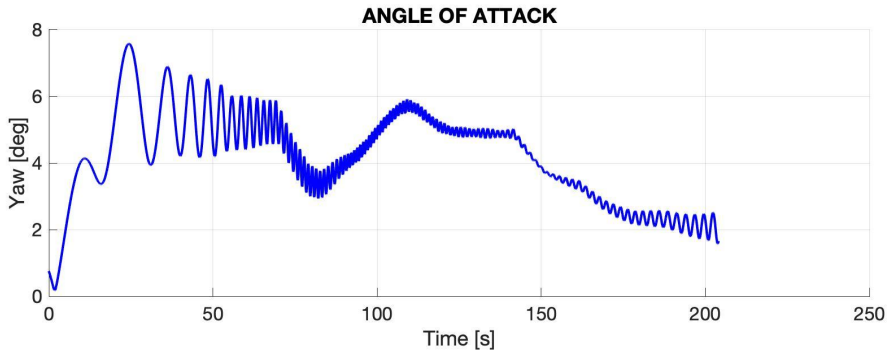

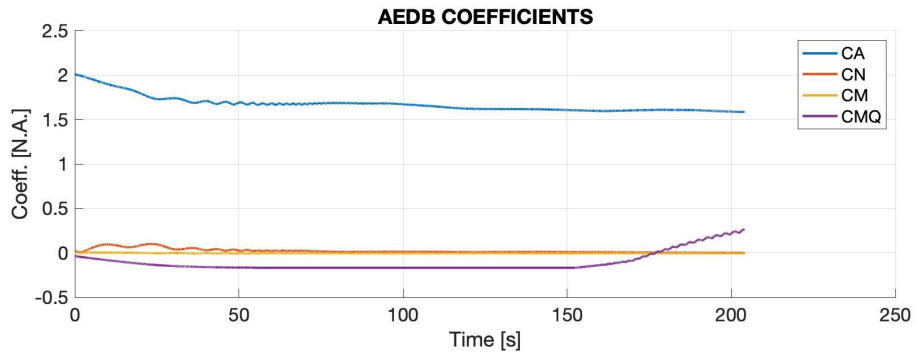

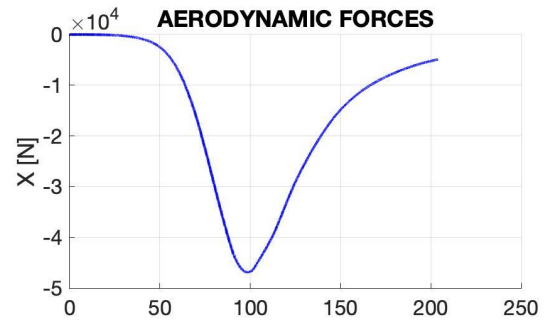

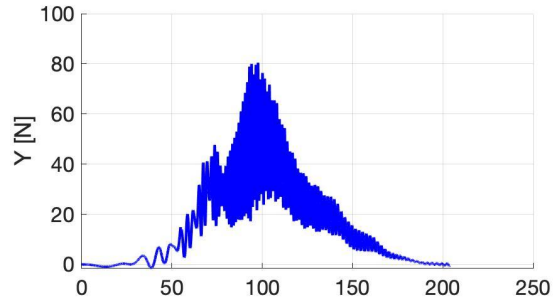

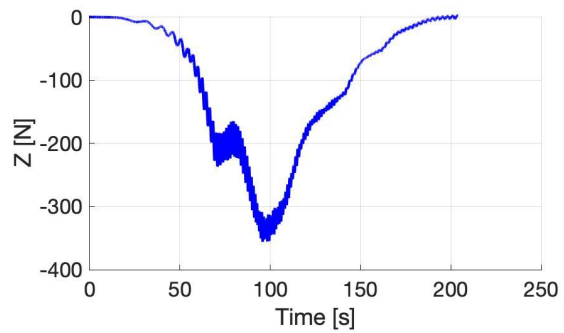

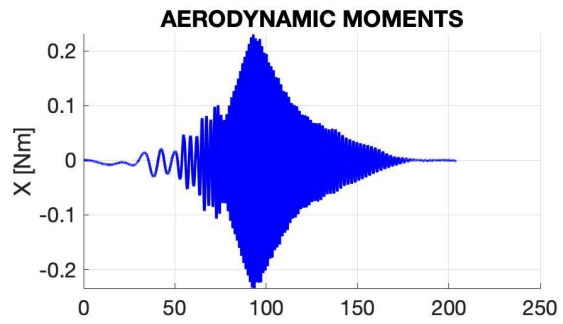

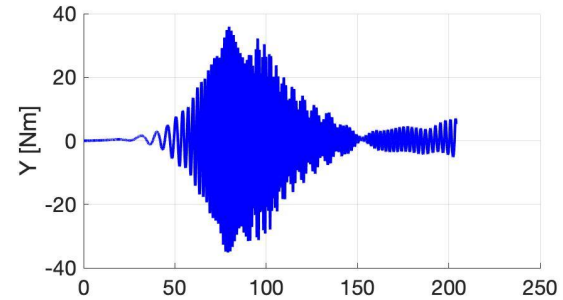

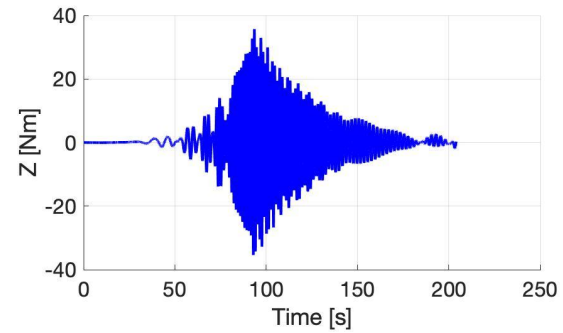

ExoMars-2016 Simulation

Simulation of IMU and Radar Altimeter measurements

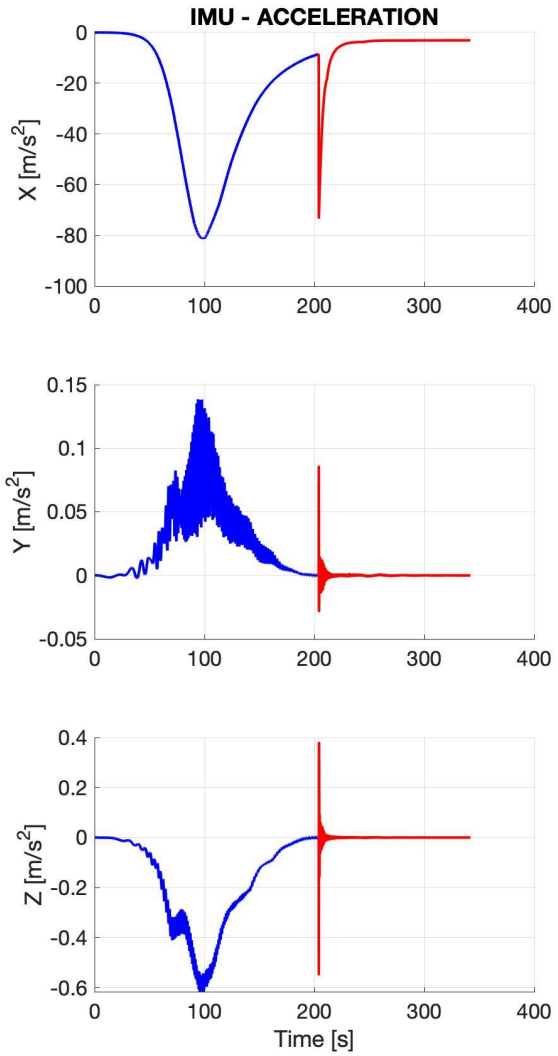

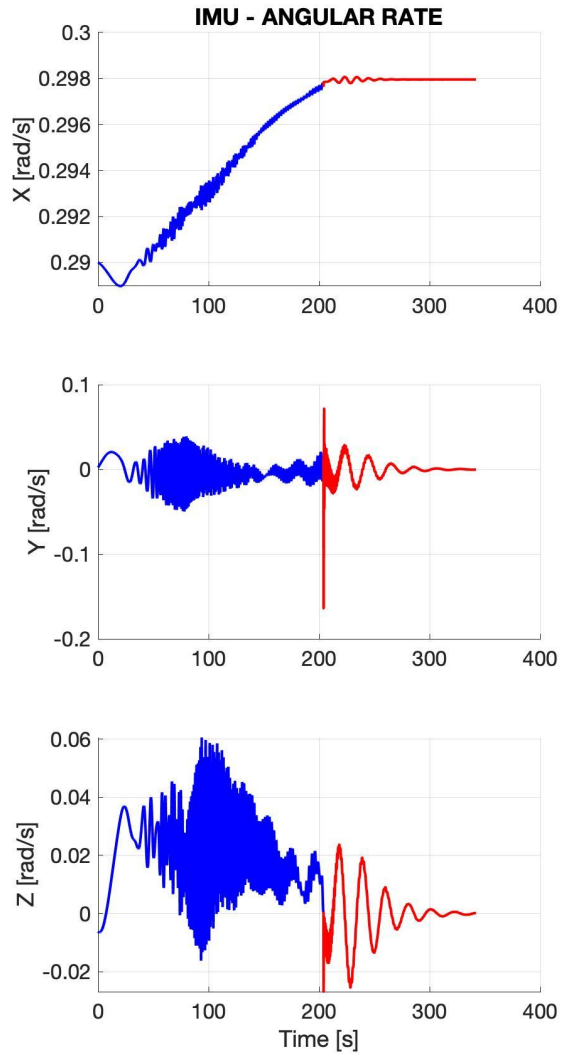

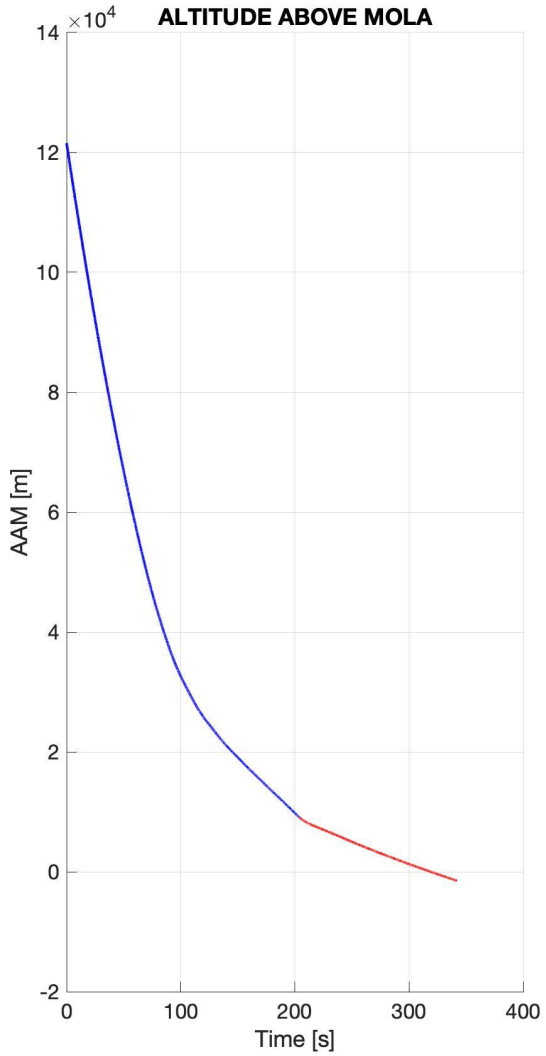

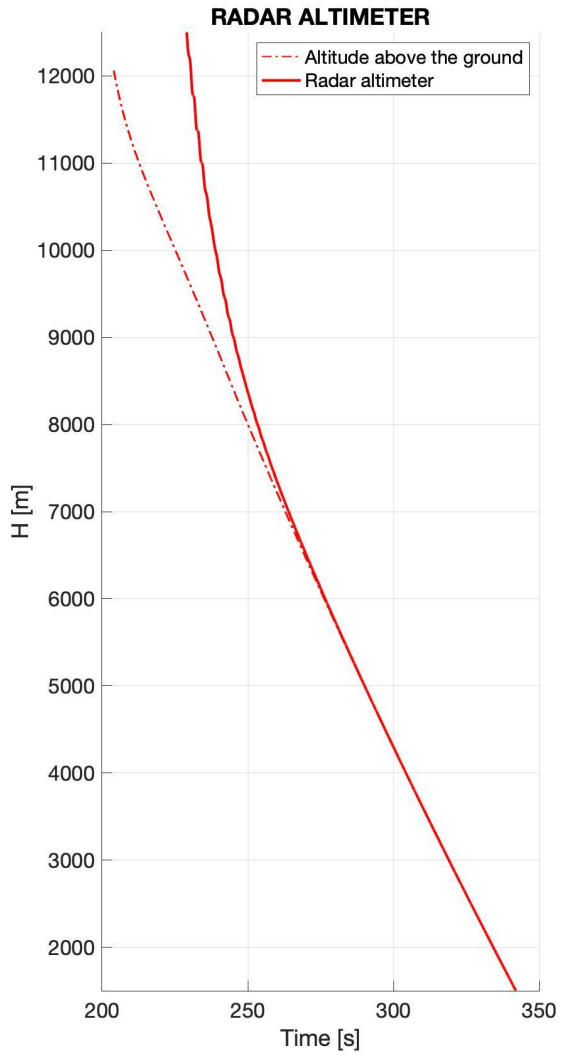

Planetary Probes
Entry and Descent Science

Part 4 - Trajectory and Atmospheric Profiles Reconstruction

Alessio Aboudan (alessio.aboudan@unipd.it), Luca Placco, G. Colombatti, F. Ferri and the AMELIA team

Introduction

- Trajectory reconstruction
  - Based on IMU data
  - Plus the assimilation of other on-board/remote sensing measurements
    - Terrain relative altitude and velocity (radar altimeter/vision systems)
    - Absolute position and speed (radio links)
- Atmospheric profiles
  - Retrieved from acc. given the trajectory
  - Simultaneous reconstruction of both trajectory and atmosphere

In general post-flight analysis requires a mission specific workflow

Equations of Motion

Assuming IMU measurements as inputs

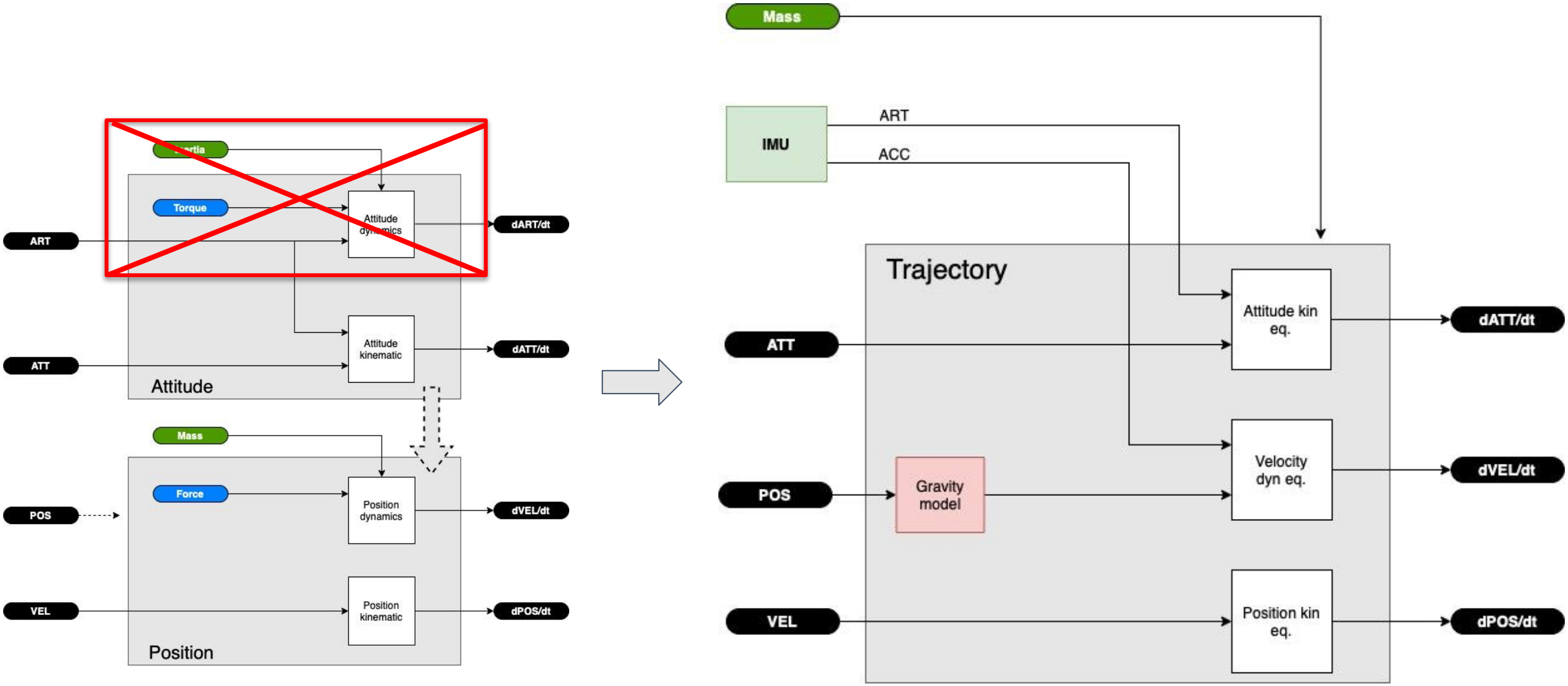

Reconstruction

General approach

- Use the ODE solver to compute the evolution of the state vector
- Starting from a given initial condition (X_0)
- Using IMU data as input
- Use the measurement model to compute the predicted sensor readings
- Compare predicted and actual measurements (compute the residuals)
- If the residuals are small wrt the sensor uncertainties then the trajectory (seq. of state vectors) is consistent with the measurements and the task is done
- Otherwise the “state” have to be updated to minimize the residuals

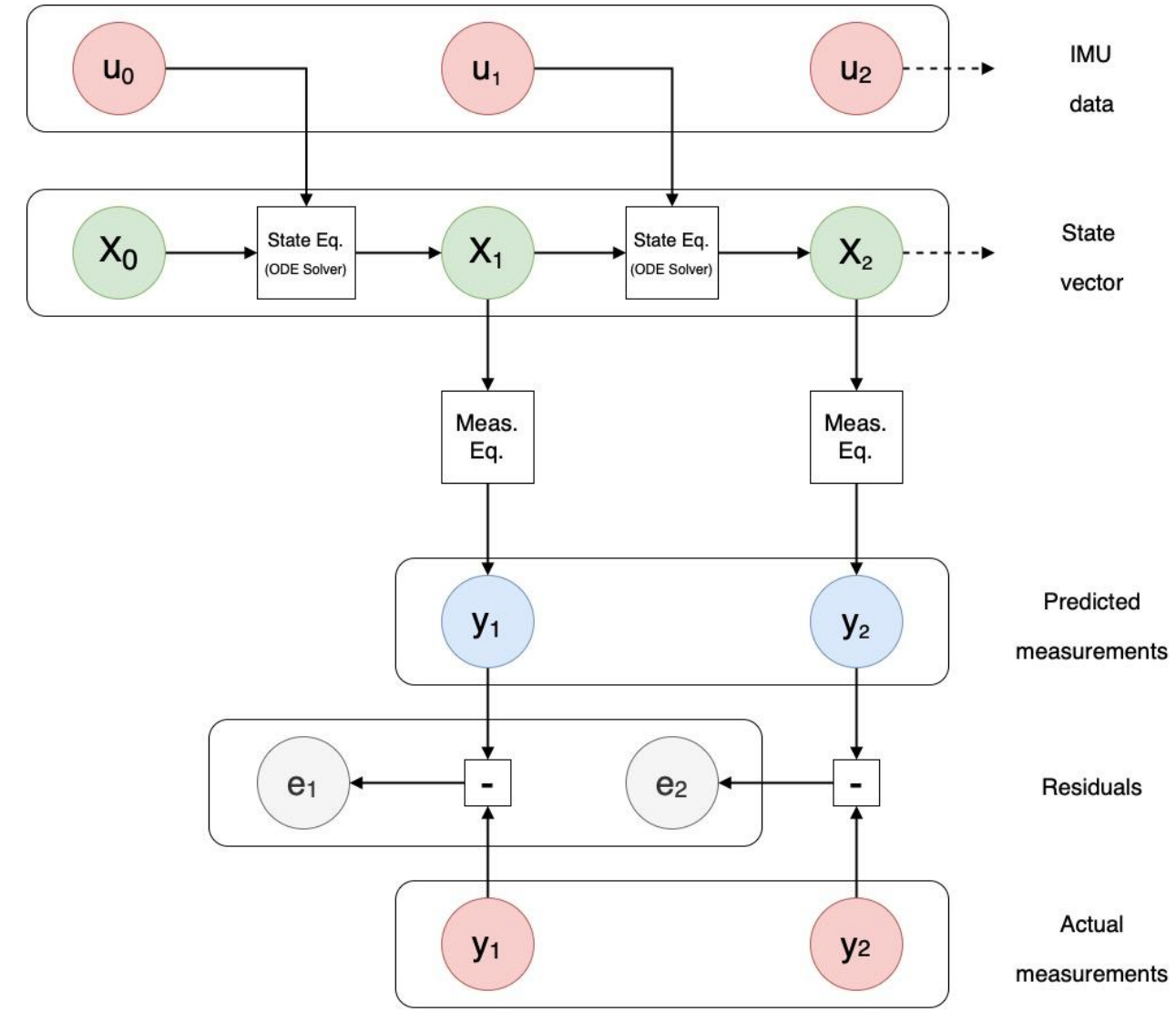

LSQ Method

- LSQ updates the initial state vector
- Producing smooth trajectory profiles
- Used to assimilate radar altimeter data and/or absolute measurements of pos/vel obtained from high res images and radioscience
- Weighted LSQ accounts for measurements uncertainty
- Requires the numerical computation of state transition matrix (see next slide)

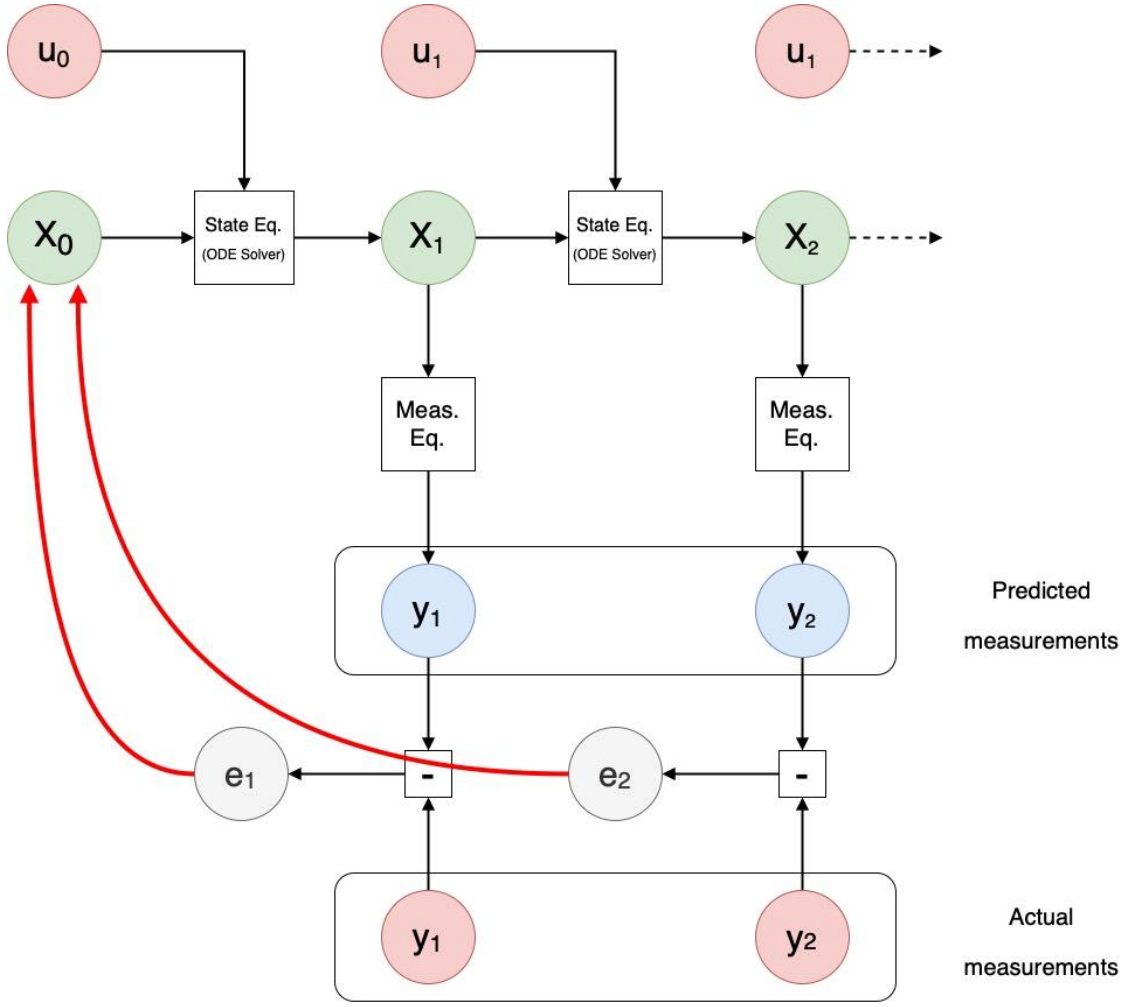

LSQ Implementation

- Find the initial state vector X_0 that minimizes the sum of squared measurement residuals

$$S = \sum_{n=1}^{N} e_n^2$$

- Using Gauss-Newton algorithm

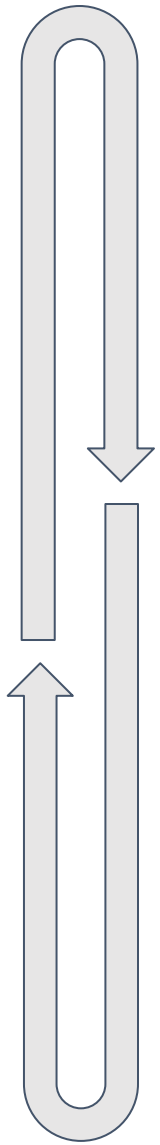

Numerical propagation:

$$\begin{cases} \dot{x} = f(t,x,u) \\ \dot{\Phi} = A\,\Phi \end{cases}$$

State eq.

State transition eq.

$$A = \nabla_x f(t,x,u)$$

Jacobian

$$\Phi(0) = I$$

Initial conditions

Update:

$$e_n = H(x_n)\,\Phi(n,0)\,\delta x_0$$

Shift eq.

$$H = \nabla_x g(t,x,u)$$

Jacobian

$$\Phi(n,0) = \Phi(n,n-1)\cdots\Phi(1,0)$$

State transition matrix

Overdetermined linear system of eq. solved using Moore-Penrose pseudo inverse method (i.e. normal equations)

$$\begin{bmatrix} e_1 \\ \vdots \\ e_n \end{bmatrix} = \begin{bmatrix} H(x_1)\,\Phi(1,0) \\ \vdots \\ H(x_n)\,\Phi(n,n-1)\cdots\Phi(1,0) \end{bmatrix} \delta x_0$$

Bayesian Filtering

Extended or Unscented Kalman Filters

- EKF/UKF updates the current estimate of state vector
- Estimate time varying parameters (e.g. atmospheric profiles or sensor biases)
- Trajectory profiles could have discontinuities/abrupt changes
- Trajectory smoothing and/or backward propagation could be needed
- Implements a complete model of the uncertainty on both the state/state model and the sensors
- Requires the numerical computation of covariance matrix (see next slide)

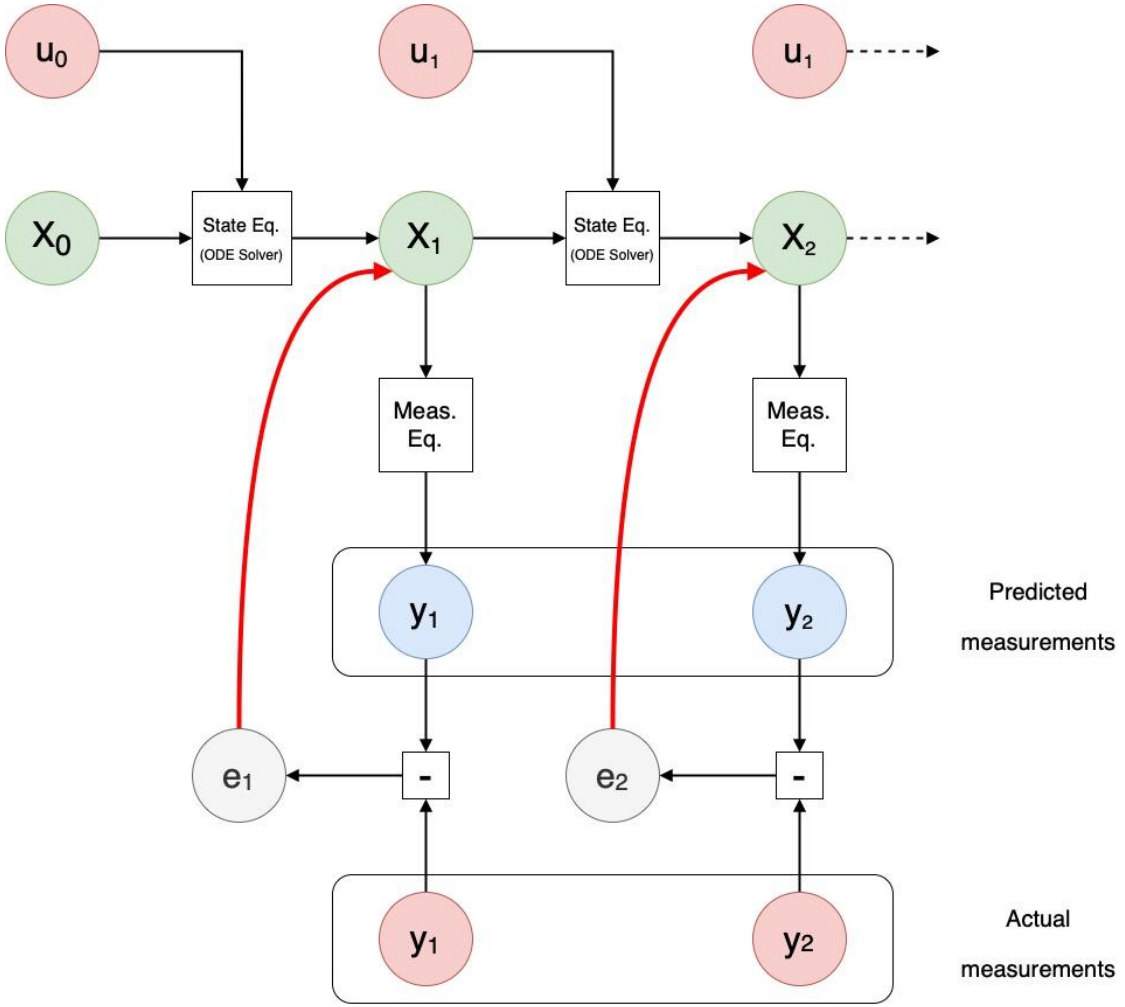

Bayesian Filtering Implementation

- The state vector is modelled using a Gaussian r.v. (mean + covariance)
- Predictor-corrector algorithms
- Specification of state/input/sensor uncertainty is required (often difficult to define)
- Tuning could be challenging and requires MC generated synthetic data

Numerical propagation:

$$\begin{cases} \dot{x} &= f(t,x,u,\eta) \\ \dot{\Sigma} &= A\,\Sigma + \Sigma\,A^T + B\,Q_u\,B^T + C\,Q_\eta\,C^T \end{cases}$$

$$\begin{aligned} A &= \nabla_x f(t,x,u,\eta) \\ B &= \nabla_u f(t,x,u,\eta) \\ C &= \nabla_\eta f(t,x,u,\eta) \end{aligned}$$

Forward update - filtering:

$$\begin{aligned} e_n &= y_n - g(x_n^-) \\ S_n &= H(x_n^-)\,\Sigma_n^-\,H^T(x_n^-) + R_n \\ K_n &= \Sigma_n^-\,H^T(x_n^-)\,S_n^{-1} \\ x_n &= x_n^- + K_n\,e_n \\ \Sigma_n &= \Sigma_n^- - K_n\,S_n\,K_n^T \end{aligned}$$

$$H = \nabla_x g(t,x,u)$$

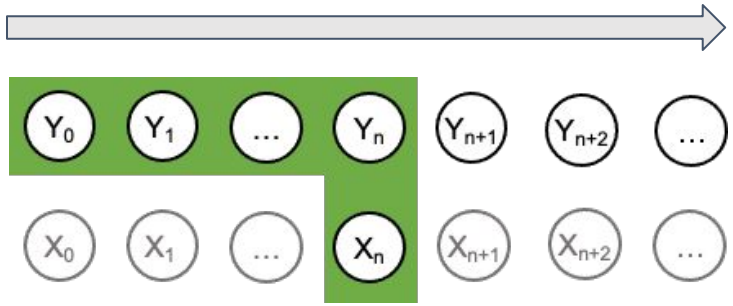

Backward update - smoothing:

$$\begin{aligned} G_n &= \Sigma_n\,A^T(x_n)\,\left[\Sigma_{n+1}^-\right] \\ x_n^s &= x_n + G_n\,\left[x_{n+1}^s - x_{n+1}^-\right] \\ \Sigma_n^s &= \Sigma_n + G_n\,\left[\Sigma_{n+1}^s - \Sigma_{n+1}^-\right]\,G_n^T \end{aligned}$$

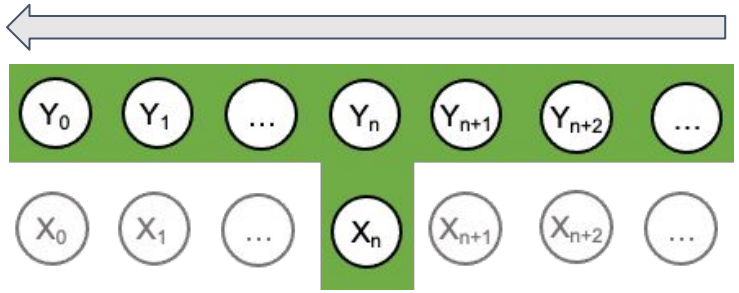

ExoMars 2016 - Schiaparelli

Reference frames and data available for the reconstruction

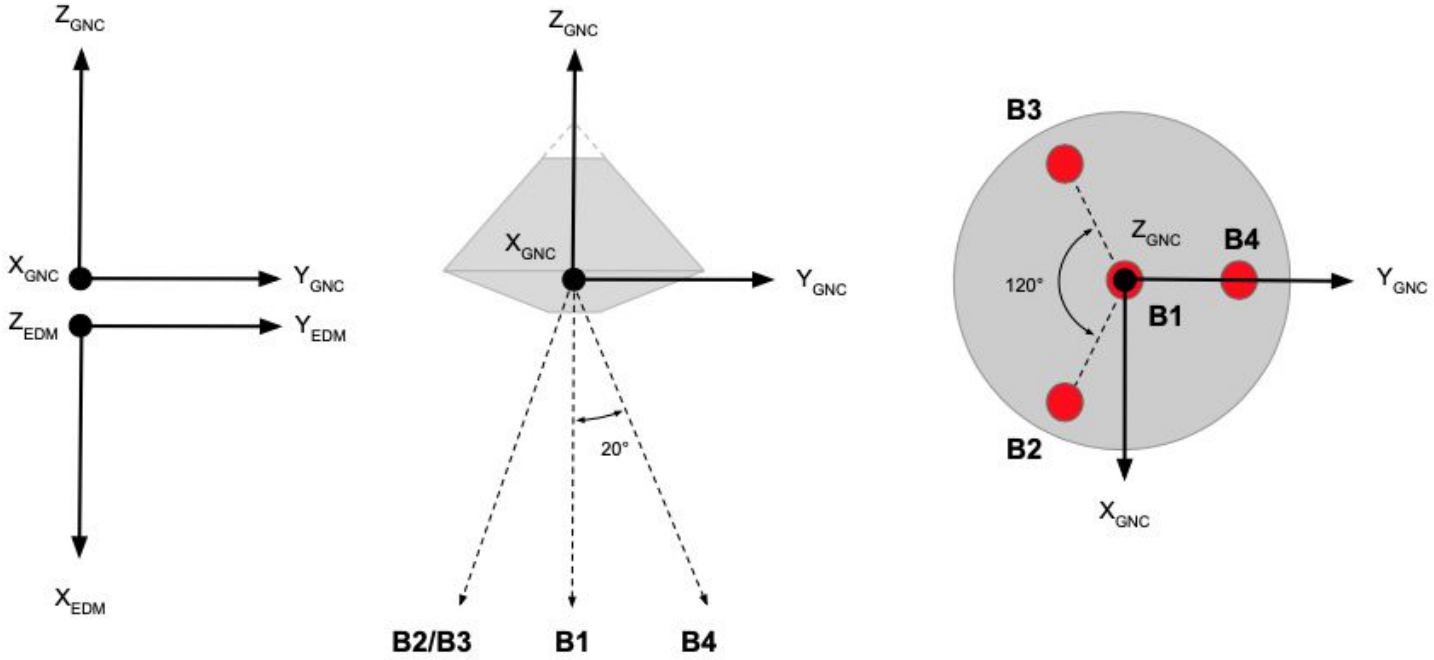

Data	Start	Stop	Samples	Rate	Ref. frame
Angular rate	14:22:43	14:46:58	11174	10 Hz	GNC
Quaternion	14:22:43	14:46:58	11174	10 Hz	MMED to GNC
Total acc.	14:22:43	14:46:45	11129	10 Hz	MMED
Velocity	14:22:44	14:46:45	1108	1 Hz	MMED
Position	14:22:44	14:46:45	1108	1 Hz	MMED
RDA slant-range	14:46:28	14:46:38	2	0.1 Hz	GNC
RDA slant-out	14:45:05	14:46:49	399	10 Hz	GNC
RDA velocity-out	14:45:05	14:46:49	399	10 Hz	GNC

- Schiaparelli crashed on Mars on 19/03/2016
- Only real-time TM produced during Entry and Descent has been produced
- Low-rate IMU and RDA data with big gaps during the plasma blackout phase (entry)

Nevertheless

- The root cause of the failure was identified
- I.e. unexpected gyroscope saturation at parachute opening
- Gyro. data during saturation was reconstructed using acc. data
- The whole trajectory, atmospheric profiles and winds profiles (descent) were retrieved

ExoMars 2016 - Schiaparelli

IMU Data

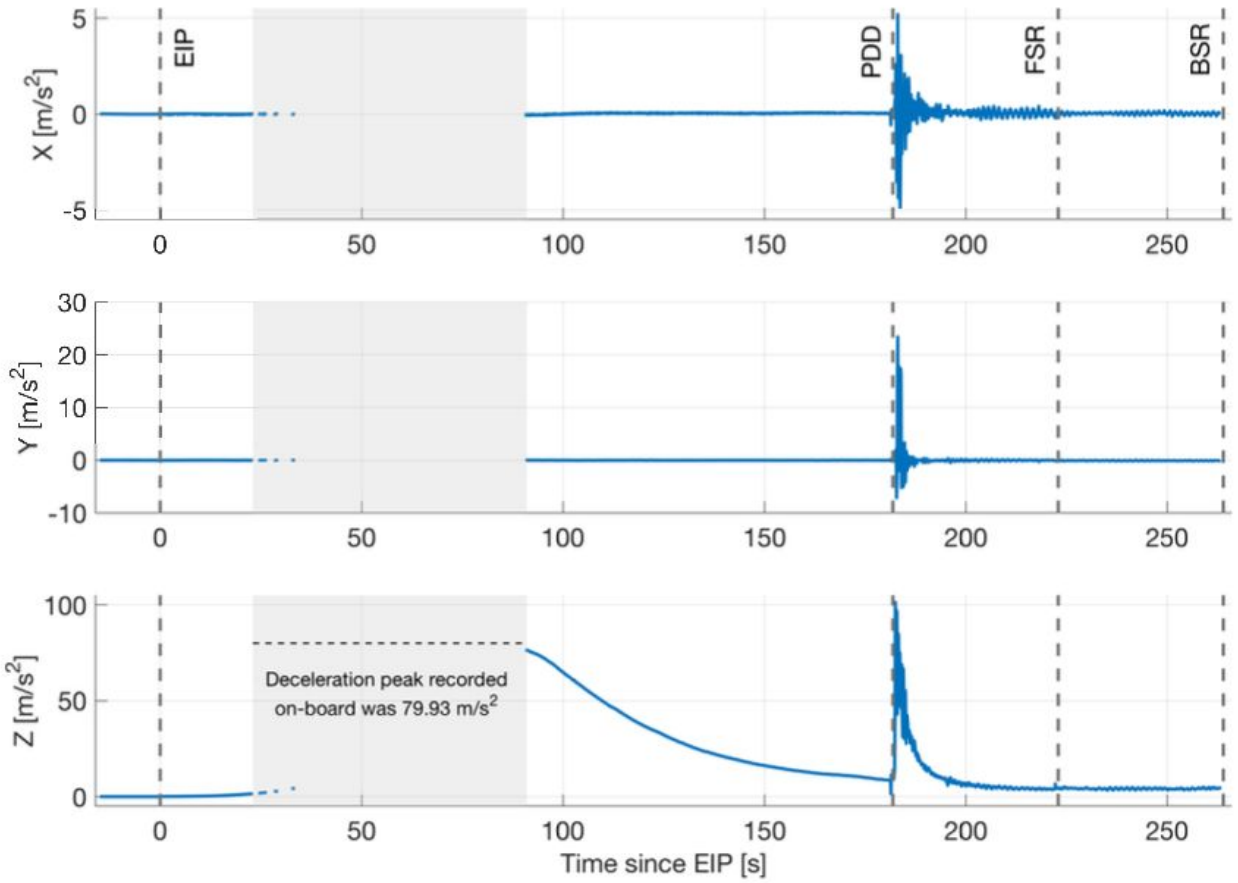

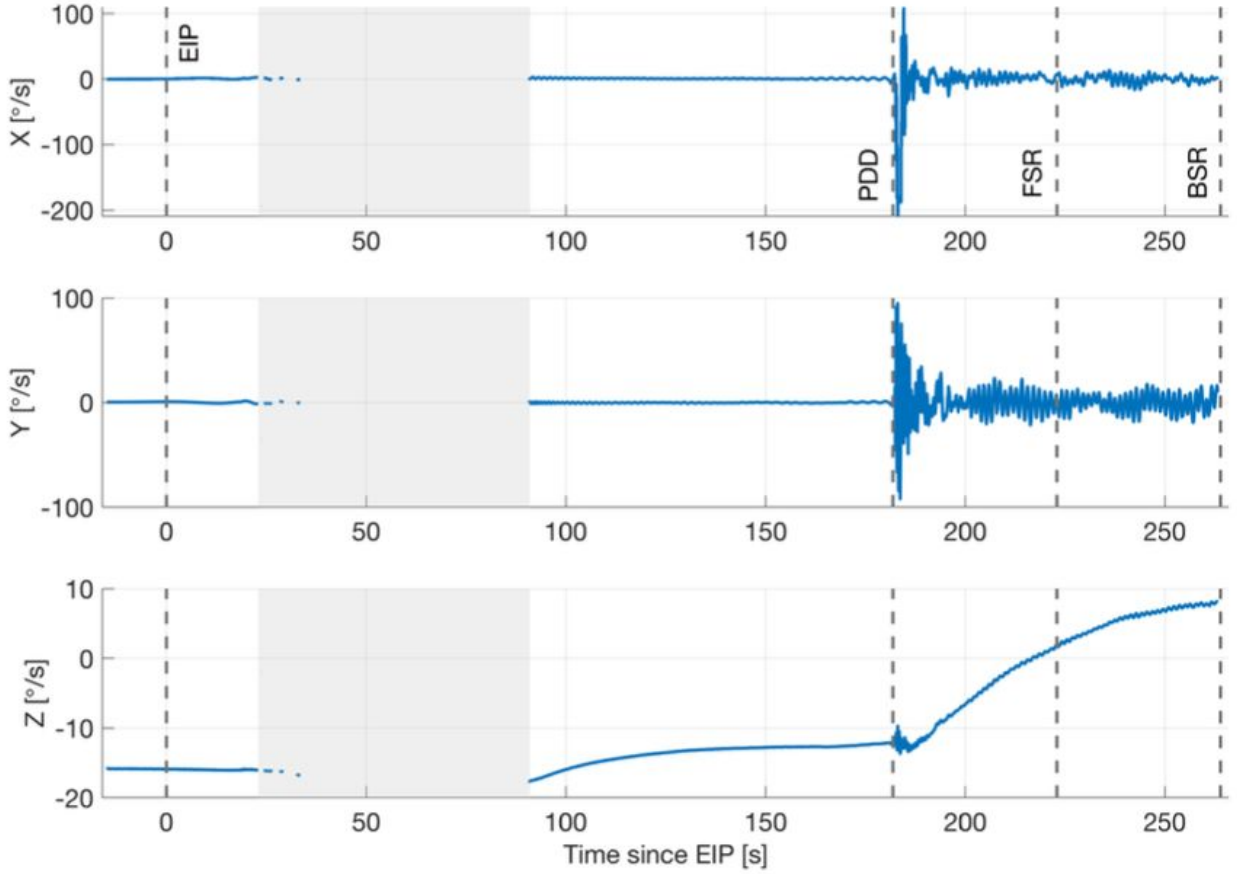

Data issues: low rate (max 10 Hz), about 70 s plasma blackout, X gyro saturated at parachute deployment

ExoMars 2016 - Schiaparelli

Recovery from X Gyro saturation

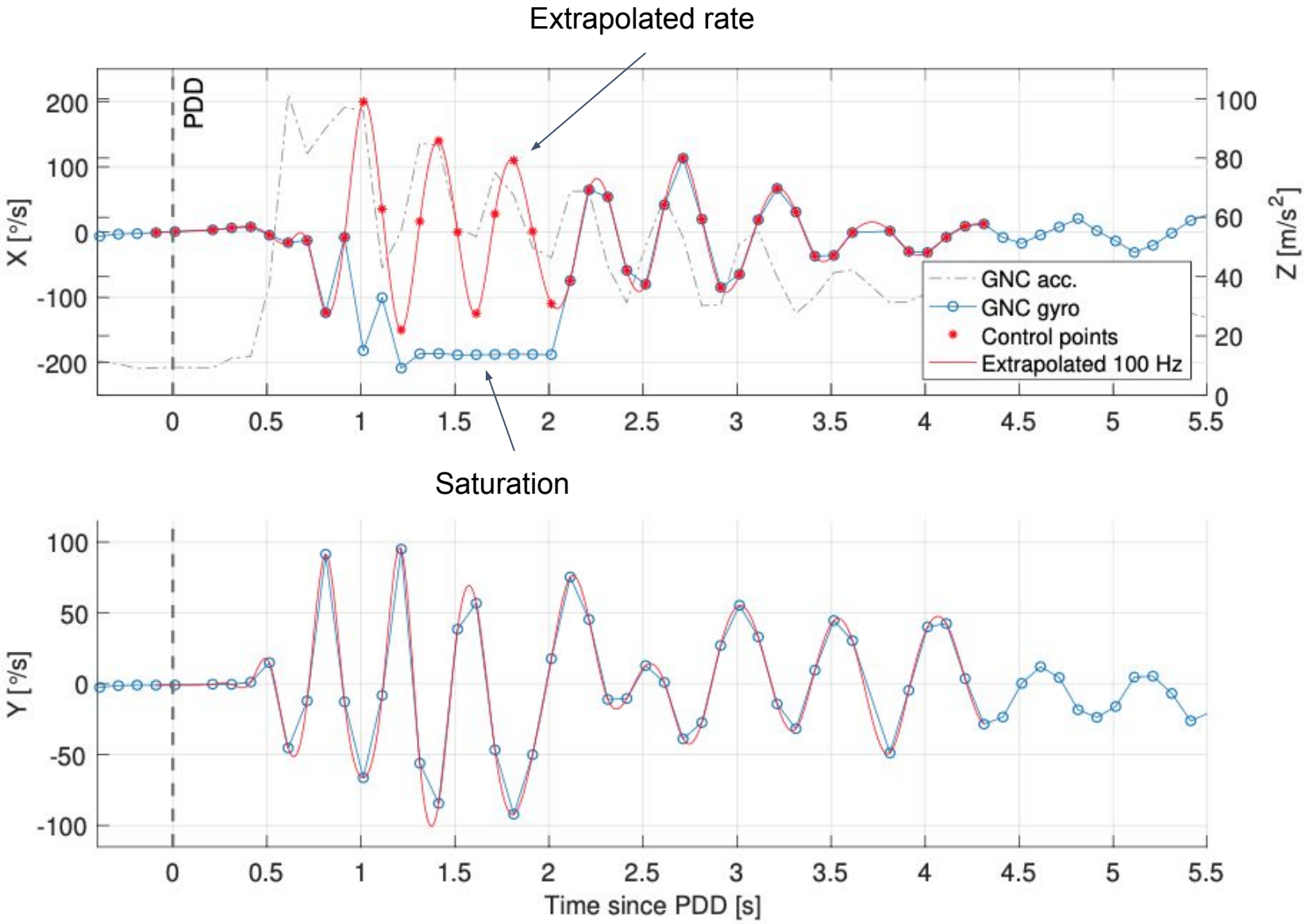

- X Gyro saturated after parachute deployment
- Extrapolated profile was defined to match acceleration data
- Angular rates were resampled at 100 Hz from 0 s to 4.25 s after PDD to improve attitude reconstruction

ExoMars 2016 - Schiaparelli

Definition of the initial state vector and general reconstruction approach

Parameter	Unit	Field	Nominal	Refined	Optimal
Quaternion	N.A.	Q1	0.7250	0.7266	-0.7268
		Q2	-0.2476	-0.2549	0.2534
		Q3	0.3916	0.3884	-0.3858
		Q4	-0.5096	-0.5064	0.5087
Velocity	km/s	X	-4.9636	-4.9614	-4.9446
		Y	-3.3138	-3.3218	-3.3383
		Z	0.8326	0.8192	0.8178
Position	km	X	-1317.4056	-1315.3245	-1317.8932
		Y	3254.8625	3254.2178	3255.1296
		Z	-223.9034	-221.2223	-219.2404

Initial state vector define 15 s after EIP (14:42:07.125)

- **Nominal:** post-separation prediction of position and velocity plus the GNC attitude refined on-board
- **Refined:** identified by dispersion analysis to get the best consistency with RDA data and events timing
- **Optimal:** obtained by RDA assimilation with Kalman smoother see next slide

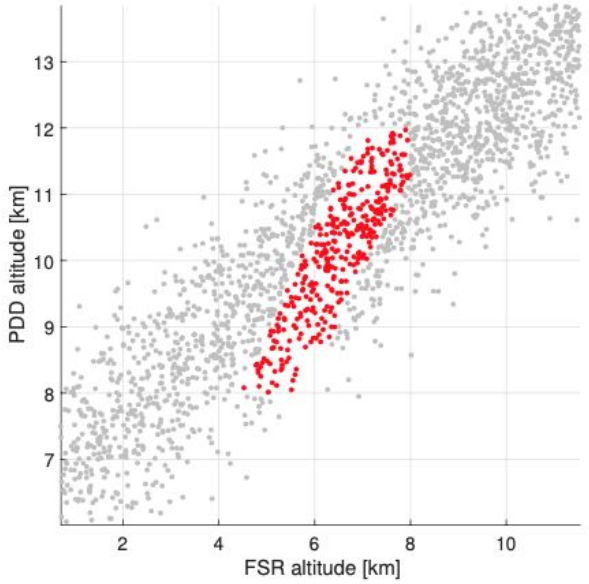

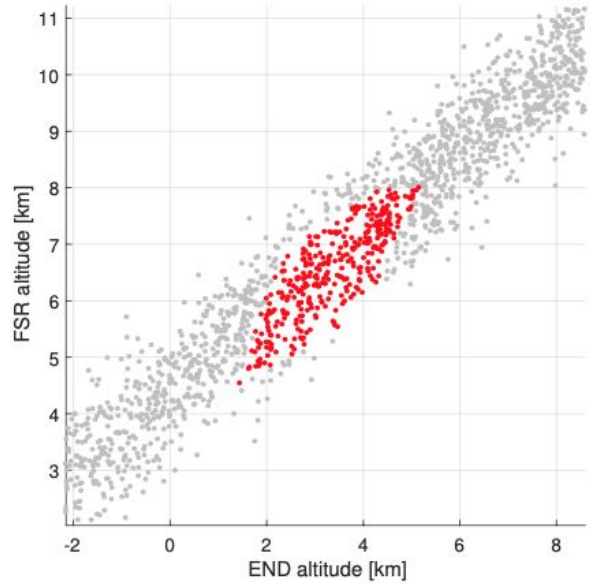

- Dispersion analysis has been performed by perturbation of Nominal initial state vector (10000 run)
- Viable trajectories (red dots) selected according to: Mach @ PDD, PDD altitude, FRR altitude, end altitude and time of impact
- Refined state obtained as the mean of the perturbed init. states of the selected trajectories

ExoMars 2016 - Schiaparelli

Optimal trajectory obtained by RDA assimilation and backward propagation

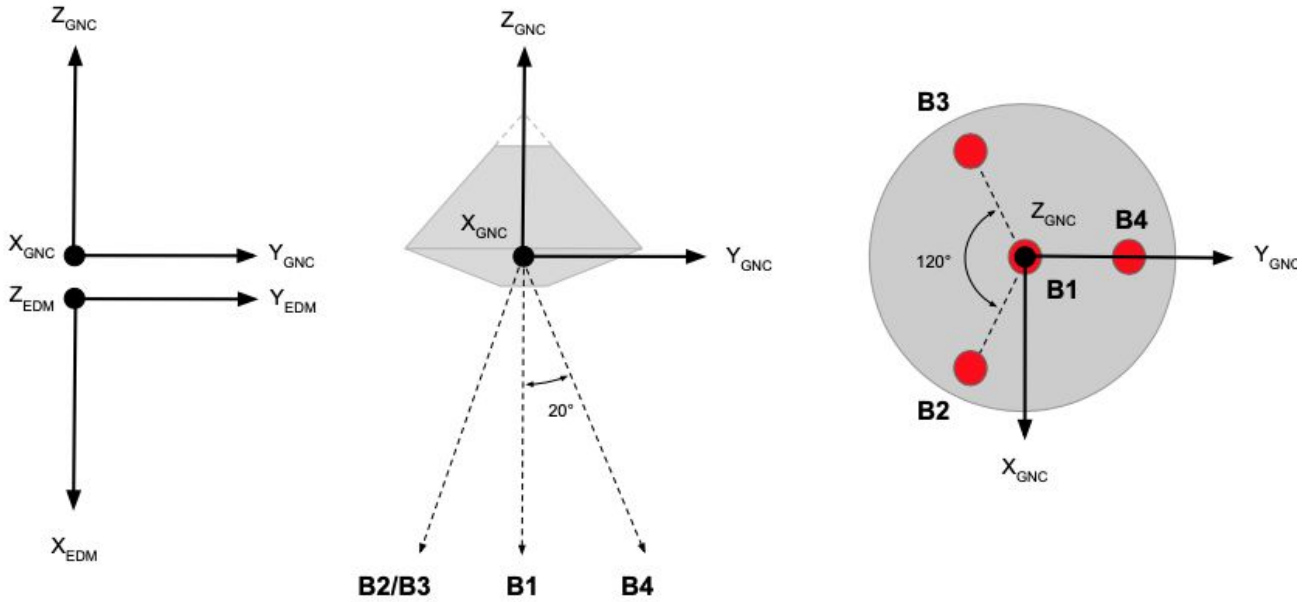

Sample	UTC	B0 m	B1 m	B2 m	B3 m	Alt. AGL m	Off-vert. °
RDA3	14:46:28.363	5932.10	6515.18	6969.29	5563.50	5544.02	20.48
RDA4	14:46:38.363	4764.35	4966.60	5051.11	5237.19	4755.66	4.89

- Input: 2 x valid points with four beams, slant-out profile, terrain relative speed (10 Hz)
- Residuals are almost Gaussian and well inside the unc. bounds
- Slant-out profile evidenced an off-vertical shift probably due to winds

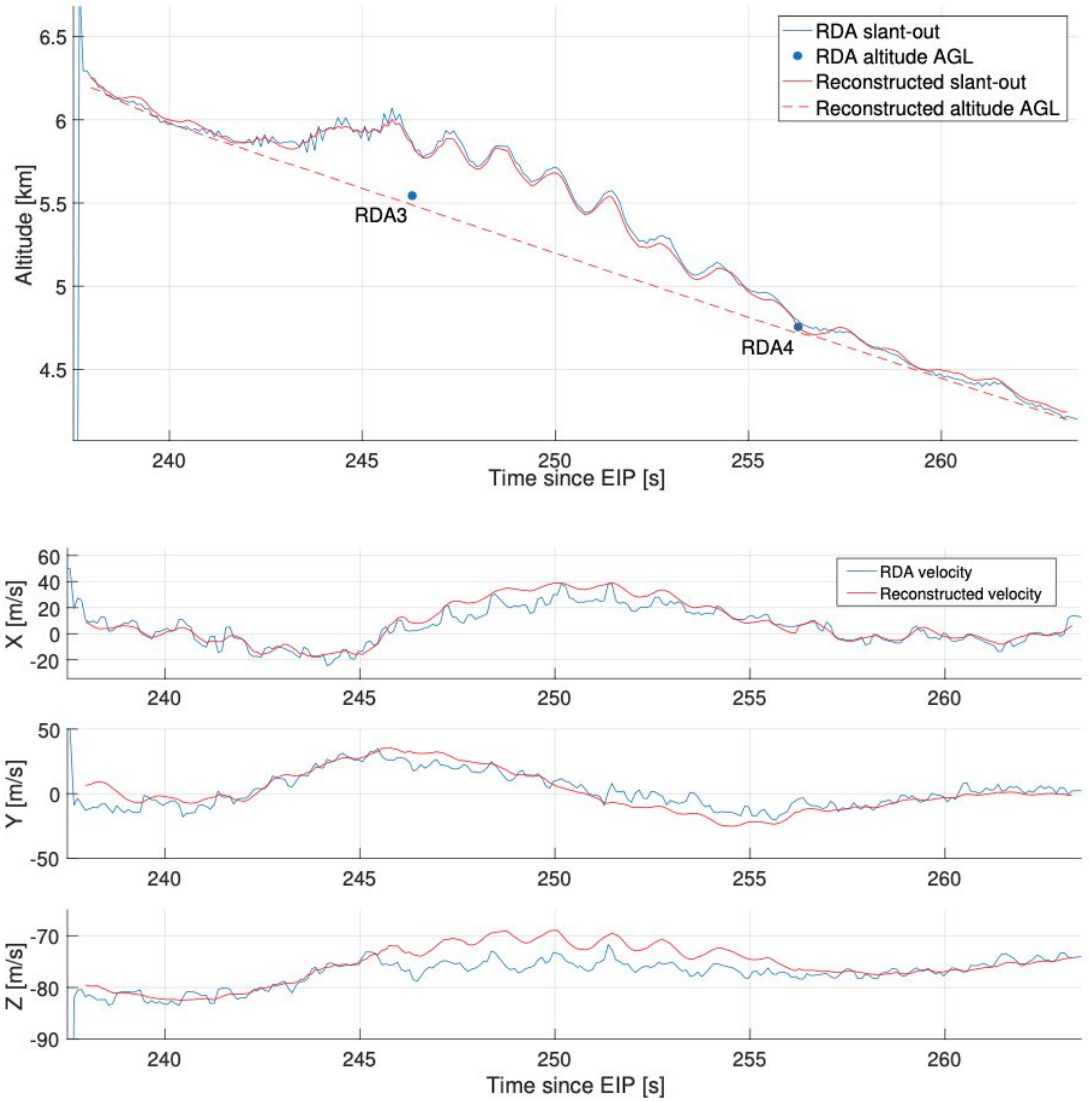

ExoMars 2016 - Schiaparelli

Reconstructed trajectory, relevant parameters at key events and related uncertainties

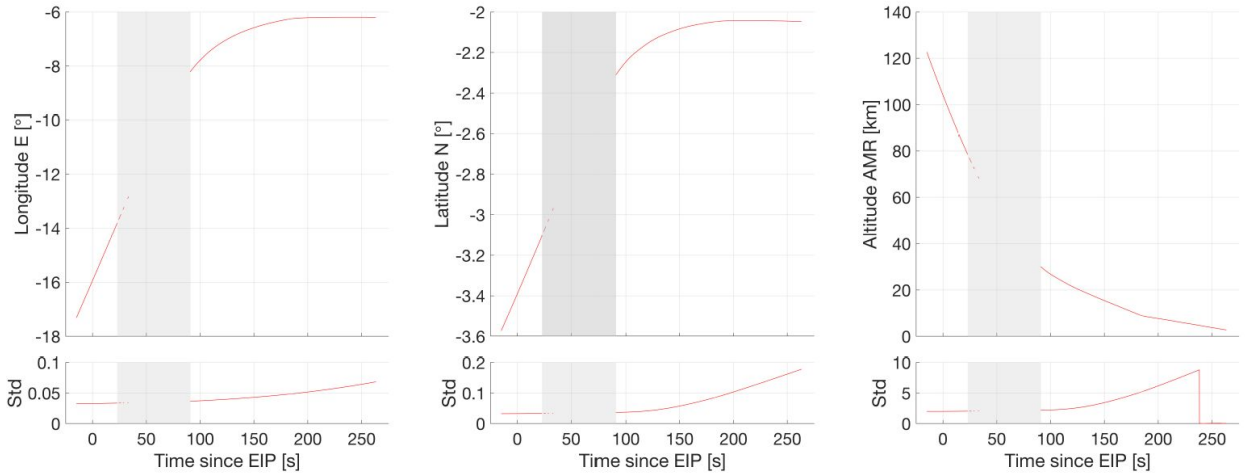

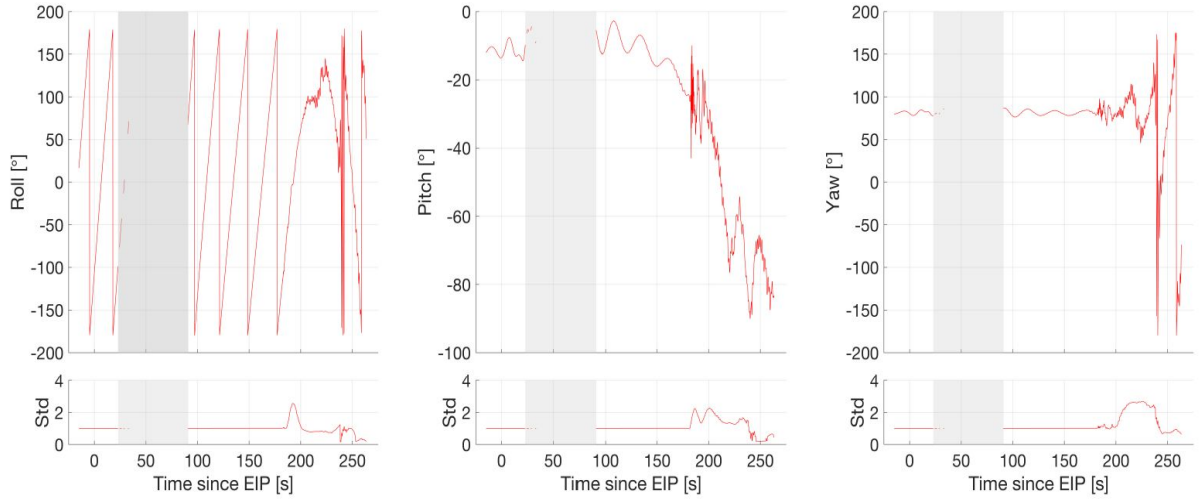

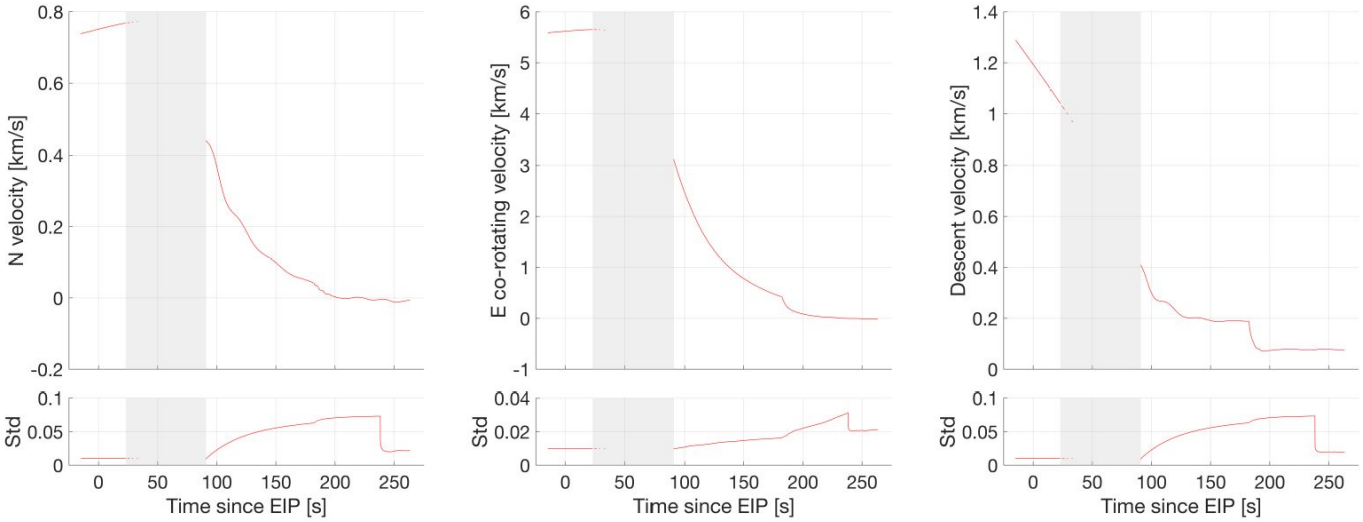

Name	Unit	First	EIP	PDD	FSR	Last
Time	UTC	14:42:07.125	14:42:22.132	14:45:23.923	14:46:05.135	14:46:45.341
Roll	◦	16.50±1.00	-105.55±1.00	-122.09±1.01	123.05±0.81	50.80±0.18
Pitch	◦	-12.03±1.00	-13.50±1.00	-26.41±1.04	-70.77±1.29	-83.19±0.44
Yaw	◦	79.88±1.00	80.36±1.00	81.54±1.02	70.55±2.66	-73.23±0.63
Vel.	km/s	6.0219± 0.0173	6.0326± 0.0173	0.6950± 0.0907	0.2724± 0.1048	0.2390± 0.0170
FPA	◦	12.36	11.41	15.74	16.73	18.12
HDA	◦	82.79	82.70	86.39	89.85	-88.33
N vel.	km/s	0.7383± 0.0100	0.7512± 0.0100	0.0421± 0.0630	0.0007± 0.0725	-0.0066± 0.0219
E vel.	km/s	5.5867± 0.0100	5.6179± 0.0100	0.4263± 0.0163	0.0199± 0.0269	-0.0137± 0.0209
D vel.	km/s	1.2895± 0.0100	1.1930± 0.0100	0.1886± 0.0632	0.0784± 0.0727	0.0743± 0.0195
Lon. E	◦	-17.3091± 0.0326	-15.9337± 0.0329	-6.2692± 0.0482	-6.1946± 0.0571	-6.1961± 0.0685
	km	± 2.0049	± 2.0100	± 2.8656	± 3.3910	± 4.0662
Lat. N	◦	-3.5723± 0.0326	-3.3897± 0.0328	-2.0488± 0.0846	-2.0430± 0.1302	-2.0473± 0.1784
	km	± 2.0010	± 2.0064	± 5.0269	± 7.7295	± 10.5831
Alt. AMR	km	122.6329± 2.0000	104.0366± 2.0056	9.3871± 5.0513	5.9022± 7.7563	2.7630± 0.0390

ExoMars 2016 - Schiaparelli

Trajectory shape and consistency with the impact points

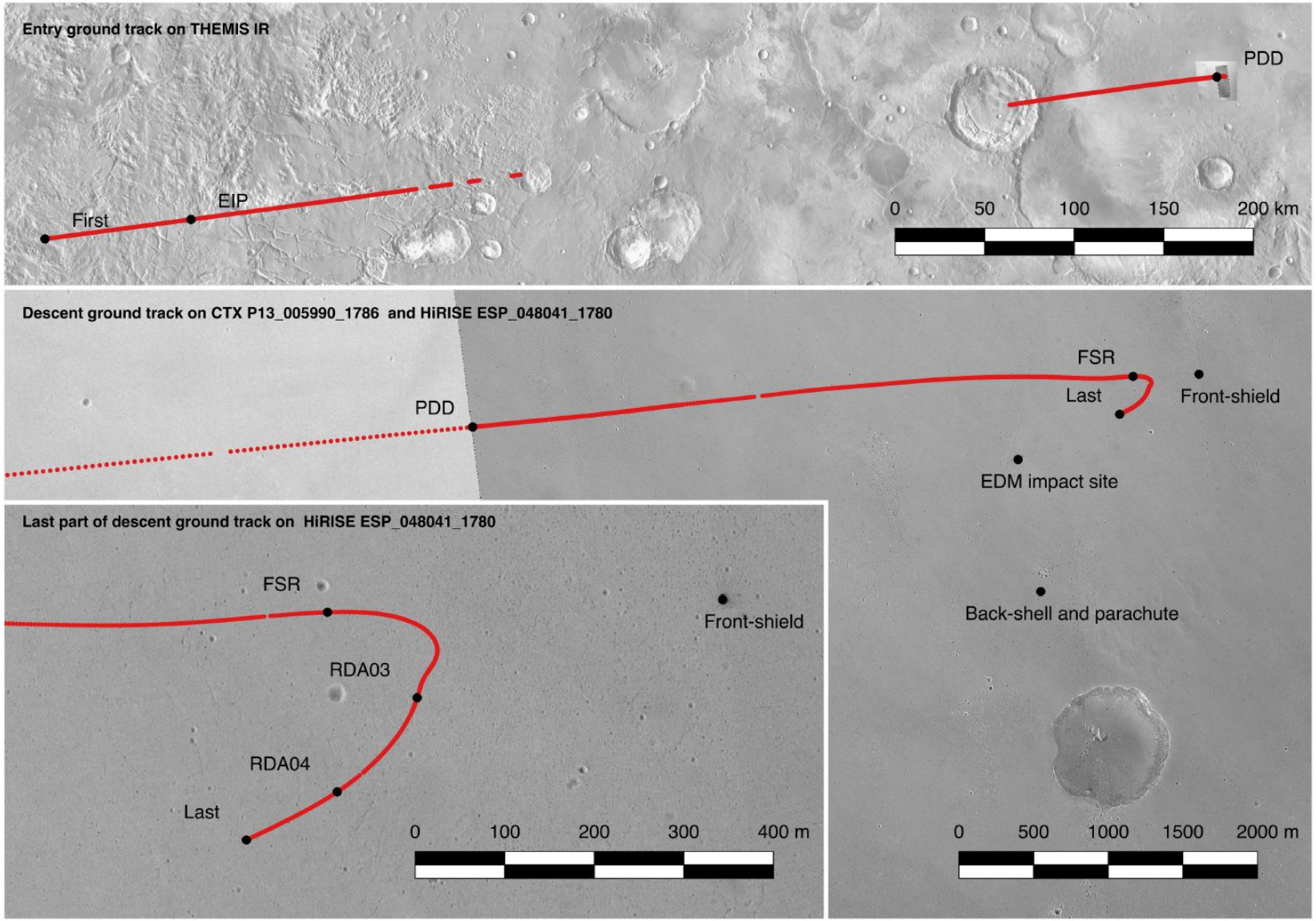

ExoMars 2016 - Schiaparelli

Reconstruction of the atmospheric structure

- Atmospheric profiles were derived from drag equation using Z axis acceleration

$$ma = \frac{1}{2}\rho v_r^2 C S \qquad\qquad v_r = \|\boldsymbol{v}_i - \boldsymbol{v}_s - \boldsymbol{v}_w\|$$

- Assumption 1: zero or negligible winds
- Assumption 2: hydrostatic equilibrium; used to compute pressure from density

$$\frac{dP}{dh} = -\rho g_h$$

- Assumption 3: Ideal gas law; used to get temperature (M = 43.41 g/mol mean molar mass of martian atmosphere)

$$T = \frac{PM}{\rho k_B N_A}$$

ExoMars 2016 - Schiaparelli

Reconstruction of the atmospheric structure given the trajectory

- Atmospheric profiles were derived from drag equation using Z axis acceleration

$$ma = \frac{1}{2}\rho v_r^2 C S$$

$$v_r = \|\boldsymbol{v}_i - \boldsymbol{v}_s - \boldsymbol{v}_w\|$$

- Assumption 1: zero or negligible winds
- Assumption 2: hydrostatic equilibrium; used to compute pressure from density

$$\frac{dP}{dh} = -\rho g_h$$

- Assumption 3: Ideal gas law; used to get temperature (M = 43.41 g/mol mean molar mass of martian atmosphere)

$$T = \frac{PM}{\rho k_B N_A}$$

- Entry

$$\rho = \frac{2 m_D a_Z}{v_r^2 C_D S_D}$$

- Descent

$$\rho = \frac{2 (m_D + m_P) a_Z}{v_r^2 (C_D S_D + C_P S_P)}$$

- For the descent phase: the mass of air dragged by the parachute must be estimated and parachute is assumed aligned with the descent module

ExoMars 2016 - Schiaparelli

Iterative atmosphere reconstruction

- Init:
  - Start from initial density and pressure profiles (eng. models)
  - Or assume a constant C_D (e.g. 1.6/1.7) and an initial value for the pressure at EIP (e.g. 7e-3 Pa)
- Loop:
  - Compute atmospheric profiles from top to bottom of the atmosphere
  - Compute Mach/Knudsen and get CD from the AEDB
- Termination after a max number of loops or when the relative variation of the density falls below a given threshold (usually 3 to 5 iterations are enough)
- For Schiaparelli an additional step was needed: <u>density during plasma blackout was interpolated</u> using an polynomial/exponential function

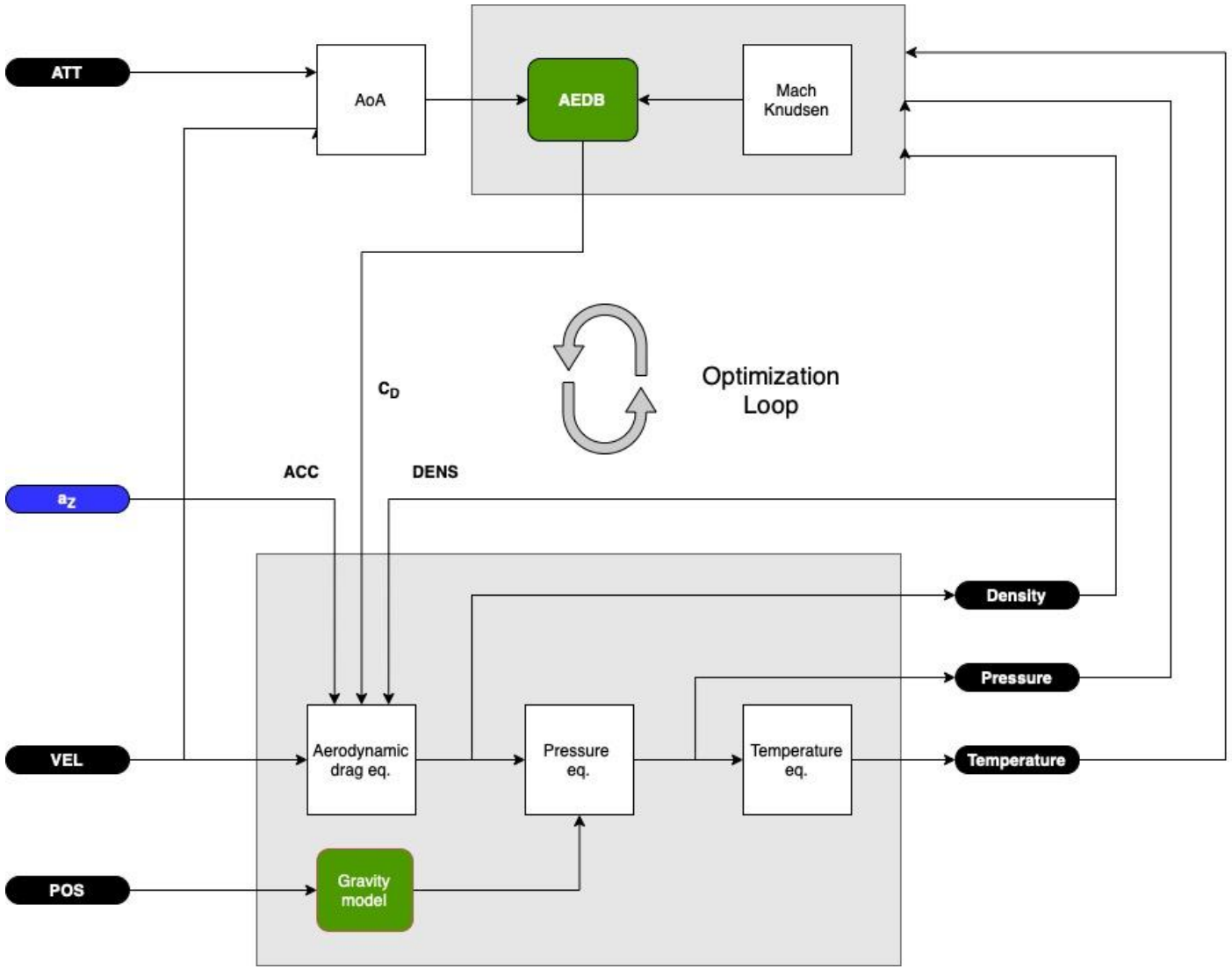

ExoMars 2016 - Schiaparelli

Comparison of computed atmospheric profiles with available models

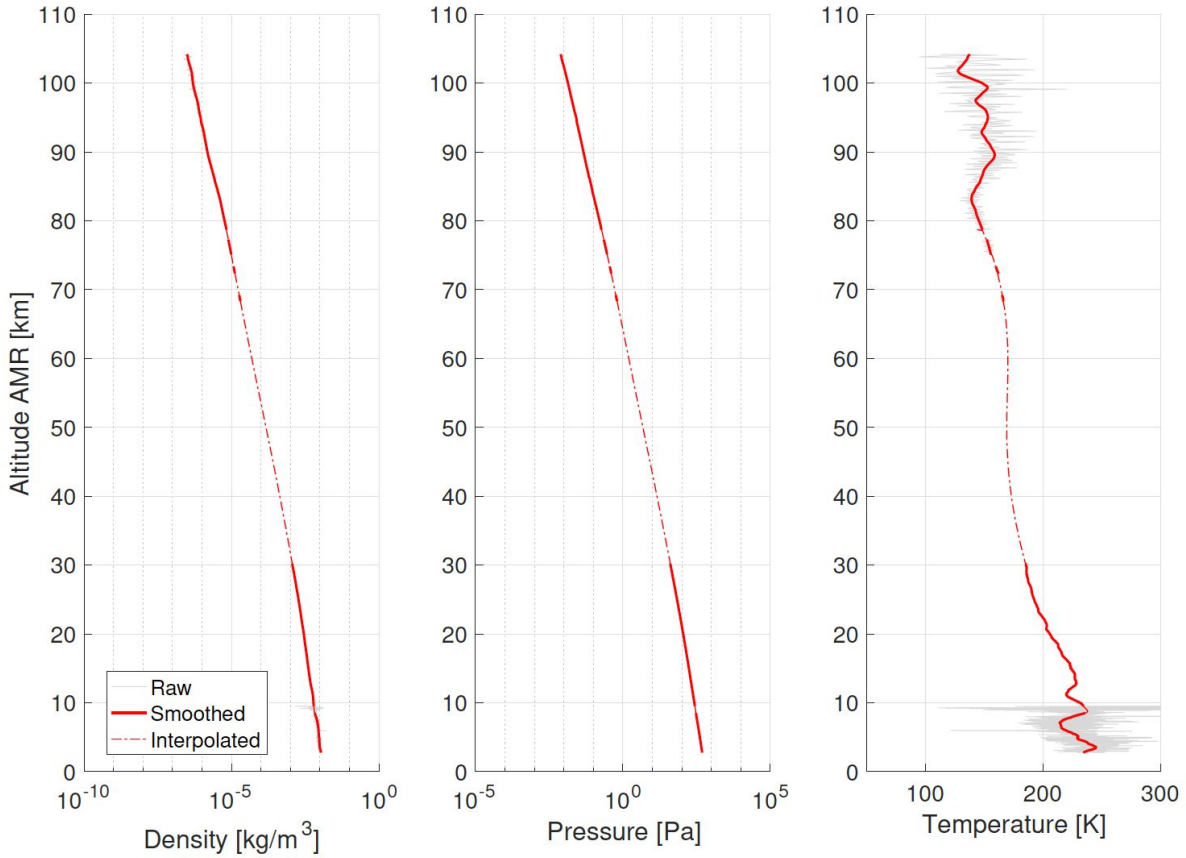

Parameter	Model	Entry before blackout min	Entry before blackout max	Entry after blackout min	Entry after blackout max	Descent min	Descent max
Density	MCD clim.	7.31	40.26	-0.60	11.70	-1.34	11.47
	MCD dust	-75.38	-58.05	1.92	13.18	2.53	18.21
	MCD cold	-14.80	15.01	0.95	12.37	0.42	13.85
	MCD warm	53.56	89.32	-3.52	17.37	-4.30	8.00
Pressure	MCD clim.	14.16	41.46	3.96	9.32	3.49	7.15
	MCD dust	-73.86	-64.74	-18.29	3.93	2.44	7.30
	MCD warm	-10.79	13.05	-2.69	6.65	3.02	7.01
	MCD cold	60.28	88.19	4.51	23.50	2.85	6.84
	MY24	-3.61	2.12	1.62	4.36	1.18	2.09
	MY25	-22.80	-17.92	-4.74	3.00	2.18	3.34
	MY26	6.44	12.10	1.24	6.01	0.31	1.29
Temperature	MCD clim.	-6.49	11.63	-3.16	4.35	-5.64	4.64
	MCD dust	-16.14	15.47	-20.30	-3.29	-11.56	1.43
	MCD warm	-9.79	11.09	-9.68	2.09	-7.78	2.33
	MCD cold	-8.23	8.78	2.59	9.25	-2.62	8.31
	MY24	-12.35	5.27	-4.56	3.32	-6.43	6.58
	MY25	-10.60	6.17	-10.16	2.14	-7.26	6.35
	MY26	-10.50	8.81	-2.20	4.16	-5.32	7.30

% min/max difference between dens/pres/temp profiles and available models: MCD climatology and MY24/26 match well

ExoMars 2016 - Schiaparelli

Comparison of computed atmospheric profiles with available models before PDD

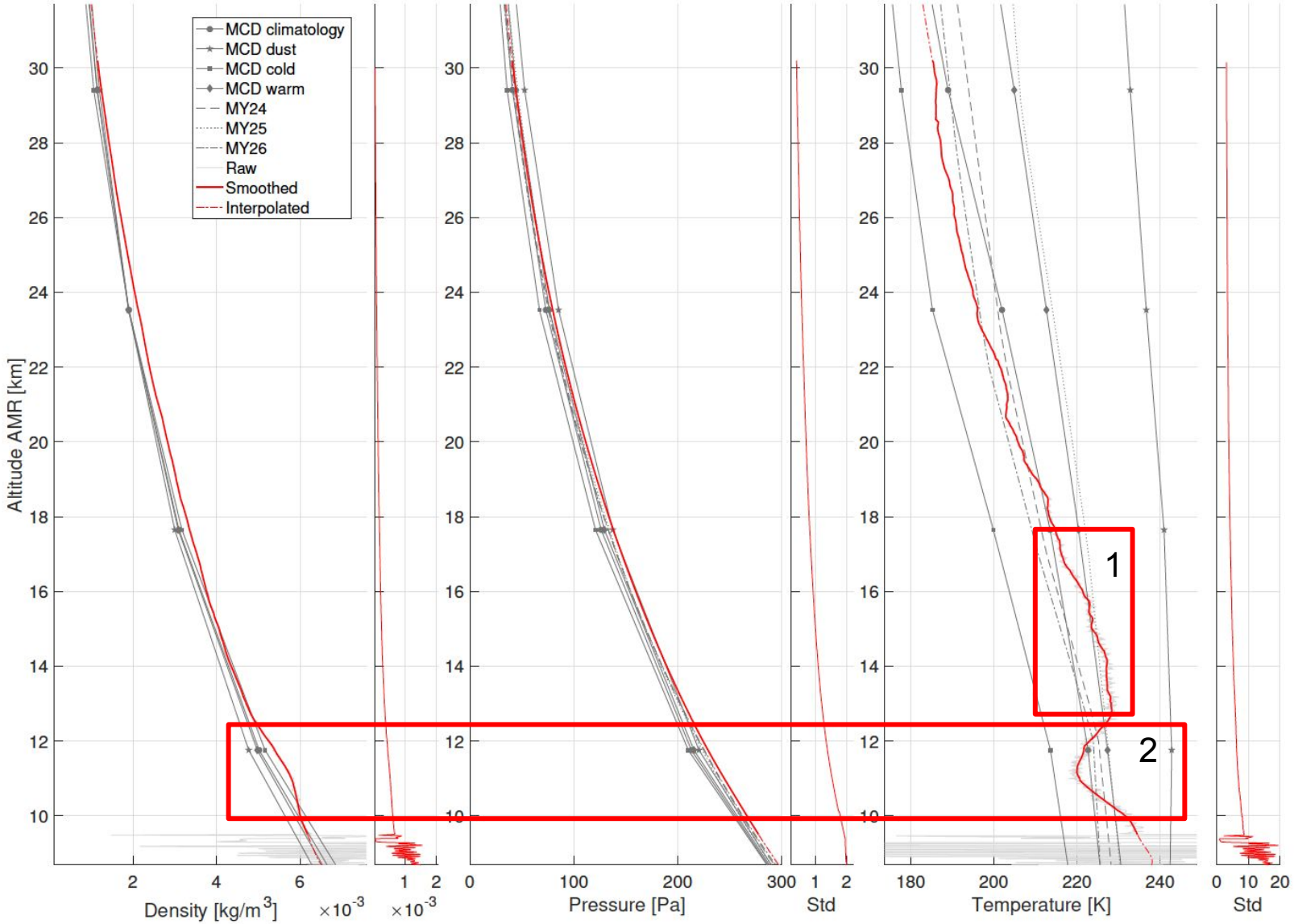

- % variation is not enough, a closer look is needed to properly compare reconstructed profiles with models
- Example: entry profiles after the blackout
- (1) Unexpected increase in temperature wrt MY and MCD clim. probably caused by inaccurate estimation of the flow angles
- (2) Temperature inversion is realistic and observed by other missions

ExoMars 2016 - Schiaparelli

Comparison of computed atmospheric profiles with available models after PDD

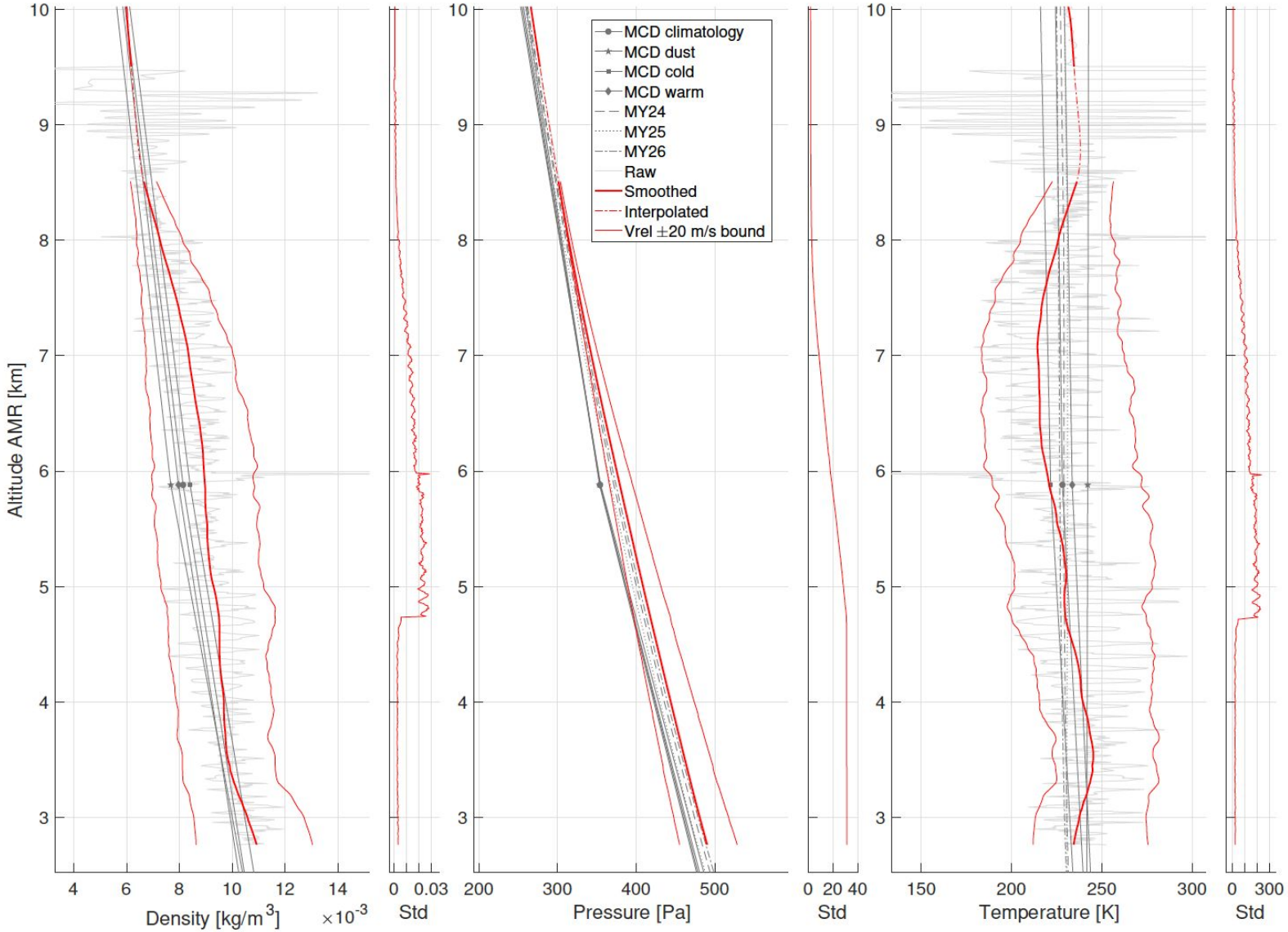

- Atmospheric profiles under parachute have high uncertainty (gray) because of high density and low speed

$$\frac{\partial \rho}{\partial v_r} = -\frac{\rho}{v_r}$$

- Nevertheless the smoothed profiles (red) are consistent with the models

ExoMars 2016 - Schiaparelli

Identification of winds during the last part of the descent

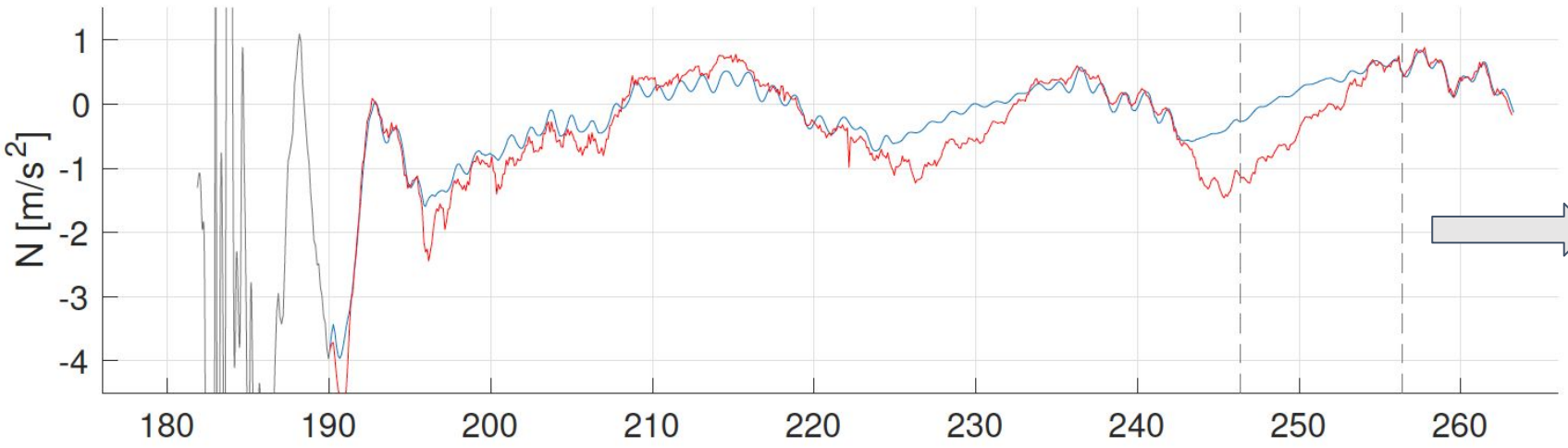

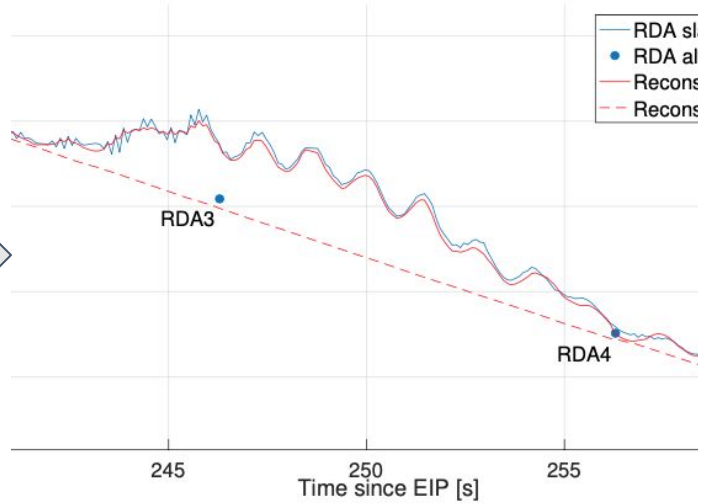

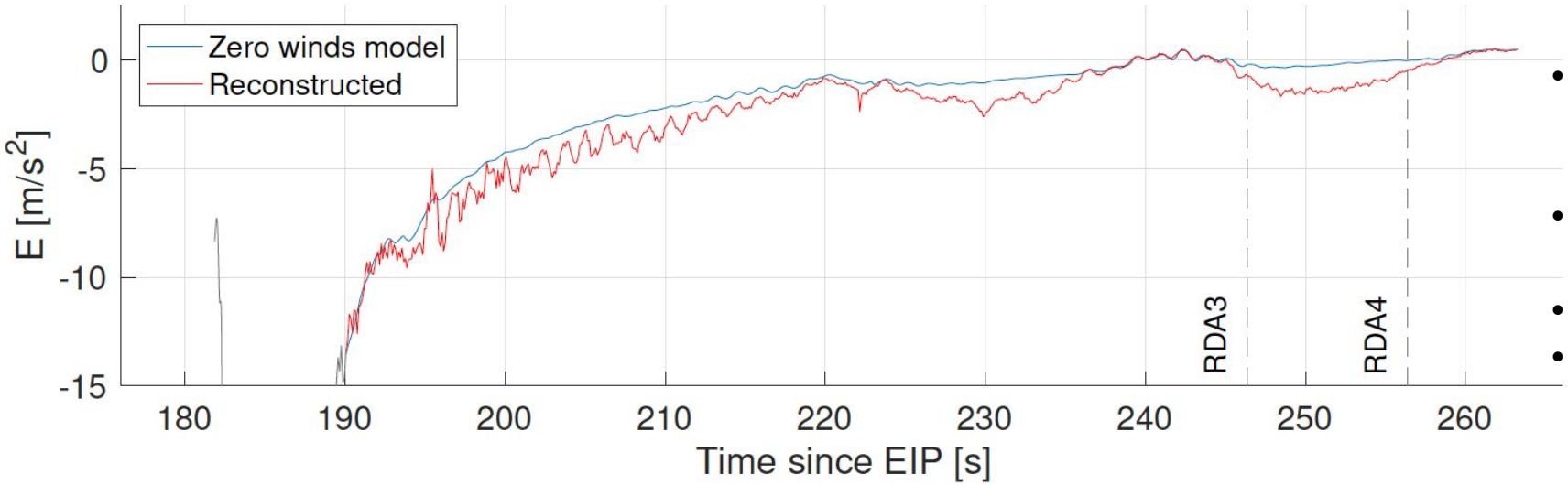

- RED: N/E acceleration measured on-board
- BLUE: N/E acceleration predicted by the 9 DoF model used for the simulator with atm. wind forced to 0
- The difference is the effect of the wind
- Confirmed by the measured slant-out
- and by the hook on the ground track

ExoMars 2016 - Schiaparelli

Identification of winds during the last part of the descent

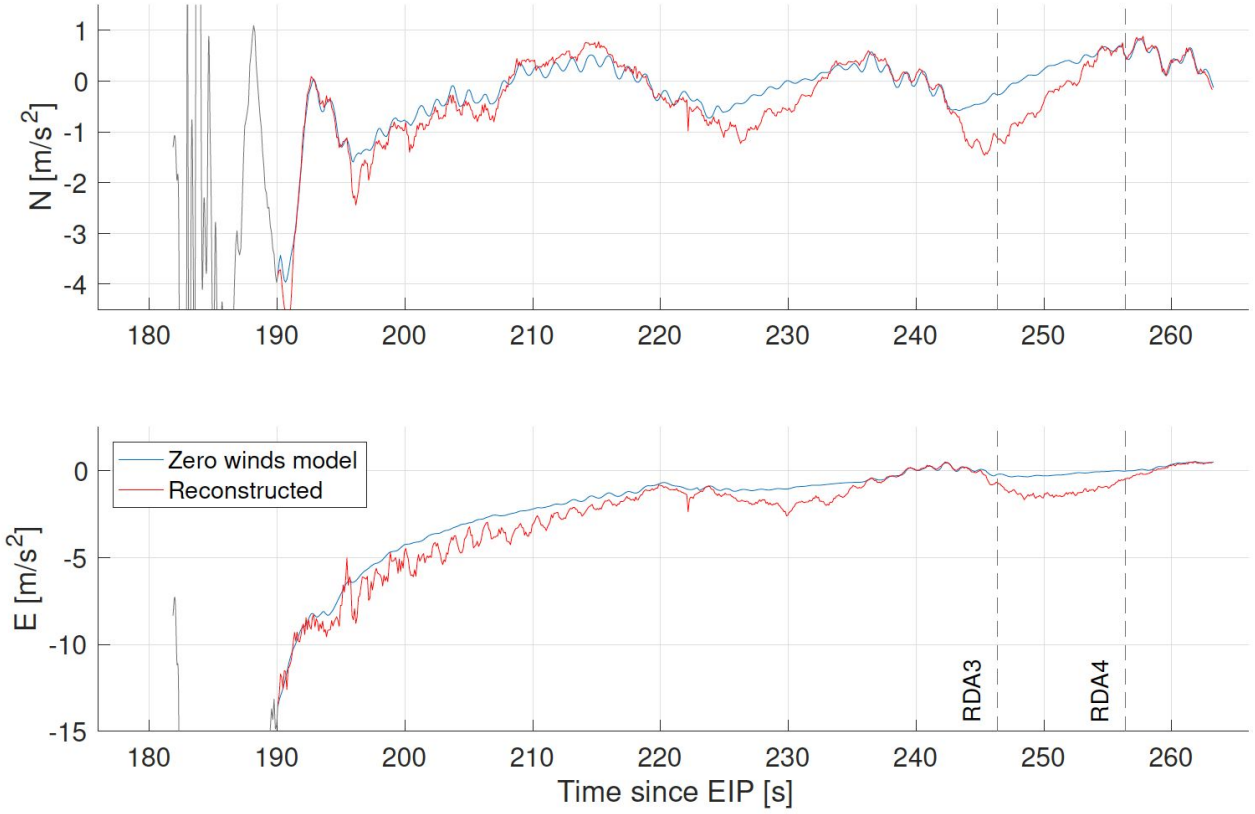

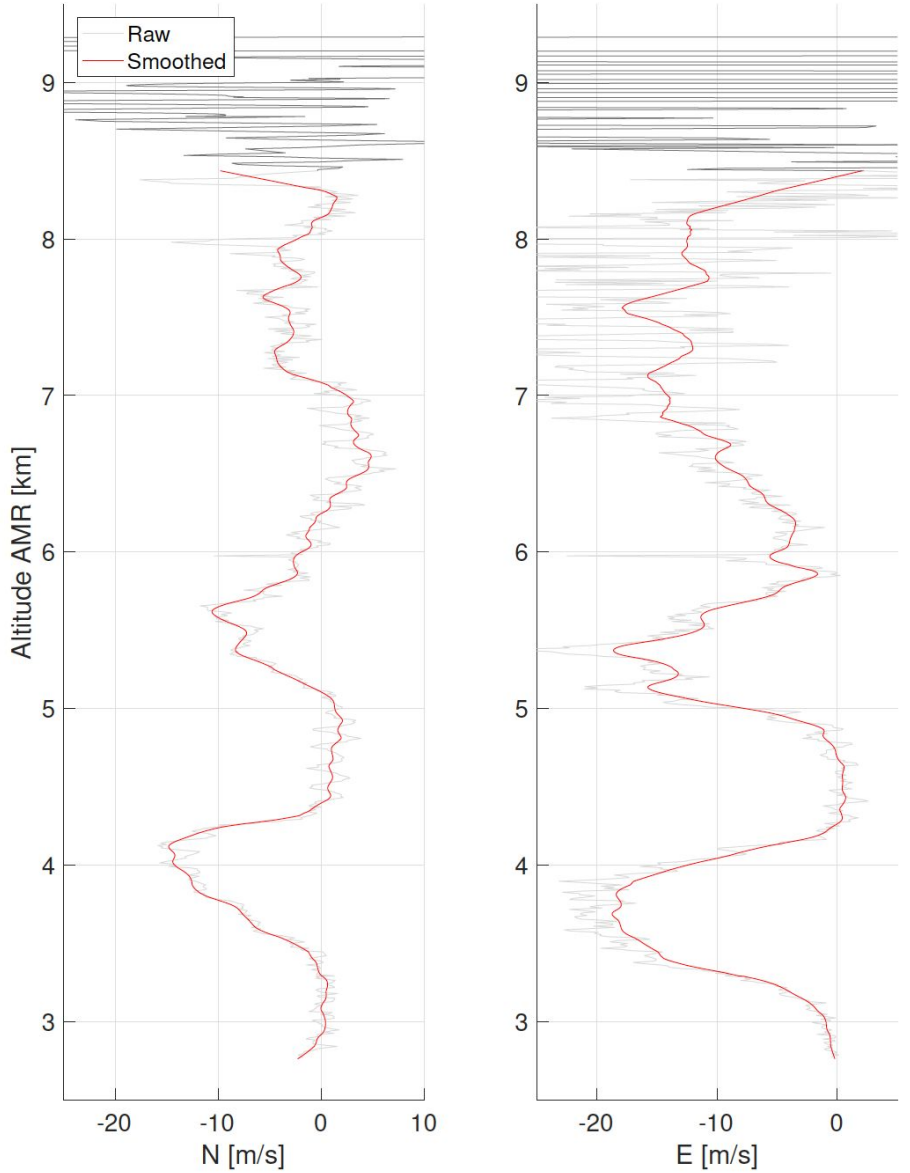

Using the AEDB it is possible to compute the wind speed (residual acc needed to obtain the red profile from the blue)

Simultaneous Trajectory and Atmosphere Reconstruction

Bayesian algorithm with an augmented state model

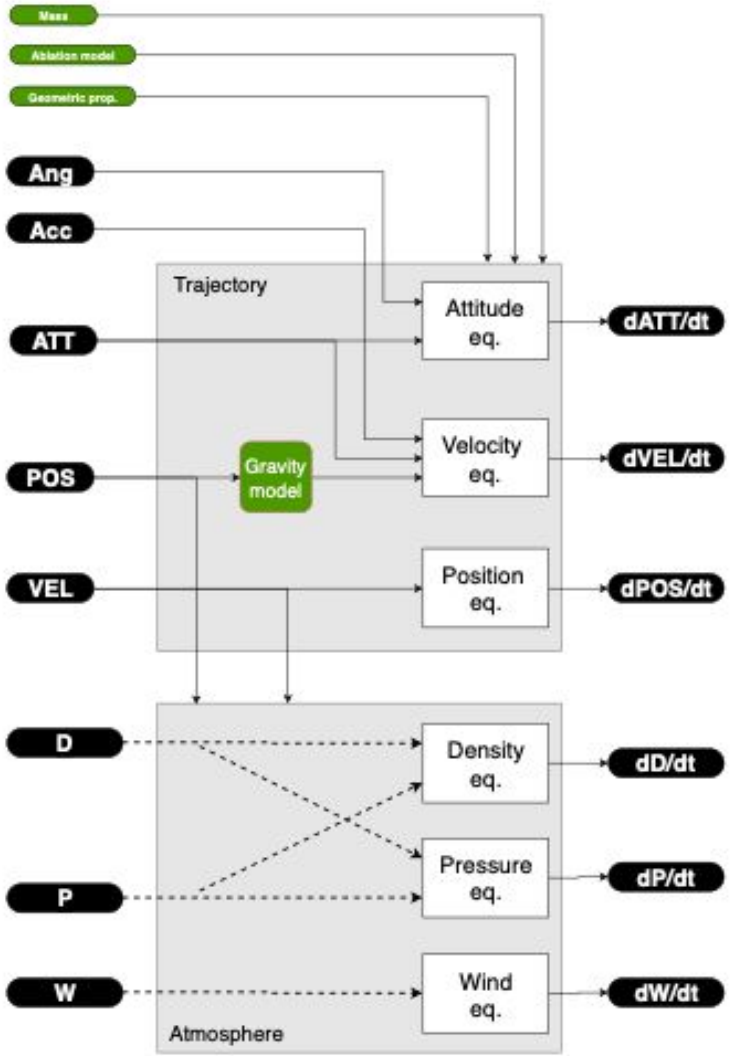

- Density, pressure and (optionally) winds are added to the state vector
- Time variation of such parameters can be formulated in different ways
- Assumptions: hydrostatic eq. and ideal gas law

A

$$\dot{\rho} = 0$$

$$\dot{p} = -g\,\rho\,v$$

$$\dot{w} = 0$$

- No constraints on density
- No constraints on winds

B

$$\dot{\rho} = \alpha\,\rho$$

$$\dot{p} = -g\,\rho\,v$$

$$\dot{w} = 0$$

- Smoothness constraint on density
- No constraints on winds

C

$$\dot{\rho} = \frac{\mu\,\rho^2\,v}{r^2\,p}$$

$$\dot{p} = \frac{\mu\,\rho\,v}{r^2}$$

$$\dot{w} = 0$$

- Density and pressure linked by hydrostatic eq. and ideal gas law
- No constraints on winds

Neptune Entry Simulation

1D Entry Simulation based on Neptune atmosphere engineering model

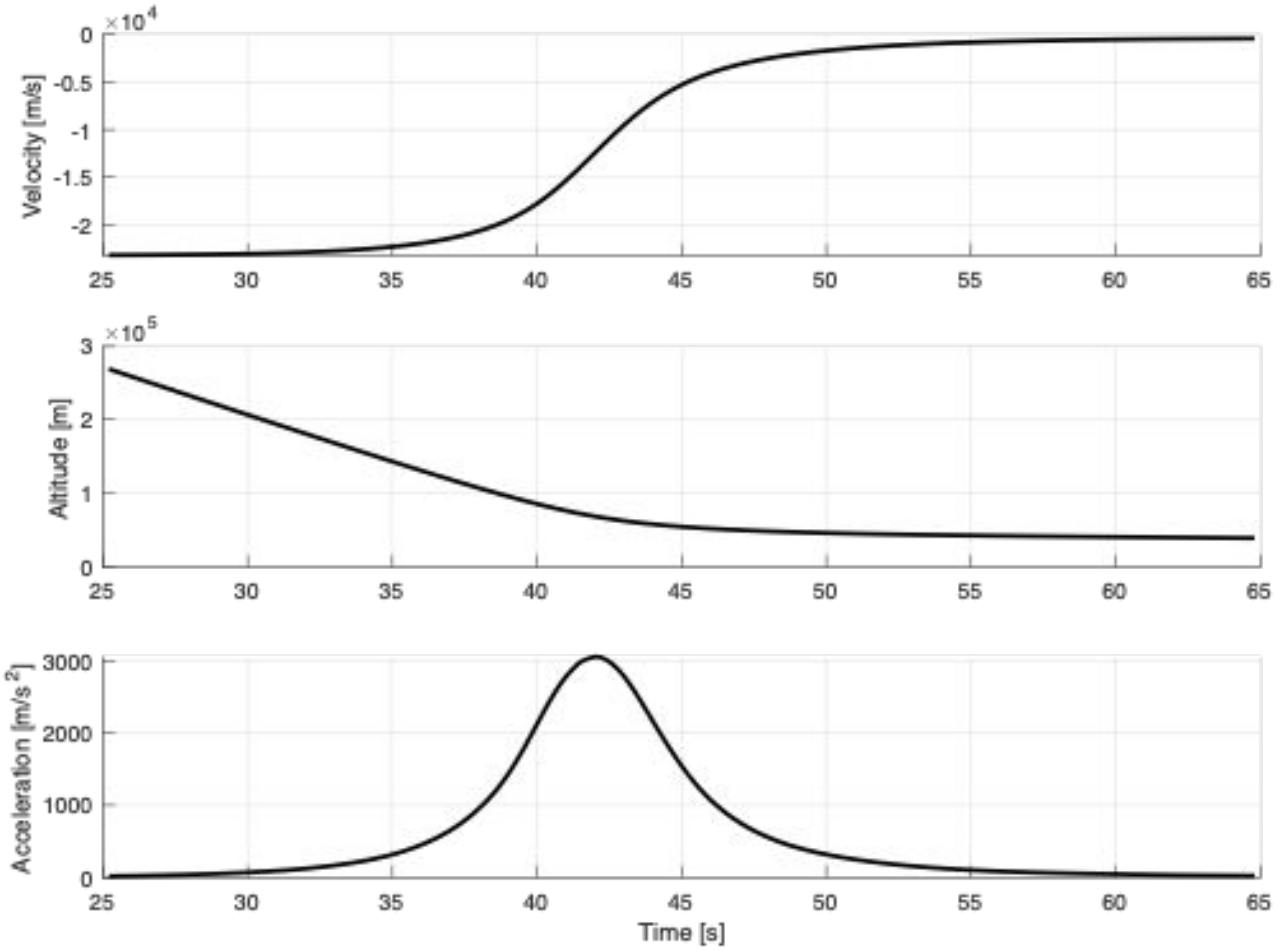

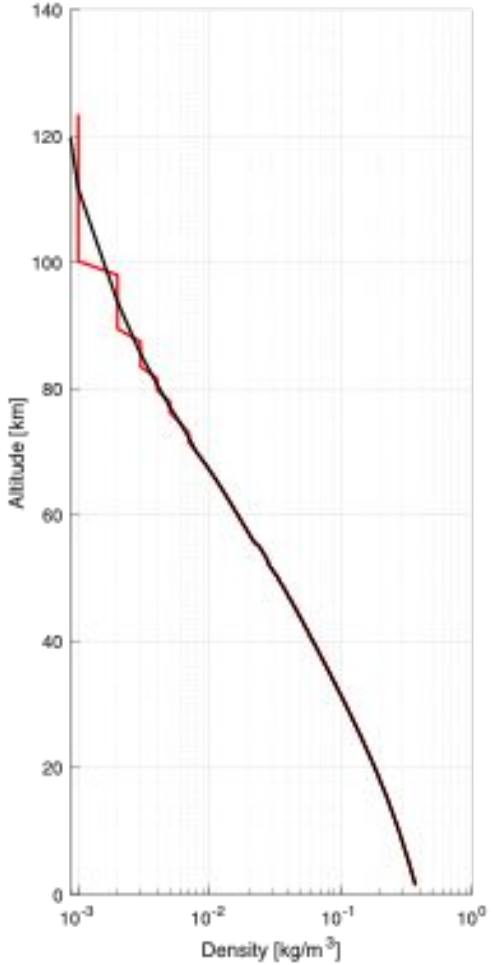

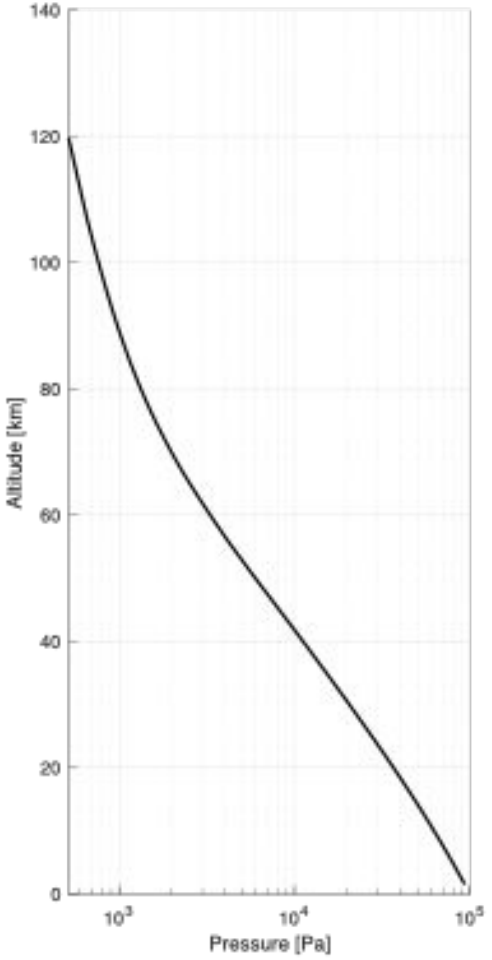

Neptune Entry Reconstruction

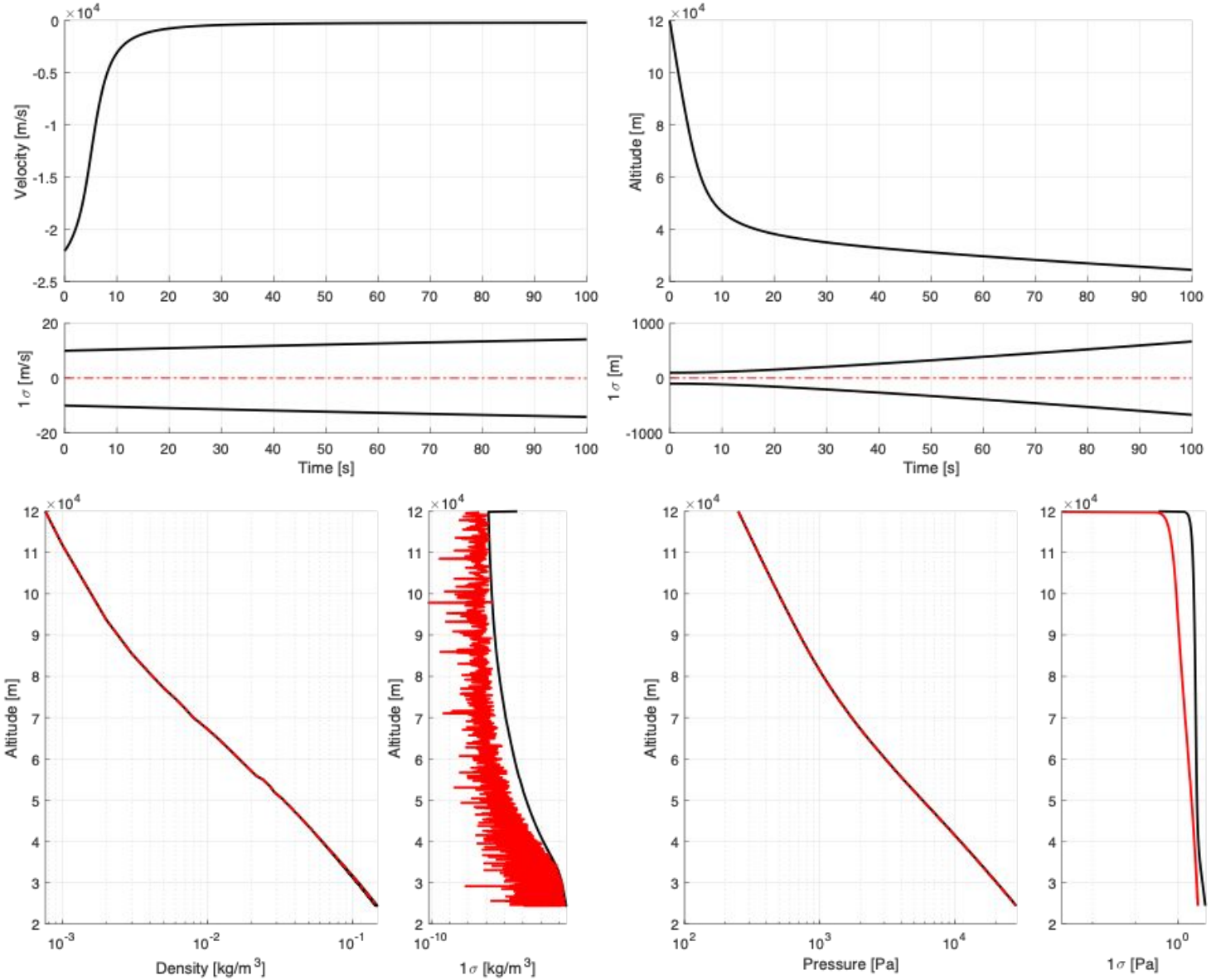

General rules to check for goodness of fit

- Simulation only: difference between the “true” and reconstructed parameters must lie in the estimated uncertainty bounds
- Both x simulation and real world data processing: measurement innovation should be Gaussian distributed